DEUTSCHES INSTITUT FÜR ERNÄHRUNGSFORSCHUNG POTSDAM-REHBRÜCKE

ABTEILUNG FÜR MOLEKULARE TOXIKOLOGIE

Role of proteolytic systems in lipotoxicity-induced hepatocellular damage

Dissertation zur Erlangung des akademischen Grades

"Doctor rerum naturalium" (Dr. rer. nat.)

in der Wissenschaftsdisziplin "Toxikologie und Pharmakologie"

eingereicht an der

Mathematisch-Naturwissenschaftlichen Fakultät

der Universität Potsdam

vorgelegt von

Ioanna Korovila

Potsdam, September 2021

Datum Disputation:

Hauptbetreuer: Prof. Dr. Tilman Grune
Betreuer: Prof. Dr. Tanja Schwerdtle
Gutachter: Prof. Dr. Jan Frank

Published online on the
Publication Server of the University of Potsdam:
https://doi.org/10.25932/publishup-55238
https://nbn-resolving.org/urn:nbn:de:kobv:517-opus4-552385

Contents

List of Figures

List of Supplementary Figures

List of Tables

Abbreviations

APS	Ammonium persulfate
ATF6	Activating transcription factor 6
Atg	Autophagy related proteins
ATP	Adenosine 5-triphosphate disodium salt
BSA	Bovine serum albumin
Cas-L	Caspase-like activity
ChT-L	Chymothrypsin-like activity
CIDEA	Cell death activator CIDE-A
CMA	Chaperon mediated autophagy
ConA	Concanamycin A
DTPA	Diethylenetriaminepentaacetic acid
DTT	Dithiothreitol
eIF2α	Eukaryotic translation initiation factor
ER	Endoplasmatic Reticulum
FFA	Free fatty acids
GAPDH	Glyceraldehyde-3-phosphate dehydrogenase
HCC	Hepatocellular carcinoma
HFD	High fat diet
HepG2	Human hepatoma G2 cell line
Hprt	Hypoxanthine Phosphoribosyl Transferase
IRE1	Inositol-requiring signaling protein 1
IRE1α	Inositol requiring enzyme 1 alpha
LAMP-1	Lysosomal-associated membrane protein 1
LC	Lactacystin
LD	Lipid droplets
MAP1LC3A/B	Microtubule-associated protein 1A/1B-light chain 3 (LC3)
MEHA	3-Methyl-N-Ethyl-N-(β-Hydroxyethyl)-Aniline
mTOR	Mechanistic target of rapamycin
NAFLD	Nonalcoholic fatty liver disease
NAS	NAFLD activity score

NASH	Nonalcoholic steatohepatitis
NEM	N-ethylmaleimide
NZO	New Zealand Obese
PA	Palmitate
PBS	Phosphate-buffered saline
PBST	PBS / 0.05% Tween 20
PE	Phosphatidylethanolamine
Pefablock	4-(2-Aminoethyl) benzene sulfonyl fluoride hydrochloride
PERK	Protein kinase RNA-like ER kinase
PI3K-III	Class III phosphatidylinositol 3-kinase
plin2	Perilipin 2
plin5	Perilipin 5
PPARδ	Peroxisome proliferator-activated receptor δ
prxs	Peroxiredoxins
prx2	Peroxiredoxin 2
prx3	Peroxiredoxin 3
prx4	Peroxiredoxin 4
puni	Punicalagin
ROS	Reactive oxygen species
Rpl13α	Ribosomal protein L13α
SD	Standard diet
SDS	Sodium dodecyl sulfate
SDS-PAGE	SDS polyacrylamide gel electrophoresis
Sqstm1	Sequestosome-1 (also known as p62)
TEMED	Tetramethyl ethylenediamine
TFEB	Transcription factor EB
TG	Triglycerides
T-L	Trypsin-like activity
Ub	Ubiquitin
Urs.acid	Ursolic acid
3MA	3-Methyladenine

Abstract

Hepatic steatosis is characterized by excessive loading of dietary lipids and chronic lipid droplet (LD) accumulation in the liver, which in turn lead to hepatocellular dysfunction. This pathogenic condition is a basic characteristic of nonalcoholic fatty liver disease (NAFLD) and a risk factor for many prevalent metabolic disorders, including obesity and type 2 diabetes. Palmitate (PA) is the most common saturated fatty acid and plays a significant role in the pathogenesis of hepatic steatosis. It has widely been used to induce lipotoxicity and study the development of LDs on cellular level. The two major proteolytic systems, ubiquitin-proteasome system and autophagy-lysosome system are involved in LD degradation and control the balance of lipid homeostasis. However, the impact of lipotoxicity on their function is still debatable. The aim of the present thesis is to investigate whether increased LD accumulation impairs the function of the proteolytic systems and if the lipotoxic effects could be reversed by enhancing their activity.

In vivo investigation in New Zealand Obese (NZO) mice, a polygenic model of obesity, demonstrated that high fat diet causes accumulation of LDs and hepatocellular injury. These effects were accompanied by a loss of autophagy efficiency and decreased proteasome subunit expression. Similar effects were observed *in vitro*, in PA-loaded HepG2 cells. PA induces LD accumulation and changes the redox status in mitochondria and endoplasmic reticulum. The function of both proteolytic systems is also affected in a time-dependent manner, considering 6 and 24h PA treatment. To investigate the role of proteasome and the autophagy-lysosome system in LD degradation, the activity of both systems was manipulated and alterations on the LD content were detected. In particular, HepG2 cells were treated with PA in presence or absence of autophagy inducer Torin 1, autophagy inhibitor 3-methyladenine, proteasome inducer ursolic acid and proteasome inhibitor lactacystin. The obtained data indicate that the autophagy-lysosome system is involved in the bulk LD degradation. It is evident that LD accumulation is associated with a failure of autophagy and leads to the disturbance of proteostasis, further contributing to LD stabilization and accumulation. Experiments with the natural autophagy inducer punicalagin, indicate that lipotoxic effects can be reversed. In particular, results show that punicalagin preserves the expression of autophagy-related proteins and restores the autophagic flux while, simultaneously, alleviating the LD content. Overall, the data of this thesis provide new insight into the role of the proteasome and autophagy-lysosome system, in PA-induced lipotoxicity. Moreover, the autophagy-inducing properties of punicalagin are underlined, proposing punicalagin a health-beneficial compound for future research on hepatic lipotoxicity.

Zusammenfassung

Lebersteatose entsteht durch eine übermäßige Zufuhr von Nahrungslipiden und ist durch eine chronische Ansammlung von Lipidtröpfchen (LD) in der Leber gekennzeichnet, die wiederum zu einer hepatozellulären Dysfunktion führen. Dieser pathogene Zustand ist ein grundlegendes Merkmal der nichtalkoholischen Fettleber (NAFLD) und ein Risikofaktor für viele weit verbreitete Stoffwechselerkrankungen, einschließlich Fettleibigkeit und Typ-2-Diabetes. Abgesehen von der Menge der aufgenommenen Nahrungsfette wird die Entwicklung der Lebersteatose auch stark von der Art der Fettsäure beeinflusst. Palmitat (PA) ist die am häufigsten vorkommende gesättigte Fettsäure und spielt eine bedeutende Rolle bei der Pathogenese der Lebersteatose. Sie wird häufig verwendet, um Lipotoxizität zu induzieren und die Entwicklung von LDs auf zellulärer Ebene zu untersuchen. Die beiden wichtigsten intrazellulären proteolytischen Systeme, das Ubiquitin-Proteasom-System und das Autophagie-Lysosom-System, sind am LD-Abbau beteiligt und kontrollieren das Gleichgewicht der Lipidhomöostase. Der Einfluss der Lipotoxizität auf ihre Funktion ist jedoch noch umstritten. Das Ziel der vorliegenden Dissertation ist es zu untersuchen, ob eine erhöhte LD-Akkumulation die Funktion der proteolytischen Systeme beeinträchtigt und ob die Effekte durch Kontrolle ihrer Aktivität umgekehrt werden können.

In-vivo Untersuchungen an New Zealand Obese (NZO) Mäusen, einem polygenen Modell für Fettleibigkeit, zeigten, dass eine fettreiche Ernährung eine Akkumulation von LDs und hepatozelluläre Schäden verursacht. Diese Effekte wurden von einem Verlust der Autophagieeffizienz und einer verminderten Expression der Proteasomaler Untereinheiten begleitet. Ähnliche Effekte wurden *in vitro* in PA-beladenen HepG2-Zellen beobachtet. PA induziert LD-Akkumulation und verändert den Redoxstatus in Mitochondrien und im Endoplasmatische Retikulum (ER). Zusätzlich beeinflusst PA die Funktion beider proteolytischer Systeme (proteasomal und lysosomal) zeitabhängig nach 6- und 24-stündiger Behandlung. Um die Rolle des Proteasome und der Autophagie beim LD-Abbau unter PA-induzierten lipotoxischen Bedingungen zu untersuchen, wurden beide Systeme inhibiert oder induziert und die Veränderungen des LD-Gehalts analysiert. Dazu wurden die HepG2 Zellen wurden mit PA in Gegenwart des Autophagie-Aktivators Torin 1, des Autophagie-Inhibitors 3-Methyladenin, des Proteasom-Aktivators Ursolsäure und des Proteasom-Inhibitors Lactacystin behandelt. Die erhaltenen Daten aus unseren Modellen belegen, dass vorrangig Autophagie am Abbau der LDs beteiligt ist. Die PA-vermittelte Lipidakkumulation könnte auf ein Versagen der Autophagie hinweisen und zu einer Störung der Proteostase sowie einer

weiteren LD-Stabilisierung und Anreicherung beitragen. Experimente mit dem natürlichen Autophagie-Aktivator Punicalagin weisen darauf hin, dass die PA-vermittelten lipotoxischen Wirkungen reduziert werden können. Insbesondere zeigen die Ergebnisse, dass Punicalagin die Expression von Autophagie-Proteinen erhält und durch PA-beeinträchtigten autophagischen Fluss wiederherstellt. Parallel dazu wird der durch PA-induzierte Gehalt an LD durch Punicalagin verringert. Zusammenfassend, liefern die Daten dieser Dissertation neue Einblicke in die Rolle des Proteasoms und des Autophagie-Lysosomalen Systems bei der PA-induzierten Lipotoxizität. Zudem werden die Autophagie-induzierenden Eigenschaften von Punicalagin aufgezeigt, die einen vielversprechenden Ansatz für die zukünftige Forschung zur hepatischen Lipotoxizität bieten.

Acknowledgements

The current project would not have been possible without the support of many people along these years. Firstly, I want to express my thankfulness to my supervisor Prof. Dr. Tilman Grune for the opportunity to work on his research group, providing me a rich environment where I could freely develop my own ideas and thoughts. I'd like to thank him for his guidance and insightful feedback. I am also grateful to my second supervisor Prof. Dr. Tanja Schwerdtle, who has held an overview of my project. Thanks to Prof. Dr. Jan Frank for reviewing and evaluating this scientific work. Warm thanks also go to my mentor Dr. Tobias Jung, a person who supported the current work by giving many useful comments, advice and helping with my experiments on imaging by confocal laser-scanning microscope.

Special thanks go to Dr. Christiane Ott whose contribution was extremely crucial for making this dissertation possible. She has been a patient listener all these years and her useful suggestions have substantially shaped the form and content of what is to be encountered below. Dr. Christiane Ott also kindly provided me with liver samples from her project. I would like to sincere thank Dr. Martin Hugo and Dr. José Pedro Castro, previous members of MTOX group and close friends who made the PhD a great experience. Our scientific discussions and their perceptive suggestions were very critical. I'd like to thank them for all the support and assistance that they gave me especially at the beginning of my work.

I am also thankful to Dr. Richard Kehm for the provision of liver samples from his project. Also significantly contributing were the biological technical assistants Stefanie Deubel, Tanina Flore, Andrea Borchert and Sabine Braune who kindly gave me their help whenever I needed on the experimental part. I would also like to thank all the members of my group MTOX and special thanks to my colleagues and close friends Raquel Fernando and Michaela Press. I would like to thank all of them by my heart for the collaboration, long discussions and willingness to help. They always made a very creative and cheerful environment despite the difficulties that sometimes there were. Special thanks also go to Dr. Thomas Laeger, Dr. Daniela Weber and Dr. Annika Höhn for the proofreading, their valuable advice and nice friendship.

Just as importantly, I wish to express my sincere thanks to my close family members, my parents Katerina and Dionysis, my brother Christos, my husband and partner in life Denis, and our little daughter Elli. Without them this achievement wouldn't have been possible and it is to them that this dissertation is dedicated.

1. Introduction

The prevalence of metabolic disorders such as nonalcoholic fatty liver disease (NAFLD), obesity and type 2 diabetes has dramatically increased over the last decades. Despite their different pathogenesis, most metabolic disorders are commonly associated with disturbed systemic lipid homeostasis and chronic lipid retention in non-adipose tissues, inducing tissue damage (lipotoxicity) [1] (Figure 1). Oversupply of dietary lipids and/or reduced capacity of lipid storage in adipose tissue are leading causes of increased circulatory fatty acids in plasma. Thus, the limited lipid storage capacity of non-adipose tissues such as liver, pancreas and heart is exceeded, leading to chronic lipid accumulation (steatosis) and subsequently to cellular dysfunction [2].

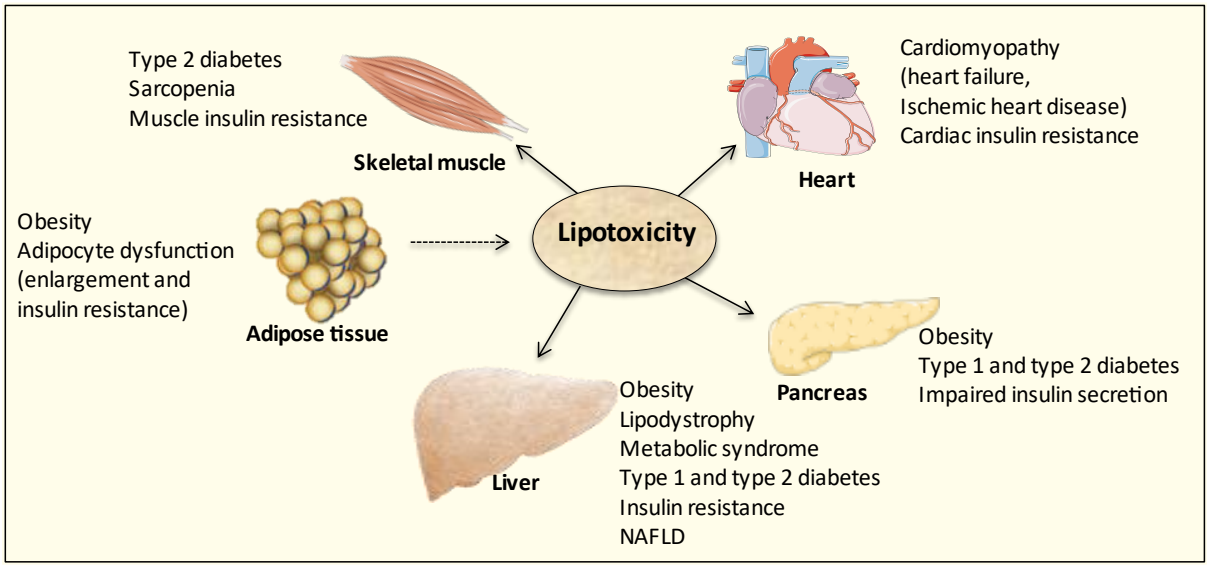

Figure 1: Ectopic lipid accumulation in non-adipose tissues is a risk factor of many prevalent metabolic disorders. (This figure has been created using the templates of human organs and tissues from Servier Medical Art:SMART [3-6]).

In the present study liver will be in the focus as it is a central and major integrator of lipid metabolism, playing a key metabolic role for the whole body. The pathogenic condition where excessive lipids accumulate in the liver (hepatic steatosis) is a basic characteristic of NAFLD. NAFLD is the most common chronic liver disease with increased predominance worldwide (reaching 25% in general population and 30% in the adult population) and it is usually consistent with the increased prevalence of obesity [7-9]. This progressive disease is a spectrum of stages, starting from simple steatosis and can develop to severe fibrotic stages leading to cirrhosis and liver failure. The lipid retention in the liver during NAFLD is not related to a history of significant alcohol abuse or other known liver disease. It involves glucose redirection from glycogenesis to lipogenesis and is usually associated with insulin

resistance [10, 11]. In the following sections, the lipid metabolism in the liver and complications which underlie disturbance of lipid homeostasis leading to hepatic steatosis will be discussed. Special emphasis will be given on proteolytic systems and their role in maintenance of lipid homeostasis.

1.1 Lipid metabolism in the liver

Liver plays one of the most important roles in human metabolism. Detoxification of xenobiotics, glucose and lipid metabolism are some of its main functions. Hepatocytes are the basic metabolic cells and the most abundant cell type in the liver. Together with blood vessels (central vein, portal triad, sinusoids) and other cell types (Kupffer cells, stellate cells, sinusoidal endothelial cells) they are organized into lobules, the smallest functional units of the liver (Figure 2) [12-15].

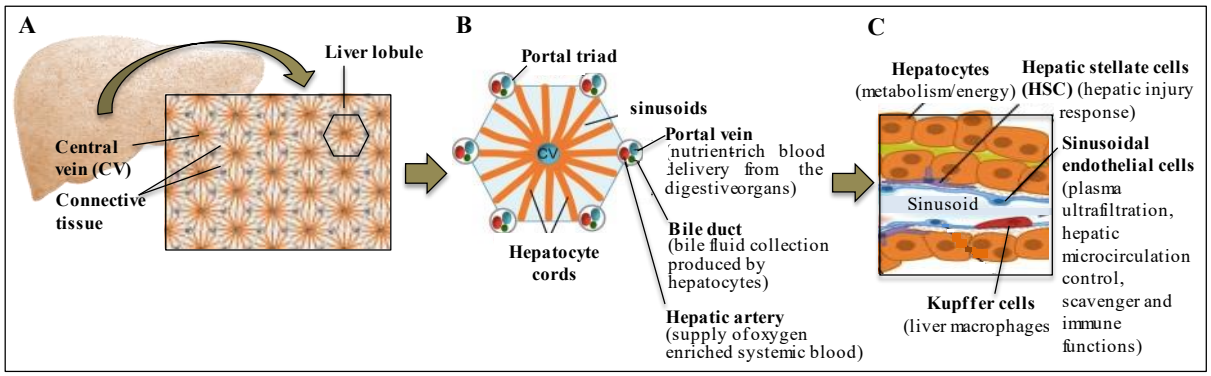

Figure 2: Structure of the liver: a complex and highly organized architecture. A. Lobular grids. The liver lobules are the functional units of the liver, arranged in lattice. **B.** Liver lobule in cross section. The liver lobules have a roughly hexagonal arrangement. Each corner contains a portal triad (portal vein, bile duct and hepatic artery) while the cental vein is located in the center. Hepatocytes are organized into plates sepatated by intervening vascular channels (sinusoids). Sinusoids constitute the hepatic circulation as they bridge the central vein with the portal triad. **C.** Cellular composition of liver lobule. (Adapted from Gordillo *et al.* [12]).

The major metabolic activity of lipids in the liver, including fatty acid uptake, esterification, oxidation and secretion, takes place in hepatocytes (Figure 3). Fatty acids in the liver derive from three primary sources: diet (15–30% of the liver fatty acid pool), remnant fatty acids released from adipose tissue during fasting and *de novo* lipogenesis (fatty acid synthesis) during feeding where excess carbohydrates are stored as lipids (5-30% of the liver fatty acid pool). Once fatty acids are imported into the liver they are temporarily stored in lipid droplets (LDs). Lipolysis or LD degradation leads to endogenous fatty acid release, which in turn is utilized for energy by β-oxidation in mitochondria or exported and delivered to other tissues by lipoprotein production. Alterations in any of these pathways of lipid import, utilization or

secretion, lead to hepatic and/or whole body imbalance in lipid homeostasis and chronic lipid accumulation in the liver, which may contribute to disease development (Figure 3) [16, 17].

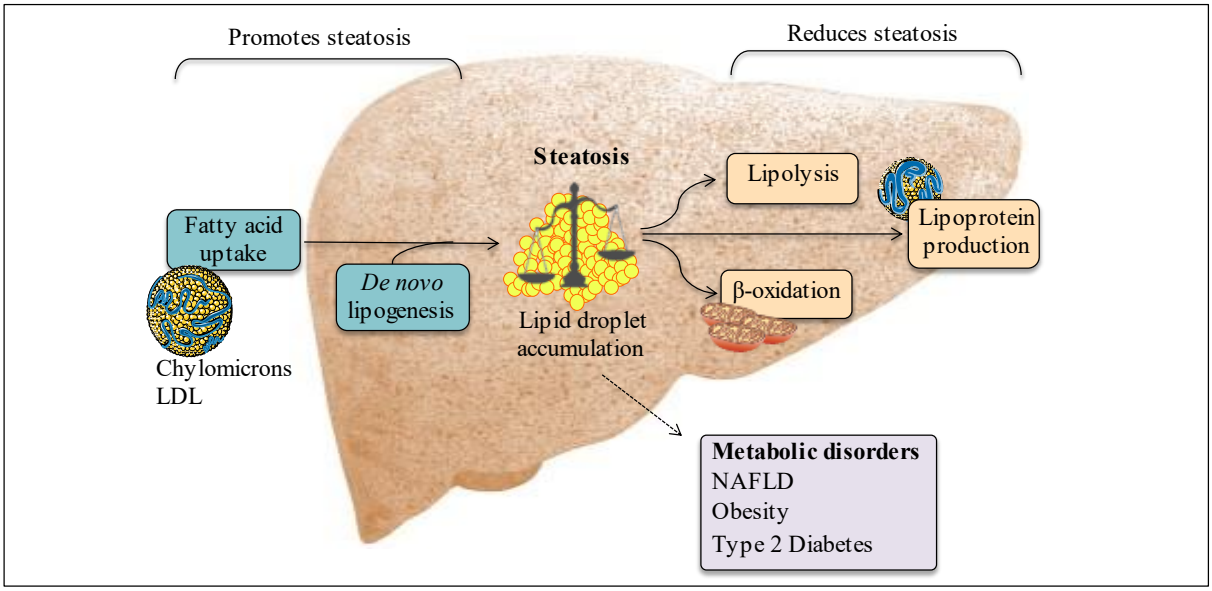

Figure 3: Hepatic steatosis results from imbalance of lipid homeostasis and is a risk factor for many prevalent metabolic diseases. Increased fatty acid uptake and *de novo* lipogenesis combined with decreased LD catabolism (lipolysis, autophagic degradation, impaired β-oxidation) and/or lipoprotein production and secretion promote hepatic steatosis (adapted from Gluchowski *et al.* [17]).

Accumulative evidence suggests that saturated fatty acids have particular contribution to hepatocellular lipotoxicity and are considered a risk factor for dyslipidemia [18]. Palmitate (PA) is one of the most abundant saturated fatty acid in human serum and in steatotic liver. Accounting for 20-30% of total fatty acids in the human body, PA can be provided in the diet (especially in Western-style diet) or synthesized endogenously via *de novo* lipogenesis from excess carbohydrate consumption [19]. PA has widely been used to induce lipotoxicity and study the development of LDs in hepatocytes, both playing a significant role in the pathogenesis of NAFLD [20-22]. Although previous studies have indicated that PA contributes to inflammation and fibrosis in the liver leading to cellular apoptosis, the exact mechanism of PA-induced lipotoxicity remains to be elucidated.

1.2 Histopathological abnormalities during hepatic steatosis

NAFLD is the term for a range of conditions caused by lipid retention in the liver. Simple steatosis is the earliest stage where only hepatocellular steatosis is observed. This stage usually remains asymptomatic and can be reversed by changes in lifestyle and diet. Hepatic steatosis can develop to nonalcoholic steatohepatitis (NASH), a condition which is accompanied by both necroinflammatory reactions and hepatocellular steatosis. NASH can in

turn progress to cirrhosis and hepatocellular carcinoma (HCC) which are irreversible severe fibrotic stages (Figure 4) [23, 24].

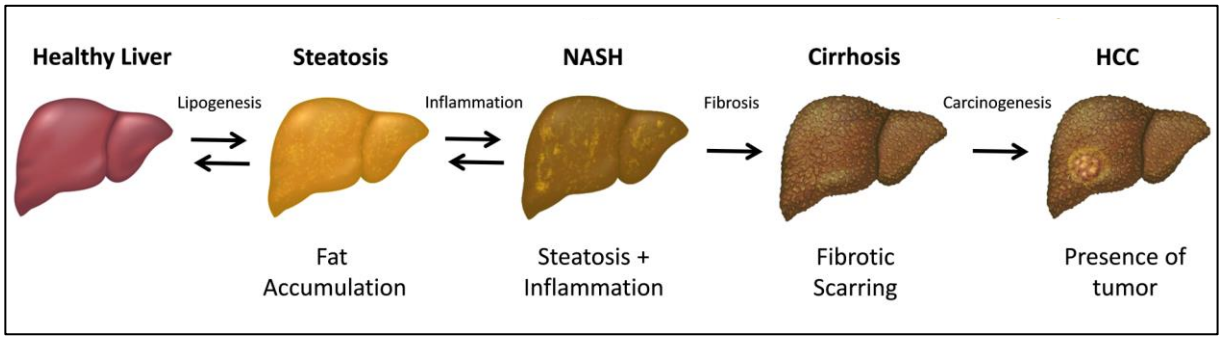

Figure 4: Progression and stages of hepatic steatosis [23].

The Pathology Committee of the NASH Clinical Research Network addressed the necessary histological characteristics of NASH and designed a scoring system (NAFLD activity score - NAS) for use in clinical research. The NAS scoring system includes the whole spectrum of NAFLD stages and evaluates the histological changes over time. It contains the following three histological features: steatosis, lobular inflammation and hepatocellular ballooning, which are necessary for the diagnosis of NASH (Figure 5).

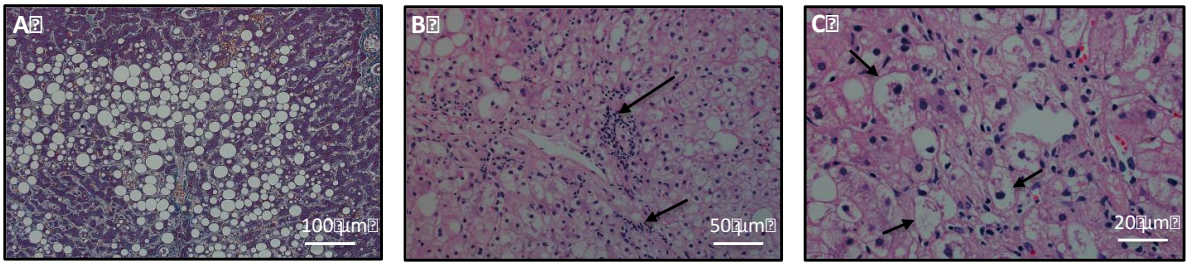

Figure 5: Histopathological features commonly seen in NASH. A. Hepatocellular steatosis (Masson trichrome staining). **B.** Lobular inflammation **C.** Hepatocellular ballooning (hematoxylin and eosin staining) [27].

Hepatocellular steatosis is recognized by increased LD accumulation (Figure 5A). It is the hallmark of NAFLD and histologically is diagnosed when intrahepatic triglyceride (TG) content is more than 5% of the hepatocytes. Lobular inflammation is characterized by necroinflammatory foci scattered in the hepatic lobule (Figure 5B). It is usually mild in NASH and consists of a variation of inflammatory cell infiltrate such as Kupffer cell aggregates and mononuclear cell clusters. Hepatocellular ballooning is also found in NASH, recognized as enlarged hepatocytes with rarefied cytoplasm and reflects hepatocellular injury (Figure 5C) [25]. The proposed NAS is the summary grade of steatosis, lobular inflammation and hepatocellular ballooning with a categorization: "not NASH", "borderline NASH" and "NASH". The term "borderline NASH" is used for cases that suggestive histological changes

are evident, although the observed patterns are not sufficient to make a definite diagnosis of NASH [26, 27].

1.3 Redox-dependent dysregulation of hepatic lipid metabolism

Several mechanisms have been proposed to explain the molecular mechanisms of lipotoxicity in hepatocytes. There is growing evidence that excessive lipid loading and chronic LD accumulation are leading causes of increased reactive oxygen species (ROS) generation in the cytosol and in cellular compartments - including mitochondria and endoplasmic reticulum (ER). The elevated ROS levels, such as hydrogen peroxide (H_2O_2), in these compartments result in mitochondrial dysfunction, ER and oxidative stress [28, 29].

In particular, major cellular sources of ROS during NAFLD are mitochondria, as these organelles are key regulators of lipid metabolism. During hepatic steatosis, the increased influx of FFA induces β-oxidation overload, leading to ROS overproduction. In addition, excess FFA serve as substrates for the formation of lipid intermediates such as lipid peroxides. The increased ROS formation and the accumulation of reactive lipids subsequently induce oxidative modifications to macromolecules (such as mitochondrial DNA, lipids and proteins of the mitochondrial machinery) eventually leading to changes in mitochondrial structure and function [30, 31].

Apart from the mitochondrial dysfunction, during FFA overload, misfolded and unfolded proteins accumulate in the ER lumen, leading to ER stress and in turn to activation of the unfolded protein response (UPR) pathway. UPR attenuates general protein translation in order to increase the protein folding capacity and facilitate the degradation of misfolded proteins. However its prolonged activation is implicated in insulin resistance, inflammation and apoptotic cell death [32-34]. Three transmembrane sensor proteins initiate and regulate the UPR pathway and induce myriad of downstream signaling cascades: protein kinase RNA-like ER kinase (PERK), activating transcription factor 6 (ATF6), and inositol-requiring signaling protein 1 (IRE1). The major substrate of PERK is the eukaryotic translation initiation factor (eIF2α), the phosphorylation of which leads to the transient attenuation of protein synthesis in an effort to relieve the burden on the ER [35].

The mitochondrial dysfunction and ER stress, which result from the elevated ROS levels in the respective compartments, in turn lead to loss of proteostasis and modulation of insulin and innate immune signaling. These effects finally alter the expression and activity of key

enzymes involved in lipid metabolism, leading to a redox-dependent deregulation of lipid metabolism [28].

The short lifespan of ROS and their rapid reactivity with other components make their direct and accurate detection quite challenging. One method to detect the redox status in cellular compartments is the determination of the redox transformations of peroxiredoxins (prxs) through their reaction with H_2O_2. Prxs are highly abundant cellular antioxidant proteins and they possess six isoforms in mammals within the cellular locations, including cytosol (prx1, -2, -6), nucleus (prx1), mitochondria (prx3 and -5), peroxisomes (prx5) and ER (prx4) [36]. As prxs are H_2O_2 scavengers, their cysteine residues are oxidized forming intermolecular disulfide bonds, during their catalytic cycle. In addition, prx oxidation occurs in the absence of widespread oxidative damage, such as lipid peroxidation or protein carbonylation. Therefore, analysis of the redox transformations of endogenously expressed prxs provides a marker of the cellular redox status and the disruptions in redox homeostasis [37].

1.4 Lipid droplet biology and implication to hepatic steatosis

During overnutrition, excess lipids are stored into LDs, which are highly dynamic organelles. They primarily function as lipid deposits during times of energy excess and energy reservoir during deprivation. Apart from their function as lipid storage, LDs are metabolically active and highly dynamic. They regulate lipid homeostasis, as they are involved in several fundamental metabolic functions such as lipid synthesis, metabolism, transportation and cell signaling. LDs are composed of a neutral lipid core surrounded by a phospholipid bilayer, in which LD-associated proteins are incorporated (Figure 6) [38].

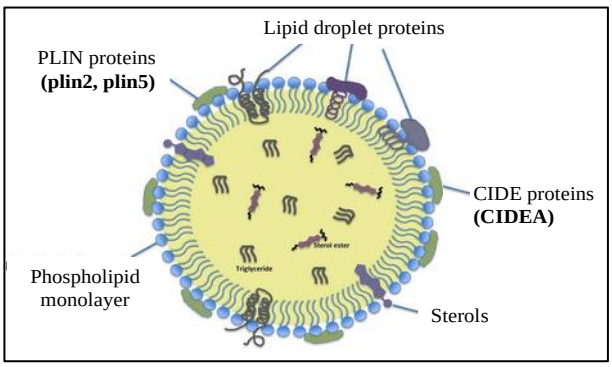

Figure 6: Structure of LDs. The LD proteins plin2, plin5 and CIDEA are highly abundant in the liver, playing significant role in the development of hepatic steatosis (adapted Onal et al. [38]).

The proteins on the LD surface have structural function and/or are highly involved in the regulation of lipid metabolism as they are enzymes involved in lipid synthesis and catabolism (lipases), membrane trafficking and cell signaling [39, 40]. Depending on the metabolic demand, the protein content of LDs can highly diverse [41]. Perilipins (plins) and cell death activators (CIDEs) are the most studied and best characterized LD-associated protein families [17].

Perilipins are proteins responsible for the maintenance of LD morphology and lipid storage-hydrolysis balance [42]. There are five known mammalian proteins which belong to perilipin family, (plin1-5) with distinct function and tissue/cell type prevalence. Among them, perilipin 2 (plin2) is highly abundant in the liver and the most upregulated perilipin in humans and rodents with NAFLD. Plin2 promotes TG accumulation, attenuates lipolysis and inhibits fatty acid oxidation [43, 44]. Perilipin 5 (plin5) is highly expressed in oxidative tissues such as muscle, heart and fasted liver, where high levels of FFA oxidation occur. It controls lipolysis and facilitates the flow of released fatty acids from lipolysis to mitochondria for β-oxidation through LD-mitochondria interaction [40, 42, 45].

The CIDE protein family includes the proteins CIDEA, CIDEB and CIDEC and play also a significant role in cellular lipid homeostasis. CIDEs have been found at LD–LD contact sites regulating LD fusion-growth and promoting exchange of lipids between LDs. Depletion of any protein of CIDE family results in numerous small LDs, while their overexpression increases the number of large LDs. Among the proteins of CIDE family, CIDEA and CIDEC have been reported to be implicated in the development of hepatic steatosis, as both proteins are increased in fatty liver diseased mice and promotes hepatic lipid accumulation [40, 46]**.** In addition, CIDEA is a sensor of saturated fatty acids, such as PA, and its expression is mediated by the transcription factor sterol response element-binding protein (SREBP) 1c [47].

1.5 Ubiquitin-proteasome system and autophagy-lysosome system: function and implication to lipid droplet degradation and steatosis

Since hepatic steatosis is characterized by increased LD retention in the liver which in turn lead to loss of proteostasis and lipidostasis, in this section the two major degradation systems of the cell: the ubiquitin-proteasome system and the autophagy-lysosome system will be on focus. Both degradation systems have dual roles, as they are responsible for the maintenance of protein and lipid homeostasis and for the cellular protein and organelle quality control. In the following paragraphs the involvement of these two degradation systems in the cellular function, LD degradation and the current knowledge regarding their association in the development of hepatic steatosis, will be discussed.

1.5.1 Lipid droplet degradation: Convergence of proteasomal and autophagic pathways

LDs dynamically cycle in size and abundance in response to the cellular fatty acid demand, such as during starvation and periods of cell proliferation, requiring membrane biogenesis.

Therefore, as mentioned above the LD proteome must be constantly adjusted to accomplish the metabolic demand. The fatty acid mobilization from LDs is mediated through the synergistic action of lipases, the autophagy-lysosome system (chaperon mediated autophagy (CMA), macroautophagy - lipophagy and microautophagy - microlipophagy) and the ubiquitin-proteasome system. In particular, the removal of proteins from the LD surface occur either by their relocalization to different cellular compartments (such as ER and cytosol) [48] or by their degradation through proteasome [49-52] or CMA [53, 54], allowing the access of lipases to act on the LD surface [55]. During the CMA pathway, chaperons transfer the proteins to lysosomes for degradation, while the ubiquitin-proteasome pathway contains a protein targeting by ubiquitination and subsequently degradation by proteasome (1.5.2) [56]. Alternatively, LDs can selectively be isolated within autophagosomes and delivered to lysosomes via macroautophagy (specifically termed as lipophagy) (1.5.4), allowing lipids as well as proteins to be degraded by the action of acidic lysosomal lipases and proteases, respectively. Apart from the entire LD, a portion can be directly engulfed into the lysosome through microautophagy (specifically termed as microlipophagy). Macroautophagy, however, is rather responsible for the bulk degradation of LDs [40, 57-59].

1.5.2 Ubiquitin-proteasome system - function

The ubiquitin-proteasome system is the central proteolytic machinery of the cell, responsible for the degradation of 80-90% of all cellular proteins. Proteasome mediates the degradation of short-lived and damaged or dysfunctional proteins, as well as the removal of fully functional and natively folded proteins which are no longer needed. Both functions retain the cellular functionality and provide a constant quality control of the functional proteome [60].

Proteolysis is mediated by the proteasome, which is a large protein complex and the degradation machinery of ubiquitin-proteasome system. The 20S core is the catalytic particle of proteasome. Several proteasomal regulators, for instance the 19S and 11S particles, can bind to the 20S core and modulate the activity and substrate specificity. However, under stress conditions the free 20S proteasome itself is able to recognize unfolded and, therefore, dysfunctional proteins due to their increased surface hydrophobicity, while the substrate degradation is occured in an ubiquitin- and ATP-independent manner [61-63].

As depicted in Figure 7A, the 20S proteasome is composed of four stacked rings, two α and two β, arranged in a cylindrical structure α-β-β-α. The outer α rings (composed of the subunits α1-7) are responsible for the entrance of substrate proteins into the inner β rings (composed of

the subunits β1-7) which provide the catalytic center. The proteolytic activity is mediated by three different subunits, the β1, β2 and β5. Although they share a common proteolytic mechanism, they have three distinct substrate specificities known as the chymotrypsin-like activity (ChT-L, cleaving after large hydrophobic amino acids, β5 subunit), caspase-like activity (Cas-L, cleaving after acidic amino acids, β1 subunit) and trypsin-like activity (T-L, cleaving after basic amino acids, β2 subunit) [64, 65].

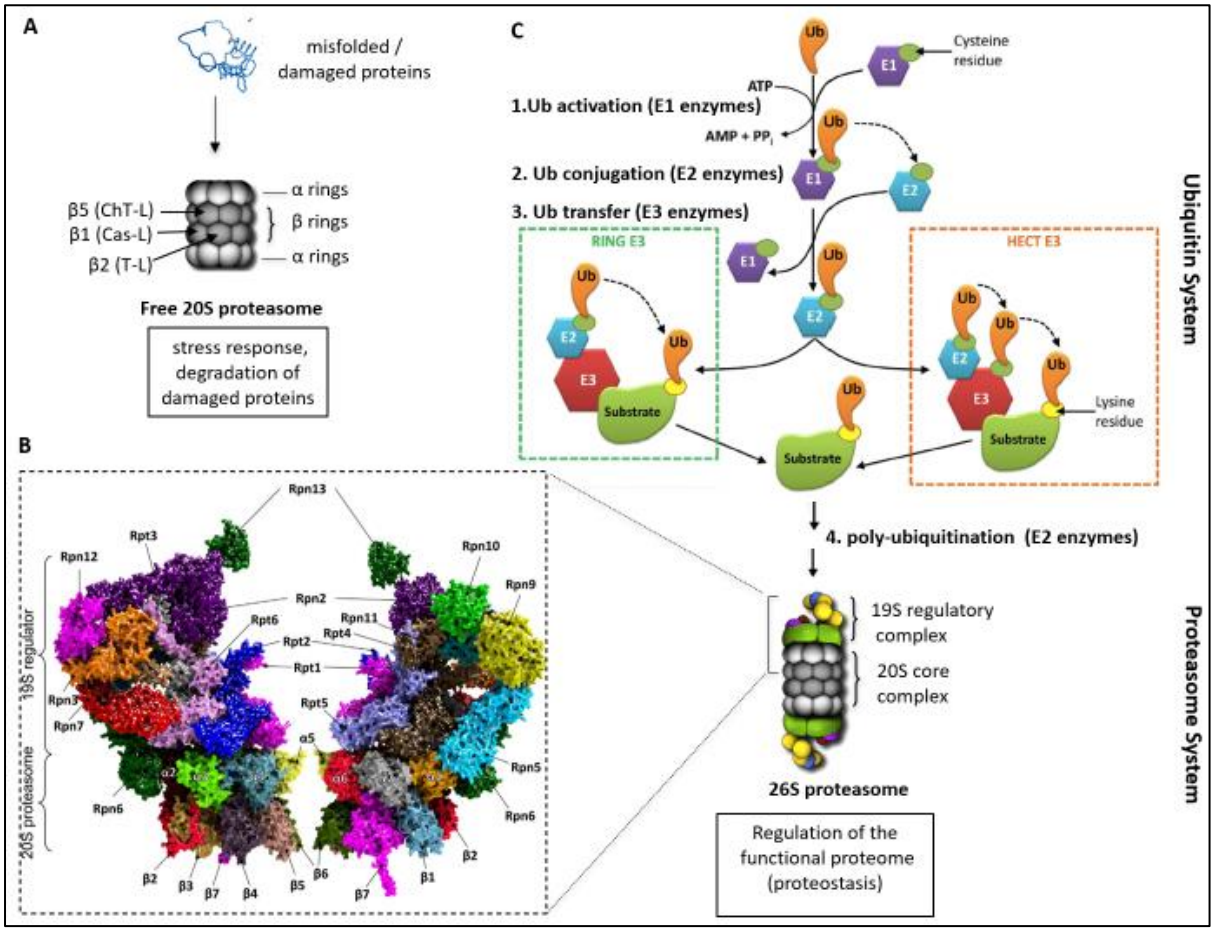

Figure 7: Protein degradation through the ubiquitin-proteasome system. A. Degradation of misfolded proteins through the 20S proteasome. **B.** Structure of 19S- half 20S regulatoty particles. (one α and one β-ring attached to the proteins of 19S regulator). **C.** Protein degradation by 26S proteasome through the ubiquitination pathway**.** The process contains activation, conjugation and transfer of a Ub molecule through E1, E2 and E3 enzymes respectively, following the elongation of Ub-labeling. Depending on the transfer mechanism, E3 enzymes can be RING type (direct transfer of Ub from E2 to the substrate) or HECT type (Ub transfer from E2 to E3 and then from E3 to the substrate) (adapted from Korovila *et al.* [56, 66]).

One of the most prominent proteasomal regulators is the 19S particle. Binding of two 19S regulatory particles to the α-rings of 20S proteasome leads to the formation of the 26S (constitutive) proteasome (19S-20S-19S). The 26S proteasome mediates the degradation of natively folded and fully functional proteins after previous substrate-targeting via polyubiquitination, necessary for substrate recognition. In contrast to the 20S proteasome, the

26S proteasome requires ATP hydrolysis to be active. The energy provided by ATP is rather necessary for substrate unfolding and not for proteolytic degradation [67, 68].

In particular, the 19S regulatory particle contains a lid-like structure which is composed of the non-ATPase dependent subunits (Rpn1-12 and Rpn15) and enables the recognition and binding of substrates. The access of protein substrates to the catalytic chamber of 20S core is restricted and depends on AAA-ATPases (subunits Rpt1–6). Rpts form the ring base of the 19S regulatory particle of the proteasome and are responsible for three functions: 1) substrate unfolding which is mediated through mechanical force via ATP binding-hydrolysis cycles, 2) gate opening and 3) substrate translocation into the proteolytic chamber of 20S core (Figure 7B) [69].

The degradation of natively folded substrates is highly specific and is mediated through polyubiquitination labeling, a process provided by the ubiquitin system (Figure 7C). The ubiquitination process contains three different types of enzymes (E1–E3). E1 enzymes initiate the process through ubiquitin (Ub) activation. E2 enzymes in turn mediate the Ub-conjugation and finally E3 enzymes transfer the Ub to substrate in a highly specific manner. After the attachment of the first Ub, the labeling is elongated, providing the degradation signal for 26S mediated proteolysis [70, 71].

1.5.3 Current knowledge regarding the implication of proteasome to hepatocellular steatosis

The role of the proteasome during hepatic steatosis is relatively poorly understood. Proteasome is involved in several cellular processes, misregulation of which underlay the pathophysiology of hepatic steatosis and thereby NAFLD. The proteasome plays a pivotal role in removal of oxidatively damaged proteins [60] and regulates the turnover of several LD proteins [49-52, 72-74] and proteins involved in lipid metabolism and insulin signaling [75-77]. Several studies in animal and cellular models have proposed an association between proteasome and insulin resistance, ER stress and cellular apoptosis in liver [78, 79] and other tissues [80-82] under lipotoxic conditions. However, systematic review in the liver regarding the role of proteasome in hepatic steatosis is limited and the impact of HFD/FFA-induced lipotoxicity in proteasome function has not been completely understood. In animal models of obesity and type 2 diabetes it has been proposed that dysfunction of proteasome is a leading cause of UPR activation, ER stress and insulin resistance [78]. Decreased proteasome activity has also been reported in mice with NAFLD [83] and HepG2 cells exposed to FFA [84]. On

the contrary, another study in HepG2 cells has demonstrated that lipotoxicity mediated by FFA does not affect the proteasome function. The same study proposed an enhanced ubiquitination and proteasomal degradation of specific insulin signaling proteins as a potential molecular mechanism of lipotoxicity-induced insulin resistance [85]. Ubiquitinome analysis of rat liver proposed that HFD alters the composition of ubiquitinated proteins, including many that participate in fatty acid metabolism [77]. In addition, transcriptomic analysis in liver of obese and diabetic mice indicated differential gene expression in response to HFD, including genes involved in ubiquitine-mediated proteolysis, fatty acid metabolism and genes encoding proteasome subunits [86].

1.5.4 Autophagy-lysosome system - function

The autophagy-lysosome system mediates the turnover of long-lived proteins, large aggregates of proteins / macromolecules as well as whole cellular organelles - including mitochondria and LDs. The system can be mediated by various cellular stresses such as nutrient deprivation, accumulation of damaged proteins or aggregates (aggrephagy), dysfunctional mitochondria (mitophagy) and by invading pathogens (xenophagy) [86]. Lipophagy has been recently reported to describe the bulk LD removal through macroautophagy, a part of autophagy-lysosome system. The process of macroautophagy - hereinafter referred as autophagy - starts by the formation of an isolation membrane (phagophore). As the phagophore expands, it incorporates the cytoplasmatic components - LDs in case of lipophagy, destined for degradation. The mature autophagosome facilitates the delivery of cargo to lysosomes via fusion, forming the autolysosome and subsequently allowing the degradation by lysosomal enzymes [87, 88] (Figure 8).

The autophagic pathway is a highly dynamic process, containing more than 30 autophagy related proteins (Atg) and other autophagy-linked regulatory proteins. Beclin-1 for instance plays a pivotal role in the early phase of the process. As a core component of the class III phosphatidylinositol 3-kinase (PI3K-III) complex, it is essential for the nucleation of the phagophore and the formation of the autophagosome [89]. During the initial phase of autophagosome biogenesis, the Atg12 protein covalently binds to Atg5 and forms the conjugate Atg5-Atg12, which exhibits E3 ligase-like activity. The Atg5-Atg12 conjugate in turn, together with Atg16 form the Atg5-Atg12/Atg16 complex. This complex supports the formation of autophagosomes [90] and the lipidation process of microtubule-associated protein 1A/1B-light chain 3 (MAP1LC3A/B, also termed as LC3) [91]. LC3 is also a key regulatory protein and a widely used marker to monitor the autophagic process. LC3 is

involved in phagophore elongation and autophagosome maturation. In particular, the non-lipidated form of LC3, LC3 I, is generated by proteolytic cleavage of pro-LC3 by Atg4 [92, 93]. LC3 I, in turn, is conjugated to phosphatidylethanolamine (PE) on the surface of phagophores, generating the lipidated form LC3 II [94, 95]. Another significant protein for selective autophagy is the macroautophagy receptor sequestosome-1 (sqstm1 also known as p62), as it sequesters and transfers polyubiquitinated proteins to autophagosomes [96]. Both LC3 II and p62 are themselves autophagic substrates and they are degraded in the autolysosomes. Turnover analysis of these proteins in the presence and absence of lysosomal degradation inhibitors, such as concanamycin A (ConA) or bafilomycin A1, is a reliable and extensively used method to estimate the autophagic flux [97].

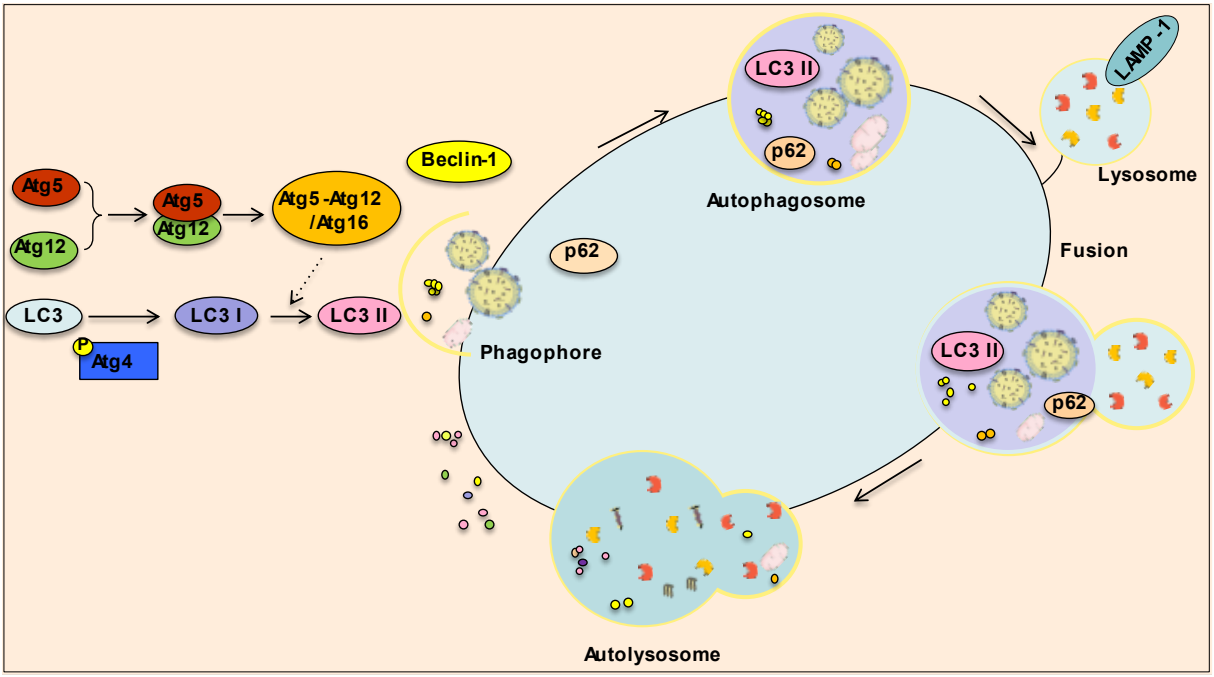

Figure 8: The autophagic pathway and its major regulatory proteins. (This figure has been created using templates from Servier Medical Art:SMART [98-100]).

The lysosomal-associated membrane protein 1 (LAMP-1) is a highly abundant protein localized in lysosomal membranes. It is thus commonly measured for the estimation of possible compensatory alterations in lysosome numbers or for determination the colocalization of lysosomes with Atgs [101]. Additionally, in lysosomes a high variety of acidic proteases, -such as cysteine cathepsins [102] and lipases, such as the lysosomal acid lipase (LAL) have been identified in order to degrade the protein and lipid cargo respectively. These enzymes display an optimum activity under acidic conditions (pH 4.5–5.5), ensured by membrane-bound ATP-consuming proton-pumps [103, 104].

1.5.5 Current knowledge regarding the implication of autophagy to hepatocellular steatosis

Since the recent discovery in 2009 that the bulk LD content can be selectively degraded through autophagy [105], many studies have been performed to elucidate its role in hepatic steatosis and thereby in NAFLD. Autophagy has emerged as an important regulator in lipid metabolism and has been widely acknowledged for its involvement in the development of NAFLD. However, the impact of HFD/FFA-mediated lipotoxicity on the autophagic function has controversially been discussed. A number of studies in mice with NAFLD and cellular models, support that HFD/FFA induces autophagy as a protective mechanism against lipotoxicity [83, 106-110]. A study by Lee and colleagues in mice with NAFLD, suggests a cross-talk between proteasome and autophagy pathway. In particular, it was demonstrated that inhibition of proteasome caused accumulation of lipid peroxides, decreased mitochondrial biogenesis and induction of autophagy / mitophagy [83]. Activation of autophagy was also suggested in response to ER stress in liver fibrosis that characterizes the advanced form of NAFLD [107, 111]. Additionally, the studies from Tu *et al.* and Cai *et al.* in human NASH, in liver tissues of HFD-fed mice and in PA-loaded hepatocytes demonstrate induced pro-survival autophagy as a protective mechanism against apoptosis [108, 110].

Besides, a recent study by Ding and colleagues proposed an initial autophagy activation, following its late inhibition upon progressive steatosis [112]. In addition, a considerable body of evidence has shown an association between impaired autophagic flux with the development of hepatic steatosis and NAFLD [113-116], while it is often discussed that induction of autophagy has protective effects [117-125]. The pathogenic mechanisms underlying the impairment of autophagy are not fully understood, although it has been suggested a link to elevated ER stress, insulin resistance and inflammation which in turn might lead to apoptosis [113-115]. In obese and diabetic mice, as well as *in vitro*, in hepatocytes with FFA-induced lipotoxicity, impaired autophagy and decreased levels of several Atg proteins have been documented [116, 125-129]. Additionally, a study in mouse liver suggested that HFD affects the vesicular fusion [130], while in patients with NAFLD decreased hepatic cathepsin expression has been found [131]. Therefore, despite extensive research, the impact of lipotoxicity on autophagy remains a debatable issue while a potential time dependent alteration of the different autophagic stages has yet to be investigated.

1.6 Targeting the proteolytic systems as approach for limiting or preventing lipotoxicity

Since both proteasome and autophagy are involved in several metabolic pathways, which accompany hepatic steatosis and NAFLD, compounds that target the protein degradation process have been examined in chronic liver diseases. Proteasome inhibitors, for instance, have made a progress in the treatment of liver fibrosis and hepatocellular carcinoma [132, 133]. Autophagy-target therapeutic strategies have also drawn growing attention. It has been reported that induction of autophagy attenuates hepatic steatosis in mice and cell-culture models with HFD/FFA-mediated lipotoxicity [117-125], although a human study suggested that long treatment with the autophagy inducer rapamycin causes liver damage and inflammation [134]. Inhibition of autophagy has been suggested for the treatment of hepatocellular carcinoma during preclinical studies, however, the implication in liver fibrosis is still debatable [135-137].

1.6.1 Punicalagin as a candidate to prevent lipotoxicity

Herbal medicine as an alternative approach in the treatment of hepatic steatosis and NAFLD is well underway [118-121]**.** One natural compound, which has been reported to benefit several chronic liver diseases is punicalagin (2,3-hexahydroxy-diphenoyl-4,6-gallagyl-glucose, Figure 9) [139, 140]. Punicalagin belongs to ellagitannins, a family of bioactive polyphenols. It accounts for more than one-half of the polyphenols in pomegranate juice and presents growing attention due to its various benefits on human health. The main biological activities include antioxidant, anti-inflammatory and hepatoprotective effects.

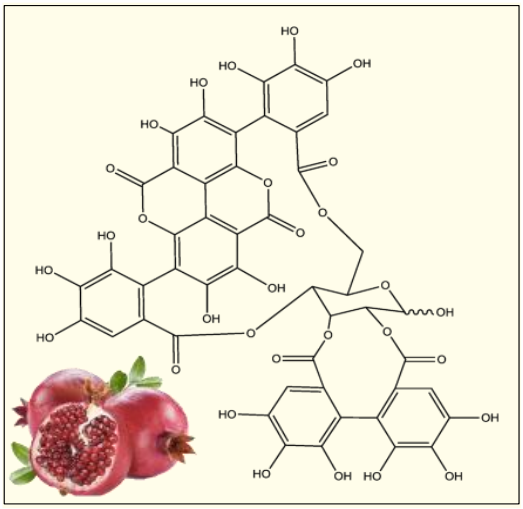

Figure 9: Chemical structure of punicalagin [138].

The potent effects of punicalagin on metabolic disorders, including NAFLD, obesity, type 2 diabetes and cardiovascular disease have recently been reported [139-143]. However, there are limited studies who investigated the protective mechanism of punicalagin and most of them have primarily concerned with its antioxidant and anti-inflammatory effects, while studies on autophagy are limited. More specifically, *in vivo* studies in adipocytes of HFD-fed mice and *in vitro* in hepatocytes, it has been reported that punicalagin attenuates lipotoxicity through induction of Nrf2-keap1 antioxidant system [140, 144]. In addition, in a HFD-

induced NAFLD rat model, improved hepatic lipid metabolism was attributed to punicalagin treatment. In particular, the fatty liver phenotype was attenuated through decreased oxidative stress, inflammation and improved mitochondrial function [139]. Interestingly, recent studies have shown that punicalagin can induce autophagy in human cell lines [145, 146]. Hence, a recent study by Cuo and colleagues showed that punicalagin could reverse the impaired autophagy flux in hepatocytes exposed to increased glucose environment [141]. However, there are no studies in hepatocytes regarding a function of autophagy under lipotoxic conditions.

2. Aims

During NAFLD, excessive lipid loading and chronic LD accumulation are the leading causes of lipidostasis imbalance which in turn result in cellular dysfunction. Apart from high lipid amount, the source of dietary fat can significantly affect the development of steatosis. PA is the most common saturated fatty acid and is considered a risk factor of NAFLD emergence. It has widely been used to induce lipotoxicity and study the development of LDs in hepatocytes. Despite extensive research in several animal and cellular models, the exact mechanism of HFD/PA-mediated lipotoxicity in hepatocytes remains to be elucidated. The two major proteolytic systems, ubiquitin-proteasome system and autophagy-lysosome system are involved in LD degradation and control the balance of lipid homeostasis. However, the impact of lipotoxicity on their function is still debatable and defining the regulatory mechanisms of both may help to better understand the occurring events *in vivo*. This work aims to understand the impact of lipotoxicity on autophagy-lysosome system and proteasome, as part of the ubiquitin-proteasome system and investigate the molecular mechanisms which underlay the lipotoxicity in hepatocytes.

In the first part of this study, *in vivo* analysis was performed on the liver of hyperphagic New Zealand Obese mice (NZO), a polygenic model of obesity and type 2 diabetes, in order to examine the following two objectives:

- Morphological alterations in the liver of NZO mice due to obesity and HFD.
- Impact of HFD-induced lipotoxicity on the proteolytic systems.

Secondly, *in vitro* analysis was performed in order to investigate the lipotoxic mechanisms in hepatocytes and the possible involvement of the proteolytic systems. To this end, HepG2 cells exposed to PA were used as *in vitro* model. The following objectives were investigated:

- Impact of PA on LD protein content and redox status.
- Impact of PA-induced LD accumulation on the proteolytic systems.
- Role of proteasome and autophagy-lysosome system in the LD degradation under PA-induced lipotoxicity.
- Whether punicalagin, a natural autophagy inducer, is able to limit or reverse the PA-induced effects.

3. Materials and Methods

Unless otherwise stated, for the present study standard chemicals such as organic solvents, salts and acids were used from Carl Roth, Sigma-Aldrich and VWR chemicals.

3.1 Animals

- *Chemicals and equipment*

New Zealand Obese mice (NZO/HIBom Dife), C57BL/6J mice (Janvier Labs), standard diet (Ssniff, Soest; V1534-300), high fat diet (Altromin, Lage; #C105789)

- *Experimental process*

The animal experiments were performed by Dr. Richard Kehm, Dr. Christiane Ott and Stefanie Deubel. Elizabeth Mayer prepared the liver tissue slices. The experimental process was performed accordingly: male NZO and C57BL/6J mice (control group) were housed in open cages of 4–5 animals under identical conditions (12/12 h light/dark cycle, 21°C room temperature and free access to water and food). Mice were kept in agreement with the National Institutes of Health (NIH) guidelines for care and use of laboratory animals. All animal procedures were performed in accordance to the guidelines of German Law on the Protection of Animals and approved by the local authorities (Landesamt für Gesundheit und Soziales, Berlin, Germany). After weaning and feeding standard diet (SD), a number of 5 weeks old NZO mice were randomly selected and received a carbohydrate-free, high fat diet (HFD, 32.1% (wt/wt) protein and 30.6% (wt/wt) fat) for 16 more weeks (Figure 10). The three above mentioned animal groups were sacrificed at week 21 of age.

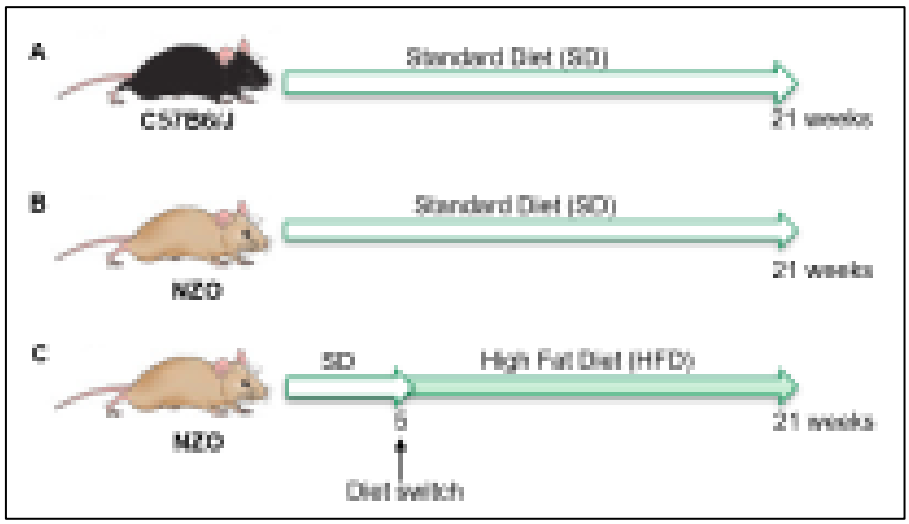

Figure 10: Experimental setup. Group of animals that were analyzed. **A.** C57BL/6J mice (n=8) and **B.** NZO mice (n=6) which received standard diet. **C.** NZO mice (n=8) mice which received high fat diet.

The liver and body weight were measured with electronic scale and liver tissue samples were either fixed in 4% paraformaldehyde for 24h with subsequent paraffin embedding or shock-frozen in liquid nitrogen and stored at −80°C for protein or mRNA isolation. For the present study, 8 liver samples from C57BL/6J-SD, 6 liver samples from NZO-SD and 8 liver samples from NZO-HFD mice were analyzed.

3.2 Free fatty acids in the liver

- *Chemicals and equipment*

NEFA-HR(2) kit (Fujifilm Wako chemicals; HP 434-91795), NEFA Standard kit (Fujifilm Wako chemicals; HP 270-77000)DC Protein Assay Lowry kit (Bio-Rad; 5000111), tissue lyser (Qiagen), autoanalyzer Cobas mira (Roche)

- *Principle of the method and experimental process*

The FFA content in liver tissues and the extracellular FFA content in HepG2 cells were determined quantitatively using NEFA-HR(2) kit. The method is based on the production of a violet-colored complex which is proportional to FFA amount and can be measured by a spectrophotometer at 546nm. The principle of the method and the reaction are summarized in Figure 11.

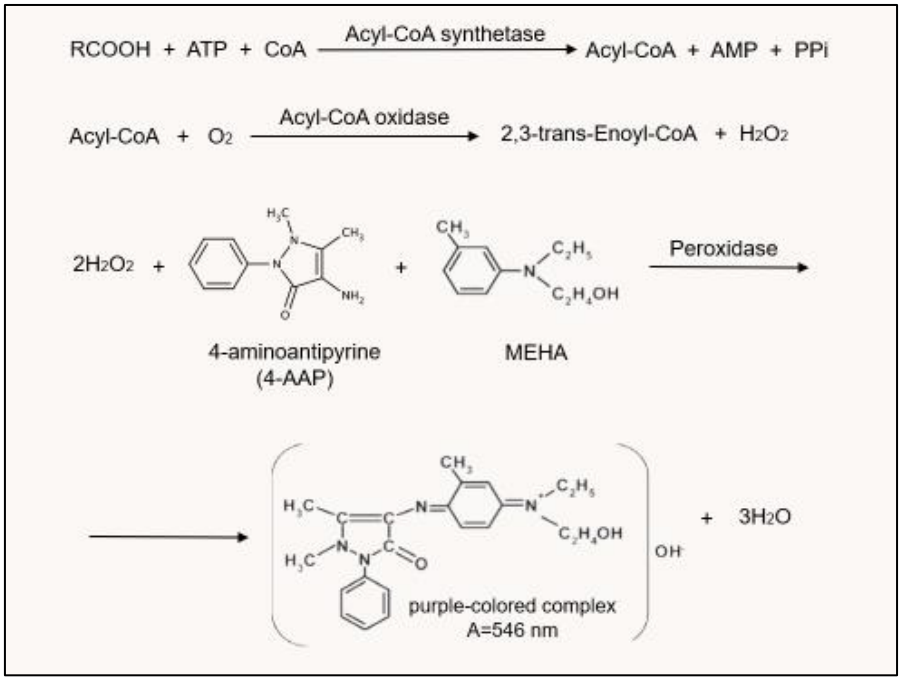

Figure 11: Determination of FFA content - principle of the method. Fatty acids are converted into a violet pigment complex (546nm) which is obtained after a series of enzymatic reactions. (CoA: coenzyme A, ATP: adenosine 5-triphosphate disodium salt, AMP: PPi: pyrophosphoric acid).

The experimental procedure was performed accordingly:

Preparation of Liver tissue extracts

20-30mg of liver tissue was lysed (20mg/400µl) with homogenization buffer (10mM $NaH_2PO_4*H_2O$, 1mM EDTA, pH 7.4, 1% Polyoxyethylene (10) tridecyl ether) and homogenized using a tissue lyser (3min, 50Hz). The lysate was subsequently centrifuged for 30min (23100g, 4°C). The supernatant was collected and shaked at 70°C (5min, 600rpm), following 5min incubation on ice and subsequently centrifugation for 30min (23100g, 4°C). The supernatant was collected and stored at -20°C, while a part was diluted 1:4 in homogenization buffer and the protein concentration was determined via Lowry protein assay as described in 3.10.1.

Supernatant collection of HepG2 cells

HepG2 cells were seeded in 24-well plates and treated with PA. After rinsing with Phosphate-buffered saline (137mM NaCl, 2.7mM KCl, 1.5 mM KH_2PO_4, 8.1mM $Na_2HPO_4*2H_2O$, pH 8.1; PBS), the supernatant was collected and stored at -20°C. A part was diluted 1:4 in PBS and the protein concentration was determined by Lowry protein assay as described in 3.10.1.

Intracellular FFA of liver tissues and extracellular FFA of HepG2 cells were measured using NEFA-HR(2) kit. The process was followed according to manufactures instruction. Briefly, 5µl of samples were mixed with 170µl Reagent 1 (containing Acyl-CoA synthetase, CoA, ATP, 4-AAP, phosphate buffer, pH 7.0 and sodium azide), 85µl Reagent 2 (containing Acyl-CoA oxidase, peroxidase and 3-Methyl-N-Ethyl-N-(β-Hydroxyethyl)-Aniline (MEHA)) and 20µl H_2O_2. The absorbance was measured at 550nm by the autoanalyzer Cobas mira. Calibration curve was developed using 0 and 1mmol/l oleic acid (provided by NEFA standard kit) and the resulting volumes were normalized to protein concentration.

3.3 Triglyceride content of the liver

- *Chemicals and equipment*

ABX Pentra Triglycerides CP kit (Horiba; A11A01640), DC Protein Assay Lowry kit (Bio-Rad; 5000111), tissue lyser (Qiagen), autoanalyzer Cobas mira (Roche)

- *Principle of the method and experimental process*

The TG content in liver tissues was quantitatively determined using ABX Pentra Triglycerides CP kit, which is an enzymatic colorimetric assay. The method is based on the production of Quinoneimine, a violet-colored substance, which is produced proportionally to

TG amount and can be measured by a spectrophotometer at 500nm. The principle of the method and the reaction are summarized in Figure 12.

The liver tissue extracts were prepared as described in 3.2 and the protein concentration was measured by Lowry protein assay (3.10.1) with dilution 1:4. The TG content was measured using the ABX Pentra Triglycerides CP kit and the process was followed according to manufacturer's instruction. Briefly, 3µl of samples were mixed with 290µl Reagent (containing PIPES free acid, NaOH, Triton X-100, Magnesium salt, p-chlorophenol, ATP, Sodium azide, Potassium ferrocyanide, 4-aminoantipyrine, lipoprotein lipase, Glycerokinase, Glycerol phosphate Oxidase and Peroxidase) and 10µl H_2O_2 and the absorbance was measured at 500nm by the autoanalyzer Cobas mira. Calibration curve was developed using 0 and 1.59mmol/l standard samples and the resulting volumes were normalized to protein concentration.

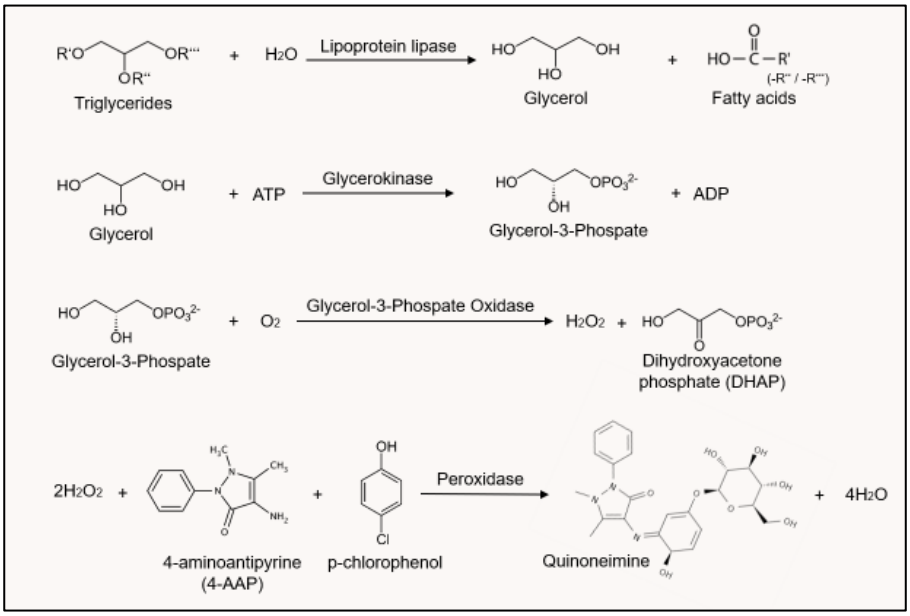

Figure 12: Determination of TG content - principle of the method. TG, after a series of enzymatic reactions, are proportionally converted into Quinoneimine and the resulting Absorption (A=500nm) is measured by a spectrometer.

3.4 Hematoxylin and eosin staining

- *Chemicals and equipment*

Roti-Histol (Carl Roth; 6640), hematoxylin solution (Sigma-Aldrich; GHS316-500ML), eosin Y solution, aqueous (Sigma-Aldrich; HT110232-1L), entellan (Merck; 1.07961.0500), MIRAX scanner (Zeiss)

- *Principle of the method and experimental process*

Histological analysis of liver samples was performed by hematoxylin and eosin staining. This method of staining is charged-based, combining hematoxylin (basophilic) and eosin (acidophilic) dyes [147]. During this procedure, nucleus and cytoplasm are stained by contrasting colors to differentiate cellular components. In particular, hematin, the oxidized form of hematoxylin, forms blue-purple colored complexes with certain metal ions, such as Fe (III) and Al (III) through salt linkages. Basophilic structures are usually those containing nucleic acids such as nucleus, endoplasmic reticulum, ribosomes and cytoplasmatic regions rich in RNA. Eosin, forms salt linkages with basic compounds, giving red-pink color. Eosin contains bromine which reacts with basic compounds such as proteins with basic amino acid residues (namely lysine and arginine). Most of the cytoplasm as well as intracellular and extracellular proteins are eosinophilic. Finally, some cellular components, such as hydrophobic fat-rich structures (LDs, adipocytes) and basal lamina are not stained allowing their clear discrimination and detection in the tissue.

The staining process was initiated by rehydrating the paraffin embedding liver sections. In particular, the slides were firstly washed twice in 100% (v/v) Roti-Histol (3min, 90rpm), following 50% (v/v) Roti-Histol (diluted in 100% (v/v) ethanol (3min, 90rpm) and twice in 100% (v/v) ethanol (3min, 90rpm). The next three washing steps are in progressively decreasing ethanolic solutions (95% (v/v), 70% (v/v) and 40% (v/v)), each step for 3min, 90rpm and finally in distilled water (3min, 90rpm). The liver slides were then stained in hematoxylin for 45s, following rinse in running tap water for 30s. The slides were then stained in eosin for 1min, following two rinses in distilled water for 10s. To achieve dehydration, the slides were washed in buffers with progressively increasing concentrations of ethanol (70% (v/v) (20s, 90rpm), 95% (v/v) (20s, 90rpm) and 100% (v/v) (2x 3min,90rpm)). The last two washing steps are in 50% (v/v) Roti-Histol (3min, 90rpm), following 100% (v/v) Roti-Histol (3min, 90rpm). Finally, the slides were fixed in entellan, dried out for 16h using MIRAX scanner. In order to evaluate the NAS score, 10 images per animal were taken. In every image the grade of steatosis, hepatocyte ballooning and lobular inflammation were evaluated according to Table 1.

The final grade for each animal was calculated by the mean of grade from the images. The proposed NAS is the summary grade of steatosis (grade: 0-3), lobular inflammation (grade: 0-3) and hepatocellular ballooning (grade: 0-2) with a categorization: "not NASH" (NAS < 3), "borderline NASH" (NAS 3-4) and "NASH" (NAS ≥ 5) [26, 27].

Table 1: NAFLD activity score (NAS)

Histological features	Description	Score
Steatosis (%)	< 5	0
	5-33	1
	33-66	2
	> 66	3
Lobular inflammation (foci per 200x field)	No	0
	< 2	1
	2-4	2
	> 4	3
Hepatocellular ballooning	No	0
	Moderate ballooning	1
	Evident ballooning	2

3.5 Immunofluorescence staining of liver sections

- *Chemicals and equipment*

Roti-Histol (Carl Roth; 6640), Antibody diluent (Dako; 50809), Normal Goat Serum (abcam; 7481), anti-perilipin-2 mouse monoclonal (R&D Systems; MAB7634), anti-LAMP1 (C54H11) rabbit monoclonal (Cell signaling; #3243), AlexaFluor 488 goat anti-rabbit (Invitrogen; A11008), AlexaFluor 594 goat anti-mouse (Invitrogen; A11032), humidified chamber (simport), FluorCare with DAPI (Carl Roth; HP20.1), confocal laser-scanning microscope (ZEISS, LSM780).

- *Principle of the method and experimental process*

Immunofluorescence is a method to visualize the localization of one or more target proteins within the same tissue sample. A protein of interest can be identified after incubation with a specific primary antibody and subsequently with a secondary antibody which is conjugated to fluorophore (indirect fluorescence, Figure 13). Incubation with secondary antibodies from different hosts and fluorophores with emission at different wavelengths, allows the detection of more than one target proteins at the same time [148].

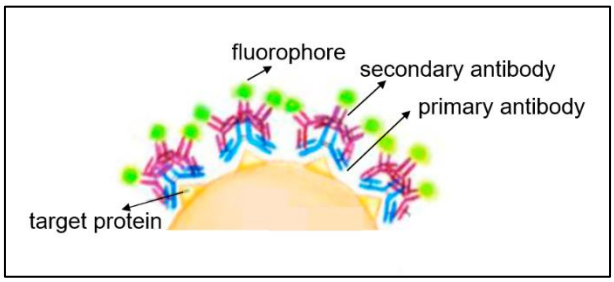

Figure 13: Principle of indirect immunofluorescence. Adapted Joshi *et al.* [142]

The process starts by deparaffinization of the paraffin-embedded tissues. The slides were firstly washed twice in 100% (v/v) Roti-Histol (3min, 90rpm), following 50% (v/v) Roti-Histol (diluted in 100% (v/v) ethanol (3min, 90rpm) and twice in 100% (v/v) ethanol (3min, 90rpm). The next three washing steps are in progressive decreased ethanolic solutions (95% (v/v), 70% (v/v) and 40% (v/v)), each step for 3min, 90rpm and finally in distilled water (3min, 90rpm). Subsequent to deparaffinization, a thermal antigen retrieval step follows, so that the formalin cross links which are formed during fixation are broken, allowing the unmasking of the antigen [149]. The antigen retrieval was performed by incubation of the slides in citrate buffer (10mM citric acid, 0.05% tween 20) for 20min at 93°C and subsequently cooling down at room temperature for 20min. The slides were then washed with PBS (3min, 90rpm) and PBS/0.05% tween 20 (PBST) (3min, 90rpm). Permeabilization step was followed, by 15min incubation of the slides to PBS/0.1% Triton X-100. Triton X-100 was used as detergent to allow antibodies to access the cellular membrane and enter the cell. After washing steps with PBS (3min, 90rpm) and PBST (3min, 90rpm) the samples were blocked with 10% Normal goat serum/antibody diluent (blocking buffer) in humidified chamber, so as to prevent unspecific binding of antibodies. The primary antibodies: anti-perilipin-2 (mouse monoclonal, 1:200) and anti-LAMP1 (rabbit monoclonal, 1:50) were diluted in blocking buffer and 50µl/slice were incubated for 1h at room temperature. After washing with PBS (3min, 90rpm) and PBST (3min, 90rpm) the samples were incubated with secondary antibodies AlexaFluor 488 anti-rabbit and AlexaFluor 594 anti-mouse), diluted 1:200 in blocking buffer. The samples were washed with PBS (3min, 90rpm) and PBST (3min, 90rpm) and embedded in FluorCare, including DAPI, allowing the nuclei visualization. 10 representative images/sample were taken by confocal laser-scanning microscope.

3.6 Cell culture

- *Chemicals*

RPMI 1640 medium (with L-glutamine, without glucose) (Corning; 10-043-CVR), glucose (Merck; 8337), Fetal Bovine Serum (FBS superior; Sigma-Aldrich; S0615), penicillin/streptomycin (Gibco; A2212), sodium PA (Sigma-Aldrich; P9767), fatty acid free bovine serum albumin (FA-free BSA; Sigma-Aldrich; A8806), ursolic acid (Sigma-Aldrich; U6753-100MG), lactacystin (LC; Enzo Life Sciences; BML-PI104-1000), Torin 1 (Cell signaling; 143795), punicalagin (Sigma-Aldrich; P0023), 3-Methyladenine (3MA; Sigma-Aldrich; M9281), Concanamycin A (ConA; Sigma-Aldrich; C9705).

- *Experimental process*

HepG2 cells were cultured at 37°C in a humidified 5% CO_2 atmosphere. RPMI 1640 growth medium (with L-glutamine, without glucose), supplemented with 5mM glucose, 10% FBS and 1% penicillin/streptomycin was used for the cell growth.

3.6.1 Media preparation with palmitate

The efficient transport of PA into the cells was achieved using fatty acid free albumin as a transporter [150]. In particular, the preparation of PA-containing media was performed as follows: sodium PA was initially dissolved in 50% (v/v) ethanol, at 70°C, to obtain 200mM final concentration. Afterwards, it was diluted in prewarmed medium, containing 1% (w/v) fatty acid free BSA, to reach a final concentration of 250 or 500μM and it was shaking for 2h at 37°C. Control cells were treated with 1% (w/v) fatty acid free BSA, containing 0.1% ethanol.

3.6.2 Regulation of proteolytic systems

Proteasome activity was manipulated using ursolic acid and lactacystin. Ursolic acid is a natural product that stimulates proteasome by opening the gate of the 20S core particle [151, 152]. By contrast, lactacystin, an irreversive proteasome inhibitor, binds to the β5 catalytic subunit of the 20S proteasome and inhibits its activity [153].

The autophagic process can be regulated by manipulating its antagonist, the mechanistic target of rapamycin (mTOR), using chemical compounds, such as Torin 1 [154]. Torin 1 is a widely used mTOR inhibitor, as it blocks the phosphorylation of both catalytic subunits mTORC1 and mTORC2 [155]. On the contrary, the autophagy inhibitor 3-methyladenine (3MA) can be used to block the autophagosome formation by inhibiting the PI3K-III, a key mTOR regulator [156]. ConA is also a specific inhibitor of V-ATPase (vacuolar type H+-ATPase) activity and it is widely used to estimate the autophagic flux [97].

The cell treatment was performed as follows: proteasome was induced by treatment for 24h with 10μM ursolic acid (20S proteasome stimulator) and inhibited for 24h with 2μM lactacystin (20S proteasome inhibitor). Autophagy was induced or inhibited by: 24h, 100nM Torin 1 (autophagy inducer via mTOR inhibition), 24h, 10μM punicalagin, 24h, 10mM 3MA (autophagy inhibitor) or 6h, 5nM ConA (lysosomal acidification blocker).

3.7 Neutral Red assay

- *Chemicals and equipment*

Neutral Red dye (Sigma-Aldrich; N6634), spectrometer (Tecan M200 Pro)

- *Principle of the method and experimental process*

The evaluation of cell viability was performed by neutral red (NR) assay. The method is based on the ability of viable cells to incorporate 3-Amino-7-dimethylamino-2-methylphenazine hydrochloride (neutral red dye) and its uptake depends on the cell capacity to maintain pH gradients. At physiological pH, this weakly cationic substance presents a net charge close to zero, enabling it to penetrate the cell membranes via passive diffusion. Inside the lysosomes, there is a proton gradient to maintain a pH lower than that of the cytoplasm. Thus, inside the lysosomes, the dye is retained as it becomes charged and it binds by electrostatic hydrophobic bonds to phosphate and anionic groups of the lysosomal matrix. Using an acidified ethanol solution, the dye is then extracted from viable cells, and the absorbance is quantified using a spectrophotometer. As cells become apoptotic or necrotic, their ability to incorporate neutral red diminishes. Thus, loss of neutral red uptake is correlated with loss of cell viability [157].

The evaluation of cell viability was performed accordingly: HepG2 cells were seeded in 24-well plate and subsequently treated with 250μM and 500μM PA for 24-72h. The cells were subsequently incubated for 1h at 37^{o}C with 0.057mM NR dye, which was diluted in growth media. After rinsing the cells with PBS, the dye was extracted by shaking for 15min with solubilization buffer (50% ethanol, 1% acetic acid). The absorbance was finally measured at 540nm on a spectrometer.

3.8 Oil Red-O staining

- *Chemicals and equipment*

24-well plate (black with clear film bottom (Eppendorf; 30741005), 4% v/v paraformaldehyde (PFA; neoLab; LC-6470.5), Oil Red-O (Sigma-Aldrich; O0625), DAPI (Roth, 6335.1), spectrometer (Tecan M200 Pro), glass bottom dishes (Mattek; P35GC-1.0-14-C), confocal laser-scanning microscope (ZEISS, LSM780)

- *Principle of the method and experimental process*

The neutral intracellular lipids were detected and analyzed by Oil Red-O staining. The method is based on the lysochrome, fat soluble diazol dye Oil Red-O ($C_{26}H_{24}N_4O$), which stains cholesteryl esters and neutral lipids but not biological membranes. The dye is hydrophobic and displays greater solubility in lipophilic substances than in the hydroalcoholic solvent (isopropanol) [158]. After staining neutral lipids, the dye is extracted from the cells, using DMSO, and the absorbance is quantified using a spectrophotometer. DAPI (4′,6-diamidino-2-phenylindole) was used to normalize the Oil Red-O values as it exhibits high affinity for DNA and therefore the number of cells per well can be estimated. More specifically, DAPI binds to adenine-thymine regions of double strand DNA and emits blue fluorescence.

The experimental procedure of Oil Red-O/DAPI staining was performed as follows: HepG2 cells were firstly seeded in 24-well plate (black with clear film bottom) and treated with PA. They were subsequently rinsed with PBS and fixed for 30min with 4% PFA. The cells were afterwards washed with PBS and stained for 30min with 0.3% w/v Oil Red-O (diluted in 60% v/v isopropanol). After rinsing the cells with water, they were incubated for 15min with 300nM DAPI and finally rinsed twice with water. The fluorescent signal of DAPI was recorded at 360/460nm by spectrometer. Afterwards, samples were lysed in DMSO and absorbance of the extracted Oil Red-O dye was measured at 520nm. The intracellular lipid content was calculated by normalizing the Oil Red-O staining to DAPI staining values. Additionally, cells were also seeded in glass bottom dishes and stained with Oil Red-O dye to obtain representative images by confocal laser-scanning microscope.

3.9 Gene expression analysis

The amount of an expressed gene can be measured by detecting and quantifying the number of copies of the gene's RNA transcripts. The process contains the following steps: a) RNA extraction from liver tissues or cells (3.9.1) b) reverse-transcription of RNA to complementary DNA (cDNA) (3.9.2) and c) amplification and detection of the cDNA using qPCR (3.9.3) [159].

3.9.1 mRNA extraction from liver tissues and HepG2 cells

- *Chemicals and equipment*

Dynabeads mRNA Direkt kit (Life Technologies; 61012), tissue lyser (Qiagen), NanoDrop spectrometer (Thermo Scientific 2000c), gauge needles and syringes (Braun)

- *Principle of the method and experimental process*

The mRNA isolation was performed using Dynabeads mRNA Direkt kit. The method is based on the oligo-Thymine ($(dT)_{25}$) residues which are covalently conjugated to magnetic beads. Thus, the poly-adenine residues at the 3'-end of most mRNA bind to magnetic beads, allowing hybridization and finally isolation of mRNA from the lysate of tissues or cells.

The experimental procedure was performed as follows:

Preparation of liver tissue extracts

Liver tissue (up to 5mg) was homogenized (2min, 30Hz) with 200µl Lysis/Binding buffer using a tissue lyser. The lysate was subsequently forced through a syringe with gauge needle in order to shear the DNA.

Lysis of HepG2 cells

HepG2 cells were seeded in 12-well plates and treated with PA. After rinsing with PBS, the cells were lysed and collected with 200µl Lysis/Binding buffer and DNA fragmentation was achieved using syringe with gauge needle.

After centrifugation at room temperature (14,000 rpm, 2min), the lysates were incubated with Dynabeads and rotated at room temperature. The vials were subsequently placed on a magnet and the supernatant was collected. After several centrifugation and washing steps according to manufacturer's instructions, the mRNA was eluted with 10mM Tris HCl (Elution Buffer). The concentration was measured by nanodrop and the RNA was stored at -80^{o}C.

3.9.2 mRNA transcription to cDNA

- *Chemicals and equipment*

SensiFast cDNA Synthesis Kit (Bioline; Bio-65054), thermal cycler (Biometra)

- *Experimental process*

The transcription of mRNA into cDNA was performed using SensiFast cDNA Synthesis Kit. For the reaction, 75-100 ng of mRNA were incubated with reverse transcriptase, 5x TransAmp Buffer (which contains random hexamer primers, RNase inhibitors and dNTPs) and RNase-free water, reaching 20µl final volume. The reaction was performed by thermal cycler under the following cycle conditions: a) primer annealing: 25°C, 10min, b) reverse

transcription: 42°C, 15min, c) inactivation: 85°C, 5min, d) hold: 4°C. The samples were diluted 1:10 in RNase-free water and stored at -20°C.

3.9.3 cDNA amplification by qPCR

- *Chemicals and equipment*

Dream-Taq-Hot Start-DNA Polymerase and DreamTaq Buffer 10x (including 20mM $MgCl_2$) (Thermo Fisher Scientific; EP1703), dNTPs (Bioline; #BIO-39028), 1x SYBR Green (Life Sciences; S7563), PCR System Stratagene Mx3005P (Agilent), MxPro qPCR Software (Agilent Technologies, Santa Clara, USA; v. 4.10)

- *Principle of the method and experimental process*

Quantitative real time-PCR (qPCR) was performed using SYBR Green as fluorescent reporter. SYBR Green binds to double-stranded DNA and emits a fluorescent signal proportional to the amount of produced DNA after each PCR cycle. Unbound SYBR Green has low fluorescence (background signal). The relative mRNA expression (number of copies of RNA transcripts), can be calculated through the threshold cycle (C_t) value which is defined as the cycle number when the fluorescence is detected above the background signal [160, 161].

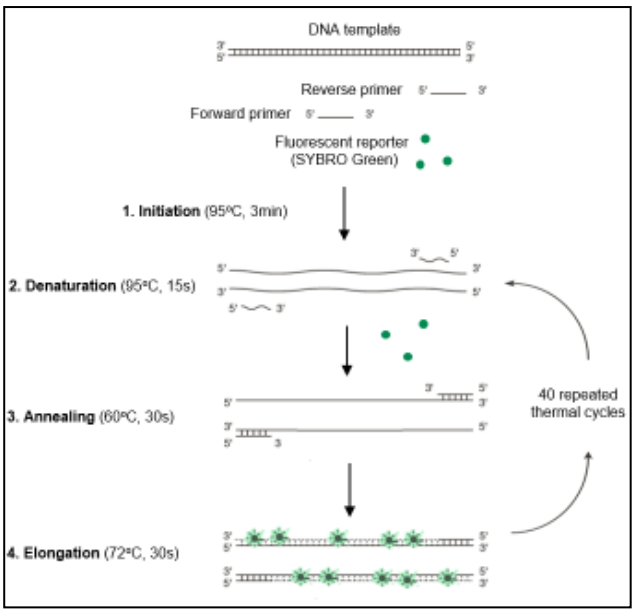

Figure 14: qPCR reaction with SYBR Green and experimental cycle conditions. (adapted Bonetta *et al*. [149])

For the qPCR reaction, 1µl cDNA template was mixed with 2.5µl 10x DreamTaq Buffer and 0.13µl Dream-Taq Hot Start-DNA-Polymerase, 2mM dNTPs, 1x SYBR Green and 1µM forward and reverse primer, reaching final volume 25µl per reaction. The cycle conditions are depicted in Figure 14. The gene expression was detected using the PCR System Stratagene Mx3005P and quantified via standard curves of amplified primer-specific cDNA (10^4, 10^5, 10^6, 10^7, 10^8 copies).

All gene expression data were normalized to the average of Ct values of housekeeping genes: Hypoxanthine phosphoribosyl transferase (*Hprt*), β-actin (*Actb*), Glyceraldehyde-3-phosphate dehydrogenase (*Gapdh*) and ribosomal protein L13α (*Rpl13a*) [162]. *Hprt*, *Actb* and *Gapdh*

were used for data normalization from C57BL/6J mice, *Hprt* and *Rpl13a* from NZO mice, *Actb* and *Rpl13a* from HepG2. The primers which were used are depicted in Table 2.

Table 2: List of primers used in qPCR analysis of liver tissues and HepG2 cells

Gene target	Host	Primer sequence
Actb	Mus musculus	fwd 5'-CACTGCCGCATCCTCTTCCT-3'
		rev 5'-GATTCCATACCCAAGAAGGAAGGC-3'
Rpl13a	Mus musculus	fwd 5'-GTTCGGCTGAAGCCTACCAG-3'
		Rev 5'-TTCCGTAACCTCAAGATCTGCT-3'
Hprt	Mus musculus	fwd 5'- GCAGTCCCAGCGTCGTG-3'
		rev 5'- GGCCTCCCATCTCCTTCAT-3'
Gapdh	Mus musculus	fwd 5'- GGGTGTGAACCACGAGAAAT-3'
		rev 5'- GTCTTCTGGGTGGCAGTGAT-3'
Plin5	Mus musculus	fwd 5'- GACTGAGGCTGAGCTAGCAG-3'
		rev 5'- GACCCCAGACGCACAAAGTA-3'
Plin2	Mus musculus	fwd 5'- CTCCACTCCACTGTCCACCT-3'
		rev 5'- GCTTATCCTGAGCACCCTGA-3'
Sqstm1 (p62)	Mus musculus	fwd 5'- AGATGCCAGAATCGGAAGGG-3'
		rev 5'- GAGAGGGACTCAATCAGCCG-3'
Map1lc3 (LC3)	Mus musculus	fwd 5'- GACCAGCACCCCAGTAAGAT-3'
		rev 5'- TGGGACCAGAAACTTGGTCT-3'
Actb	Homo sapiens	fwd 5'-CAAGAGATGGCCACGGCTGCT-3'
		rev 5'-TCCTTCTGCATCCTGTCGGCA-3'
Rpl13a	Homo sapiens	fwd 5'- AGCCTACAAGAAAGTTTGCCTATCTG-3'
		rev 5'- TAGTGGATCTTGGCTTTCTCTTTCCT-3'
Cidea	Homo sapiens	fwd 5-GACTCAAGGGCCTGCTGA-3'
		rev 5'-GAGAAACTGTCCCGTCACCT-3'
Plin5	Homo sapiens	fwd 5'- GGGAGTCTCAGTGATGGTCTG-3'
		rev 5'- TATGACTCCATGGCGGAACT-3'
Plin2	Homo sapiens	fwd 5'-TCAGCTCATTCTACTGTTCACC-3'
		rev 5'-CCTGAATTTTCTGATTGGCACT-3'
Sqstm1 (p62)	Homo sapiens	fwd 5'-AGCTGCCTTGTACCCACATC-3'
		rev 5'-CAGAGAAGCCCATGGACAG-3'
Maplc3 (LC3)	Homo sapiens	fwd 5'- CTGTGGACCCAGCCGAC-3'
		rev 5'- CCCTTGTAGCGCTCGATGAT-3'

3.10 Determination of protein concentration

The protein concentration of lysates or supernatants was determined by Lowry or Bradford protein assay. Both methods are colorimetric with high sensitivity. The method was chosen dependently on the content of dilution buffers, as in Bradford method basic conditions and detergents such as SDS and Triton X-100 interferes with the reaction, leading to precipitation of reagents, while in Lowry method, acids, phenols and dithiothreitol (DTT) interfere with chromophore production [163]. The principle of the methods and the experimental procedures are described on the following paragraphs.

3.10.1 Lowry protein assay

- *Chemicals and equipment*

DC Protein Assay Lowry kit (Bio-Rad; 5000111), spectrometer (Tecan M200 Pro)

- *Principle of the method and experimental process*

The process for protein determination by Lowry assay contains two steps which lead to blue color development [164]. Firstly, the reaction of proteins with copper under alkaline conditions. The resulting monovalent copper ion subsequently reacts with Eolin reagent, leading to its reduced form which is a blue colored substance. The color development is primarily due to the amino acids: tryptophan and tyrosine and the absorbance can be measured through a spectrophotometer at 750nm.

The experimental procedure was performed using the DC Protein Assay Lowry kit. Briefly, 5µl of sample was added into a 96-well plate and incubated with 25µl Reagent S (surfactant solution, which was diluted 1:50 with Reagent A - alkaline copper tartrate solution) and 200µl Reagent B (Eolin reagent). After shaking (100rpm) for 15 min, at room temperature, the absorbance was measured at 750nm by spectrometer. BSA standards (0, 0.2, 0.4, 0.6, 0.8, 1, 1.2, 1.4 mg/ml) were also measured in order to develop calibration curve.

3.10.2 Bradford protein assay

- *Chemicals and equipment*

Bio-Rad protein assay dye reagent (Bio-Rad; 5000006), spectrometer (Tecan M200 Pro)

- *Principle of the method and experimental process*

The determination of protein concentration by Bradford method was performed using Bio-Rad protein assay [165]. The process contains the Coomassie Brilliant Blue G-250 dye which exists in three forms: cationic (doubly protonated form, red/brown), neutral (green) and anionic (unprotonated form, blue). Under acidic conditions, the protonated (red) dye binds to proteins, through electrostatic interactions with the amino acid groups of proteins and Van der Waals forces with the carboxyl groups of the proteins. The resulting blue-colored complex is due to the stably bound Coomassie G-250 which is in unprotonated form (blue). This leads to change in absorbance from 465nm to 595nm which is proportional to protein amount and can be measured by a spectrophotometer.

The experimental procedure was performed accordingly: 4µl of sample was added into a 96-well plate and incubated with 200µl Bio-Rad dye reagent (acidified solution of Coomassie G-250). After 5 min incubation at room temperature, the absorbance was measured at 590nm by spectrometer. BSA standards (0, 0.2, 0.4, 0.6, 0.8, 1, 1.2, 1.4 mg/ml) were also measured in order to develop calibration curve.

3.11 Protein analysis by immunoblot

The detection of target proteins was mediated by protein immunoblot analysis. According to this process, proteins were extracted from liver tissues or HepG2 cells and the concentration was determined by Lowry protein assay (3.10.1). Proteins were subsequently separated according to their molecular weight by Sodium dodecyl sulfate (SDS) polyacrylamide gel electrophoresis (SDS-PAGE) (3.11.1, 3.11.2). The proteins were finally transferred to nitrocellulose membrane by electroblotting (semi-dry blotting) and detected by indirect fluorescence through Odyssey imaging system (3.11.3).

3.11.1 SDS-PAGE gel electrophoresis under reducing sample conditions

- *Chemicals and equipment*

cOmplete Protease Inhibitor Cocktail Tablets (Roche Life Science; 11697498001), tissue lyser (Qiagen), ultrasonic device (Hielscher; UP100H), Chameleon Duo Pre-

stained Protein Ladder (LI-COR Biosciences GmbH; 928-60000), Mini-Protean Electrophoresis system (Bio-Rad), PowerPac Basic power supply (Bio-Rad)

- *Principle of the method and experimental process*

SDS-PAGE is a method where proteins, in denatured state can be separated according to their molecular weight. Proteins are initially treated with strong reducing agents (SDS, β-mercaptoethanol, DTT, heating) so as to remove their secondary and tertiary structure, allowing the polypeptide separation in polyacrylamide gel. Apart from partial protein denaturation that SDS is used for, SDS also binds to proteins through hydrophobic interactions, imparting a uniform net negative charge.

The samples are next loaded into the wells of polyacrylamide gel. As proteins are negatively charged covered, when voltage is applied, they migrate towards the positively charged (higher voltage) anode through the acrylamide pores of the gel. Smaller proteins migrate faster through the pores, allowing the separation according to their size. A polyacrylamide gel is composed of two gels with different pH and pore size in order to improve the protein resolution (stacking gel and separating/running gel). The stacking gel has greater pore size and lower pH and it is used to stack the proteins on a narrow area, allowing higher resolution of the proteins as they enter to the separating gel.

The protein extraction was performed as follows:

Preparation of liver tissue extracts

Liver tissue was lysed (5mg/100µl) with lysis buffer (10mM Tris HCl pH 7.5, 0.9% NP-40, 0.1% SDS and 1mM Pefablock), containing protease inhibitor cocktail. Homogenization was performed using a tissue lyser (2min, 30Hz, 2x). The lysate was subsequently centrifuged for 15min (13,000rpm, 4^{o}C) and the supernatant was collected and stored at -80^{o}C for further analysis.

Lysis of HepG2 cells

HepG2 cells were seeded in 24-well plate and treated with PA. After rinsing with PBS, the cells were lysed and collected with 100µl lysis buffer. Ultrasonic lysis was performed on ice at 80% amplitude, 0.5 cycle, 10 times/sample and the lysates were stored at -80^{o}C for further analysis.

A part of the lysates was diluted 1:10 (lysate from liver tissues) or 1:4 (cell lysate) in lysis buffer for determination of protein concentration via Lowry assay (3.10.1). Protein extracts

were subsequently diluted in reducing Laemmli buffer 4x (0.25M Tris pH 6.8, 8% SDS, 40% Glycerol, 0.03% Bromophenol blue, 8% β-mercaptoethanol) and boiled at 95°C for 5min. The protein separation was performed on 5% stacking gel and either 10% or 15% separating gel, depending on the molecular weight of the target protein. The consistence of gels is depicted in Table 3. 20 μg proteins/lane was loaded in each well, electrophoresis buffer (50 mM Tris, pH 8.5, 0.38 M glycine, 0.1% SDS) was filled in the tank of the electrophoresis system and 100V was applied by power supply. Protein marker was also loaded for the estimation of the protein's molecular weight in the sample.

Table 3: Composition of gels for SDS-PAGE.

Stacking gel		**Separating gel**		
components	**5%**	**components**	**10%**	**15%**
dH_2O (ml)	5.4	dH_2O (ml)	7.92	4:6
1.5M Tris pH 6.8 (ml)	1	1.5M Tris pH 8.8 (ml)	5	5
30% Acryl/Bis (ml)	1.34	30% Acryl/Bis (ml)	6.68	10
SDS (μl)	80	SDS (μl)	200	200
10% APS (μl)	80	10% APS (μl)	200	200
TEMED (μl)	8	TEMED (μl)	8	8

3.11.2 SDS-PAGE gel electrophoresis under non-reducing conditions for prx detection

- *Chemicals*

Catalase (Sigma-Aldrich; C9322-5G), cOmplete Protease Inhibitor Cocktail Tablets (Roche Life Science; 11697498001),

- *Principle of the method and experimental process*

The redox state of cellular compartments in HepG2 cells was measured by determination of the oxidation and dimerization levels of compartment-specific prxs. As prxs are H_2O_2 scavengers, during their catalytic cycle the cysteine residues are oxidized in presence of H_2O_2, forming intermolecular disulfide bonds. During electrophoresis, the oxidized protein is running as a dimer under non-reducing conditions, allowing the separation from the non-oxidized (reduced) form which is monomer (Figure 15) [36]. The principle of the method is to trap the oxidized and reduced forms during protein extraction from the cells and monitor the proportions of monomer and dimer.

A critical step during sample preparation is the rapid alkylation of reduced cysteines so as to prevent artefactual oxidation of prxs. Thus, high concentration of N-ethylmaleimide (NEM) is used in washing buffer/lysis buffer for alkylation of reduced thiols in prx monomers. Catalase is also included in washing buffer so as to limit the H_2O_2 levels. The samples were prepared under non-reducing conditions in order to preserve the disulfide bonds of dimers. Therefore, β-mercaptoethanol or DTT were not included into the Laemmli buffer and the samples were not boiled before loading on the gel for electrophoresis.

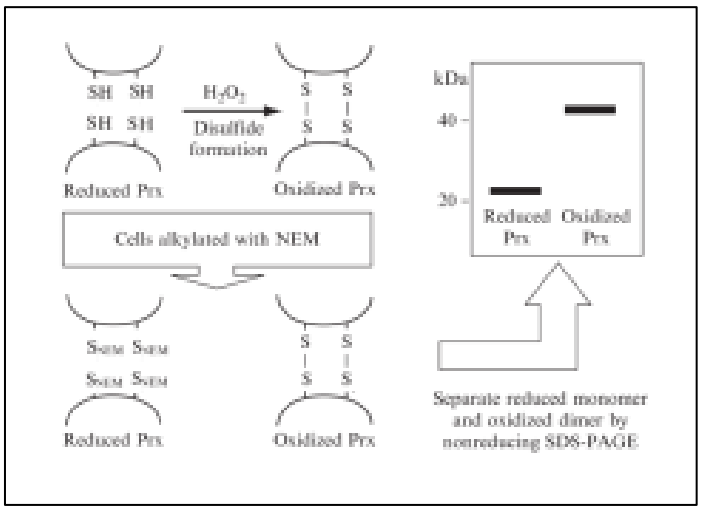

Figure 15: Immunoblot method under non-reducing conditions to detect prx oxidation. The method involves the alkylation of reduced thiols on prxs (monomers) with NEM and subsequently, their electrophoretic separation from the oxidized dimers under non-reducing conditions [37].

The experimental procedure was performed as follows: after PA treatment, the cells were washed twice with ice-cold alkylation buffer (100mM Na_3PO_4, 0.1mM diethylenetriaminepentaacetic acid (DTPA) pH 7.4, 10μg/ml catalase and 100mM NEM, protease inhibitors (1:100)). Catalase was added 30min prior to use and NEM immediately prior to use), lysed with lysis buffer (alkylation buffer, 0.1% SDS) and incubated at room temperature for 1h. The protein content was measured by DC Protein Assay Lowry as described on 3.10.1. The protein extracts were diluted in 4x non-reducing buffer (0.25M Tris, pH 6.8, 40% glycerol, 8% SDS, and 0.03% bromophenol blue), resolved by SDS-PAGE electrophoresis in 15% gels and transferred to a nitrocellulose membrane as described in 3.11.1 and 3.11.3.

3.11.3 Electrophoretic transfer of proteins to a membrane and immunostaining

- *Chemicals and equipment*

0.42µm or 0.2µm pore size nitrocellulose membranes (Whatman®, GE Healthcare, Dassel, Germany), Ponceau S (Sigma-Aldrich; P71170-11), Odyssey® Blocking Buffer (LI-COR Biosciences, No. 927-70001), secondary antibodies: IRDye®800CW Goat anti-Rabbit IgG (LI-COR Biosciences; 925-32211), IRDye 680LT Goat anti-Rabbit IgG (LI-COR Biosciences; 926-68021), IRDye 800CW Goat anti-Mouse IgG (LI-COR Biosciences; 926-32210), IRDye 680LT Goat anti-Mouse IgG (LI-COR Biosciences; 926-68020), TransBlot Turbo Transfer System (Bio-Rad), Image Lab software version 5.2.1 (Bio-Rad), Odyssey® imaging system (LI-COR image studio version 5.2, Bad Homburg, Germany)

- *Principle of the method and experimental process*

The transfer of the separated proteins was performed by semi-dry blotting. During that process, the negatively charged proteins migrate from cathode to anode and through polar and ionic interactions they are transferred into the nitrocellulose membrane (Figure 16). To confirm the uniformity of protein transfer and for normalization of target protein in the end, staining of total proteins was mediated through Ponceau S. This dye is negatively charged and reversibly binds to positively charged groups of amino acids and to non-polar regions of proteins, giving a red color to the protein bands of the blot membrane. To visualize the protein of interest on the membrane, the immunostaining procedure was performed after incubation with specific primary antibody and subsequently with secondary antibody, conjugated to infrared fluorophore (indirect fluorescence). Blots were visualized by LI-COR imaging system which includes two separate lasers and detectors. Thus, incubation with secondary antibodies, originated from different host animals and conjugated to fluorophores with different emission wavelengths, allow the simultaneous detection of two target proteins on the same membrane.

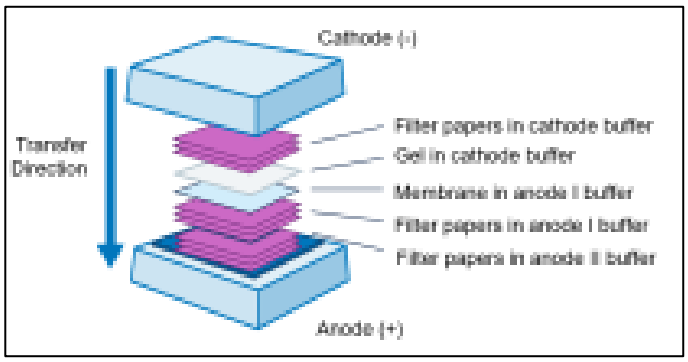

Figure 16: Semi-dry blotting.

The experimental procedure was performed as follows: subsequent to the electrophoretic separation, proteins were transferred to 0.42µm nitrocellulose membranes (0.2µm for

detection of proteins with low molecular weight, such as LC3I/II) by semi-dry blotting. In particular, as depicted in Figure 16, 3 papers soaked in Anode buffer II (20% methanol, 30mM Tris base, pH 10-11) were placed on blotting apparatus, following 3 papers soaked in Anode buffer I (20% methanol, 300mM Tris base, pH 10-11). The membrane was also incubated in Anode I buffer and placed on top of the papers. Finally, the gel and 3 papers were positioned, both soaked in Cathode buffer (40mM 6-aminocapronic acid, 20% methanol, 25mM Tris base, pH 9-10) and proteins were transferred at 25V for 30min, via TransBlot Turbo Transfer System. The membrane was stained by Ponceau S and the protein lanes were scanned and quantified by Image Lab version 5.2.1. Blocking was performed using Odyssey Blocking Buffer diluted 1:2 in PBS for 1h at room temperature, followed by incubation of primary antibodies overnight at 4°C (Table 4).

Table 4: Primary antibodies used for immunoblot

Target protein	Specificity/host	Dilution	Company
Atg4B	rabbit monoclonal	1:1000	cell signaling; #13507
Atg5, Atg5/Atg12	mouse monoclonal	1:1000	nanotools; #0262
Beclin-1	rabbit polyclonal	1:1000	cell signaling; #3738S
eIF2α	rabbit polyclonal	1:1000	cell signaling; #9722S
GAPDH [6C5]	mouse monoclonal	1:20000	abcam; ab8245
GAPDH	rabbit polyclonal	1:2500	abcam; ab37168
IRE1α (14C10)	rabbit monoclonal	1:1000	cell signaling; #3294S
LAMP1 (C54H11)	rabbit monoclonal	1:1000	cell signaling; #3243
LC3A/B (D3U4C)	rabbit monoclonal	1:1000	cell signaling; #12741S
p62	mouse monoclonal	1:5000	abcam; ab56416
p-Atg4B (Ser383)	rabbit polyclonal	1:1000	cell signaling; #19386
p-eIF2α (Ser51)	rabbit polyclonal	1:1000	cell signaling; #9721S
p-IRE1α (S724)	rabbit polyclonal	1:1000	NB100-2323JF646
plin2	mouse monoclonal	1:2500	R&D Systems; MAB7634
prx2	mouse monoclonal	1:2500	abcam; ab50862
prx3	rabbit polyclonal	1:4000	Sigma-Aldrich; P1247
prx4	mouse monoclonal	1:1000	abcam; ab68344
Rpt6	mouse monoclonal	1:1000	Enzo; BML-PW9265
α4	mouse monoclonal	1:1000	Enzo; PW8120
β1	rabbit polyclonal	1:1000	santa cruz; sc-67345
β5	rabbit polyclonal	1:1000	abcam: ab3330

The membranes were next probed with fluorescent-labeled secondary antibodies. Both primary and secondary antibodies were diluted in Odyssey Blocking Buffer/PBS (1:2), containing 0.1% Tween 20. Detection and quantification of immunoblots were performed in a linear range with the Odyssey imaging system. The proteins which were extracted from liver tissues were normalized to total protein amount *via* Ponceau S staining, while the proteins from HepG2 cells were normalized to the housekeeping protein GAPDH.

3.12 Enzymatic activity of proteolytic systems

The proteasome and cathepsin activity were determined by measuring the amount of released fluorescent peptide AMC (7-amino-4-methylcoumarin) after applying specific AMC-tagged peptide substrate to the lysates. The process includes protein extraction from liver tissues or HepG2 cells and determination of concentration by Bradford protein assay (3.10.2) and subsequent measurement of enzymatic activity (3.12.1, 3.12.2).

3.12.1 Proteasomal activity

- *Chemicals and equipment*

Tissue lyser (Qiagen), ultrasonic device (Hielscher; UP100H), spectrometer (Tecan M200 Pro), Suc-LLVY-AMC (Enzo Life Sciences; BML-P802-0005), Concanamycin A (ConA; Sigma-Aldrich; C9705)

- *Principle of the method and experimental process*

The chymotrypsin-like activity of 20S and 26S proteasome was measured after incubating the substrate succinyl-Leu-Leu-Val-Tyr-AMC (Suc-LLVY-AMC) with the protein extract. Since ATP is essential for the 26S proteasome activity, it was additionally added to the reaction buffer. On the contrary, in order to measure the activity of 20S proteasome, ATP was depleted after including deoxyglucose and hexokinase on the reaction buffer. The resulting fluorescence from cleavage and release of AMC, was recorded by spectrometer and the experimental procedure was performed as follows:

<u>Preparation of liver tissue extracts</u>

Liver tissue was lysed (10mg/150µl) with lysis buffer (25mM HEPES, 250mM sucrose, 20mM $MgCl_2$, 1mM EDTA, pH 7.4, supplemented with 1.6mM DTT) and homogenized using a tissue lyser (2min, 30Hz). The lysates were subsequently centrifuged for 15min

(13,000rpm, 4°C) and the supernatant was collected for determination of protein concentration by Bradford assay (3.10.2) and enzymatic activity measurement.

Lysis of HepG2 cells

HepG2 cells were seeded in 6-well plate and treated with PA. After rinsing three times with ice-cold PBS, the cells were collected with 100µl lysis buffer and lysed by three freeze-thaw cycles. The lysates were centrifuged for 15min (13,000rpm, 4°C) and the supernatant was collected for determination of protein concentration by Bradford assay (3.10.2) and subsequent measurement of enzymatic activity.

The proteasomal chymotrypsin-like activity was measured by determining the cleavage rate of the fluorogenic peptide suc-LLVY-AMC. After measuring the protein content of supernatants, samples were diluted to a concentration of 1µg/µl. 10 µl (10 µg) of sample was placed into a black 96-well plate and incubated with 100µl of reaction buffer (150mM Tris, 30mM KCl, 7.5mM MgOAc, 10mM $MgCl_2$, containing either 100µM ATP for measuring the 26S activity, or 15mM deoxyglucose and 0.1mg/ml hexokinase for ATP depletion and measuring the 20S activity). The reaction was started by addition of 10µl suc-LLVY-AMC diluted in DMSO. AMC liberation was measured with a spectrometer (360/485nm) and monitored every 15min for 2 h at 37°C. The chymotrypsin-like activity was determined as the increase in AMC fluorescence and calculated using free AMC standards (0, 0.5, 1, 2, 5, 10µM) in order to develop calibration curve. 2µM LC was also added as negative control.

3.12.2 Lysosomal cysteine cathepsins activity

- *Chemicals and equipment*

Tissue lyser (Qiagen), ultrasonic device (Hielscher; UP100H), fluorogenic peptide Z-Phe-Arg-AMC (Enzo Life Sciences; BML-P139), Concanamycin A (ConA; Sigma-Aldrich; C9705), spectrometer (Tecan M200 Pro)

- *Principle of the method and experimental process*

Cysteine cathepsins activity was measured by applying the fluorogenic peptide Benzyloxycarbonyl-Phe-Arg-AMC on the protein extract, which is the substrate of most cathepsins (cathepsins B, C/DPP-I, F, K/O2, L, L2/V, O, S, and X/Z). The resulting fluorescence from cleavage and release of AMC, was recorded by spectrometer.

The experimental procedure was performed accordingly: liver tissue was lysed (10mg/150µl) with 1mM DTT and homogenized using a tissue lyser (2min, 30Hz). HepG2 cells were seeded in 6-well plate and treated with PA. After rinsing with PBS, the cells were lysed and collected with 150µl, 1mM DTT. Tissue and cell lysates were subsequently shaken in a thermomixer for 1 h, 1000rpm at 4°C, sonicated on ice at 80% amplitude, 0.5 cycle, 10 times/sample, and subsequently centrifuged for 30min (13,000rpm, 4°C). The supernatant was collected for determination of protein concentration by Bradford assay (as described in 3.11.1.1) and all samples were diluted to a concentration of 0.25µg/µl. 10 µl (2.5 µg) of sample (triplicates) were placed into a black 96-well plate and incubated with 100µl reaction buffer (150 mM Na-acetate, 24 mM cysteine∗HCl, and 3 mM EDTA dihydrate, pH 4.0) for 10min. The reaction was started by addition of 10µl fluorogenic peptide Z-Phe-Arg-AMC at 166µM final concentration. AMC liberation was measured with a fluorescence plate reader (360/460nm) and monitored every 15min for 2 h at 37°C. The activity of cysteine cathepsins was determined as the rate of AMC fluorescence increase and calculated from standards of free AMC (0, 0.5, 1, 2, 5, 10µM) in order to develop calibration curve. 2µM ConA was also added into some wells as negative control.

3.13 Statistical analysis

Statistical analysis, of at least 3 biological replicates, was performed using GraphPad Prism (GraphPad Software, San Diego, USA; v. 8.0.0). Differences between groups were assessed by one-way ANOVA followed by Tukey's post-hoc test, unpaired t-test, Mann–Whitney test or one sample t-test (using a hypothetical value of 1). Shapiro–Wilk test was used for testing the Gaussian distribution. Statistical significance was considered and indicated at $p < 0.05$ and results are presented as mean values ± standard deviation.

4. Results

In order to get a first impression regarding the impact of HFD on the proteolytic systems, a first *in vivo* screening was performed by analyzing the liver of C57BL/6J and NZO mice (4.1). The next aim was to investigate the mechanism of LD-mediated cellular dysfunction and the role of proteolytic systems, on cellular level (4.2). Finally, in the third part of the thesis, a reversion of the LD-induced effects was addressed, by stimulating the autophagic system through punicalagin (4.3).

4.1 Impact of high fat diet on the liver of NZO-obese mice – *in vivo* analysis

The mouse liver samples were provided by Dr. Richard Kehm and Dr. Christiane Ott. Liver slices of C57BL/6J and NZO mice were analyzed and compared according to two parameters: 1. strain (comparison of C57BL/6J and NZO mice on SD) and 2. diet (comparison of NZO mice on SD and HFD).

4.1.1 Effects of strain and diet on liver's morphology

Body and liver weight were measured as depicted in Figure 17. NZO mice have significantly increased body and liver weight in comparison to C57BL/6J mice. Both, body and liver weight were distinctly higher in NZO mice on HFD, reaching almost the double weight in comparison to NZO SD.

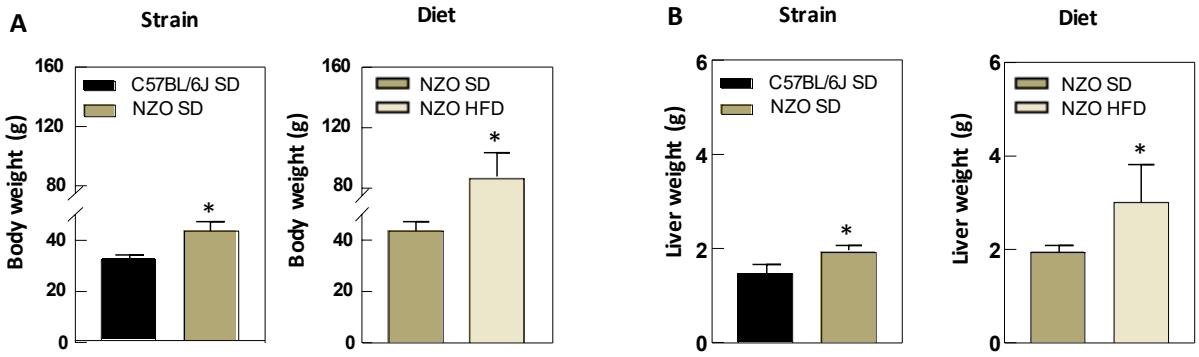

Figure 17: Body and liver weight of C57BL/6J SD, NZO SD and NZO HFD mice. Statistical significance was given by unpaired t-test at *p < 0.05. C57BL/6J SD n=8, NZO SD n=6, NZO HFD n=8.

TG and FFA content in the liver was next measured (Figure 18). The TG content was significantly lower in NZO vs C57BL/6J mice on SD. However, TGs were substantially higher in NZO mice due to HFD. On the contrary, the amount of FFA were not significantly altered by strain and diet.

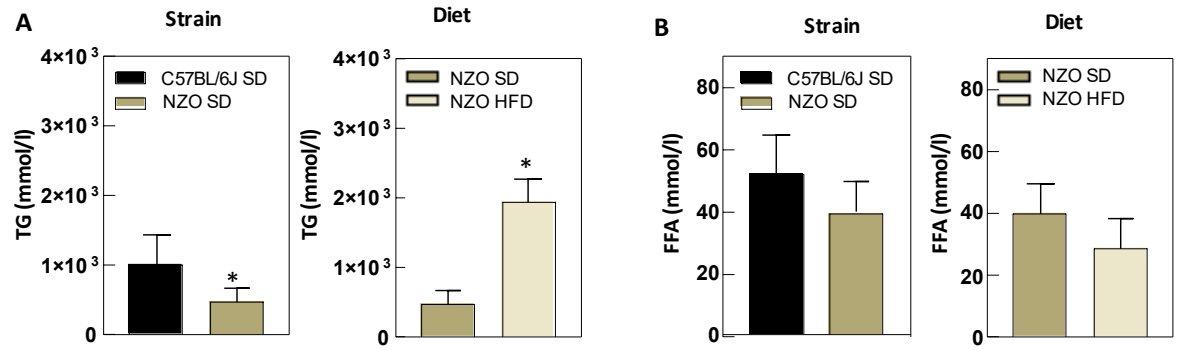

Figure 18: TG and FFA content in the liver. Statistical significance was given by unpaired t-test at *p < 0.05. C57BL/6J SD n=8, NZO SD n=6, NZO HFD n=8.

Changes in liver's morphology due to strain or diet were additionally examined by histological analysis. As depicted in Figure 19 the NAFLD activity score (NAS) was evaluated, by assessing three parameters: steatosis, lobular inflammation and cellular ballooning. C57BL/6J SD mice have NAS score: 0, NZO SD mice showed a few ballooning cells, giving NAS score: 1 and NZO HFD mice have many prominent ballooning cells and LDs, giving NAS score: 3.7.

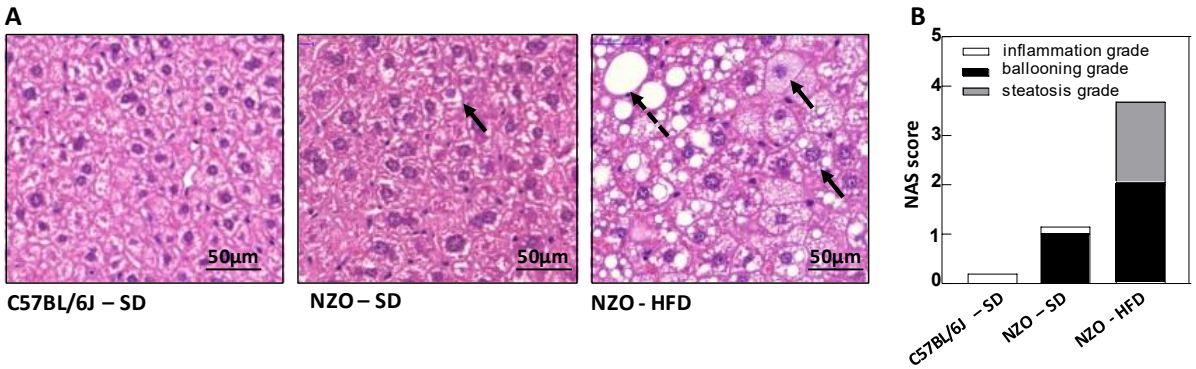

Figure 19: Liver histology. A. Representative images of hematoxylin and eosin-stained liver sections (magnification 40x). Nuclei, rough ER, and ribosomes are basophilic, therefore stained in purple. Most cellular organelles, extracellular matrix and cytoplasm are eosinophilic, stained in pink. Non-stained components such as the hydrophobic LDs are in white. Ballooning cells (black arrows) and LDs (dotted arrows) are depicted in the images. **B.** NAS score evaluation within each group. The heigh of the bars corresponds to the mean of individual NAS components. The white part of the bar corresponds to the inflammatory score, the gray part to the ballooning score, and the black part to the steatosis score. (C57BL/6J SD n=7, NZO SD n=6, NZO HFD n=8).

The mRNA expression of the LD proteins *plin5* and *plin2* was measured, as well as the protein levels of plin2 (Figure 20). Both *plin5* and *plin2* genes were less expressed in NZO SD mice in comparison to C57BL/6J SD mice. However, during HFD the *plin5* levels were further decreased, in contrast to *plin2* which was dramatically increased (Figure 20A, B). The protein levels of plin2 were detected by immunoblot and increased by strain and diet (Figure

20C). Additionally, Figure 20D shows immunostaining of plin2 in liver slices. Interestingly, plin2 is only obvious in NZO HFD mice, surrounding the LDs.

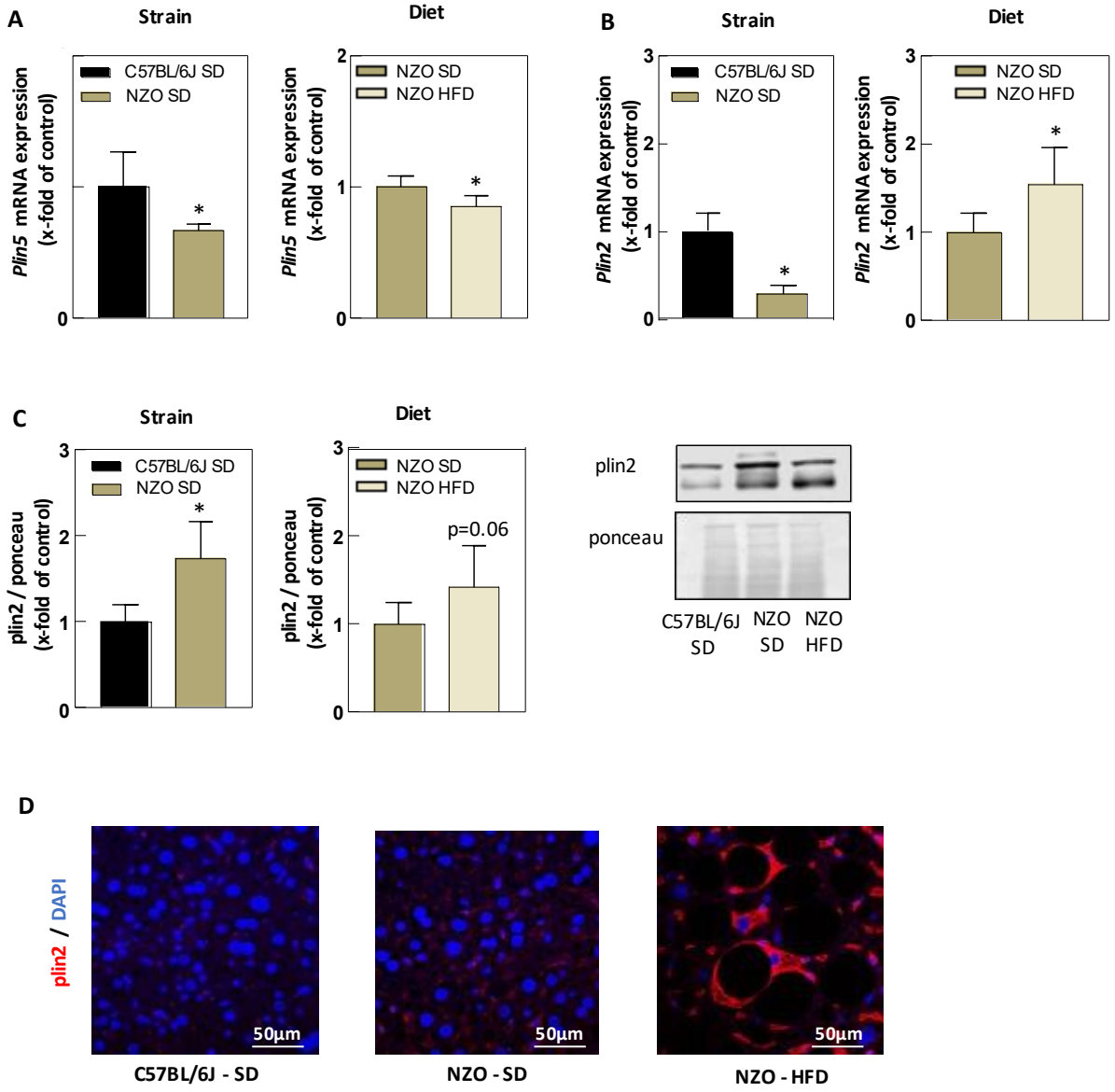

Figure 20: Alterations of LD proteins. A, B. mRNA expression of the LD proteins *Plin5* (A) and *Plin2* (B). **C.** Immunoblot analysis of plin2. Quantification and representative immunoblots. Ponceau was used as protein loading control. **D.** Representative images of immunostaining by confocal laser-scanning microscope (magnification 10x). Statistical significance was given by unpaired t-test at *p < 0.05. Trend was given by p=0.06. C57BL/6J SD n=8, NZO SD n=6, NZO HFD n=8.

4.1.2 Impact of strain and diet on proteasome system

In order to study whether the proteasome is also affected due to strain and diet, proteasome subunits were firstly detected. As depicted in Figure 21, the catalytic subunit β5 was significantly lower in NZO SD mice in comparison to C57BL/6J SD. However, there are no significant changes on the levels of β1 catalytic subunit in NZO SD vs C57BL/6J SD. On the contrary, the levels of Rpt6, the component of the 19S regulatory particle, was significantly increased in NZO SD vs C57BL/6J SD.

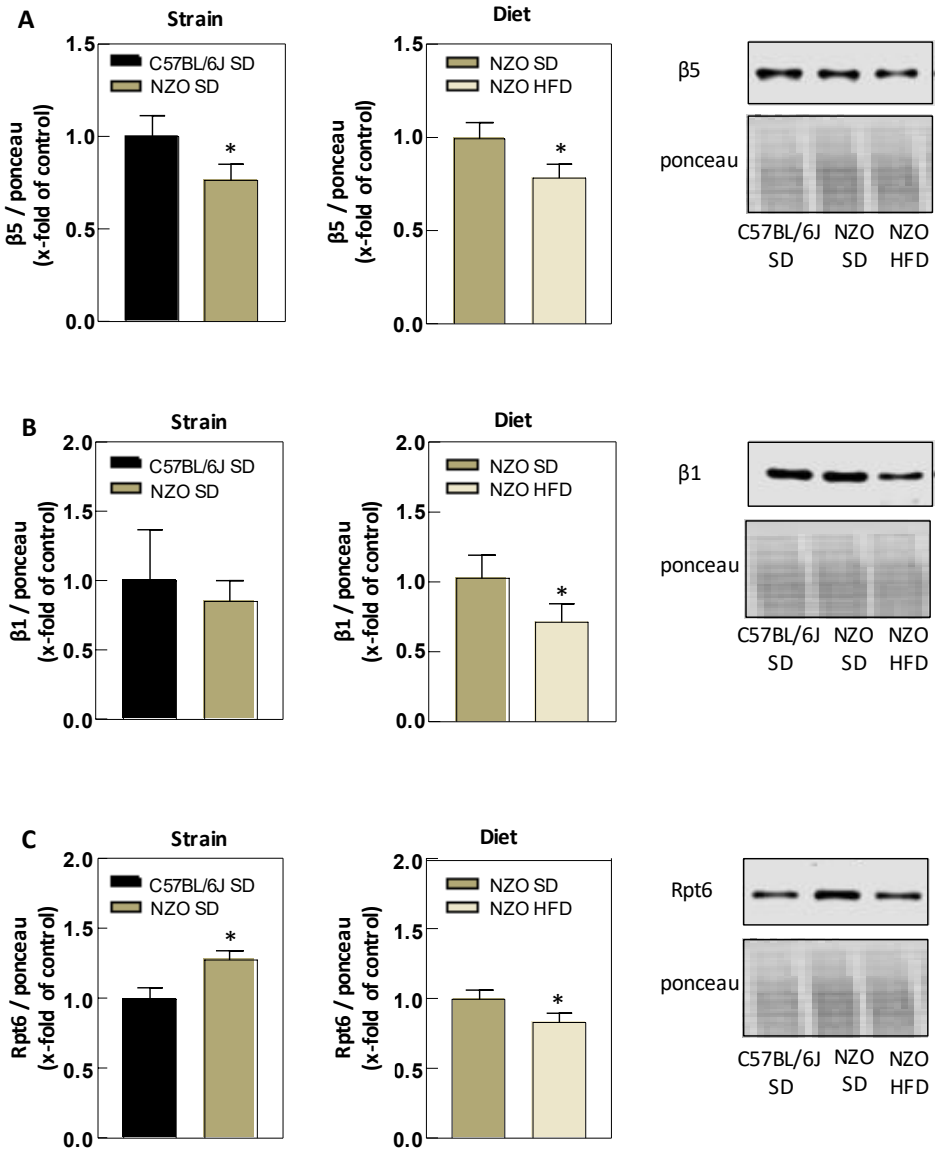

Figure 21: Impact of strain and diet on proteasome subunits. A-C. Immunoblot analysis of the proteasome subunits β5, β1 and Rpt6. Quantification and representative immunoblots. Ponceau was used as protein loading control. Statistical significance was given by unpaired t-test at *$p < 0.05$. C57BL/6J SD n=8, NZO SD n=6, NZO HFD n=8.

Interestingly, all above-mentioned proteasome subunits were significantly lower due to HFD in NZO mice. However, these changes on proteasome subunits didn't affect the proteasome activity (chymotrypsin-like activity) of both 20S and 26S proteasome (Figure 22).

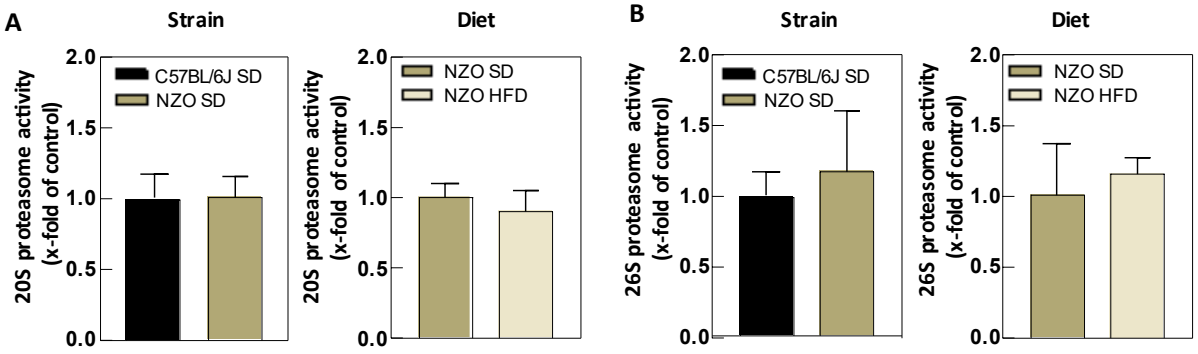

Figure 22: Proteasome activity of NZO mice is not affected by strain and diet. A. 20S chymotrypsin-like proteasome activity **B.** 26S chymotrypsin-like proteasome activity. Statistical significance assessed by unpaired t-test (*$p < 0.05$). C57BL/6J SD n=8, NZO SD n=6, NZO HFD n=8.

4.1.3 Impact of strain and diet on the autophagy-lysosome system

In order to study the effects of strain and diet on the ALS, the autophagy-related proteins Beclin-1, Atg5 and Atg5-Atg12 complex were initially detected by immunoblot, all involved in the first phase of the autophagic process (Figure 23). In NZO SD mice these proteins are significantly high, in comparison to C57BL/6J SD mice and low in comparison to NZO HFD mice.

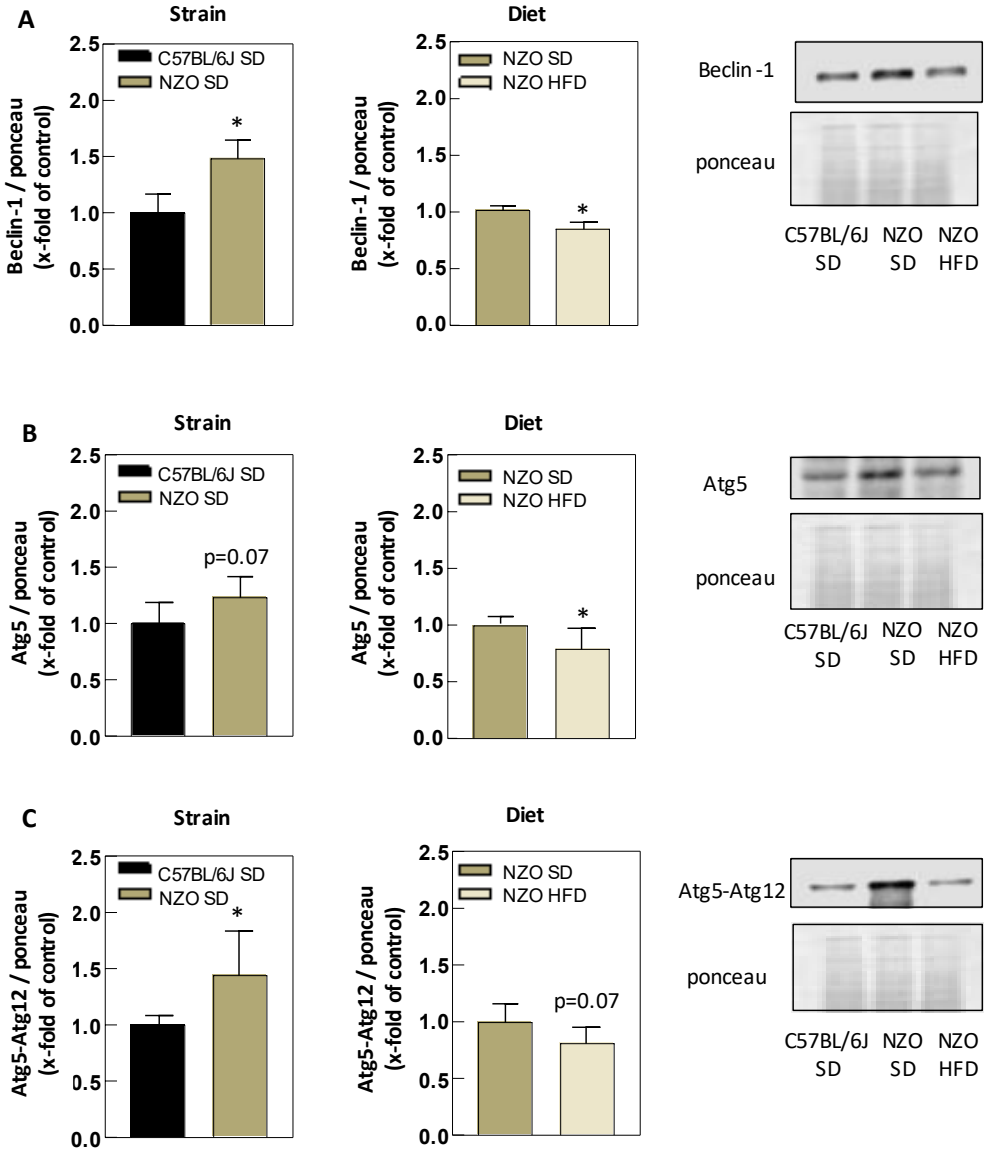

Figure 23: Effects of strain and diet on early stages of the autophagic pathway. A-C. Immunoblot analysis of autophagy-related proteins Beclin-1 (A), Atg5 (B) and Atg5-Atg12 (C). Quantifications and representative immunoblots. Ponceau was used as protein loading control. Statistical significance was given by unpaired t-test at *p < 0.05. Trend was given by p=0.07. C57BL/6J SD n=8, NZO SD n=6, NZO HFD n=8.

The gene and protein levels of LC3 were next determined (Figure 24A-C). The mRNA expression of *Map1lc3* (LC3) was significantly higher in NZO SD mice vs C57BL/6J SD. LC3 I also tended to be highly formed, in contrast to LC3 II which clearly tended to be lower in NZO SD mice, comparing to C57BL/6J SD (p=0.052).

HFD did not bring any further changes on *Map1lc3* gene expression and LC3 II formation. Interestingly enough though, the protein levels of LC3 I are significantly down as a diet effect, which was not observed as a strain effect.

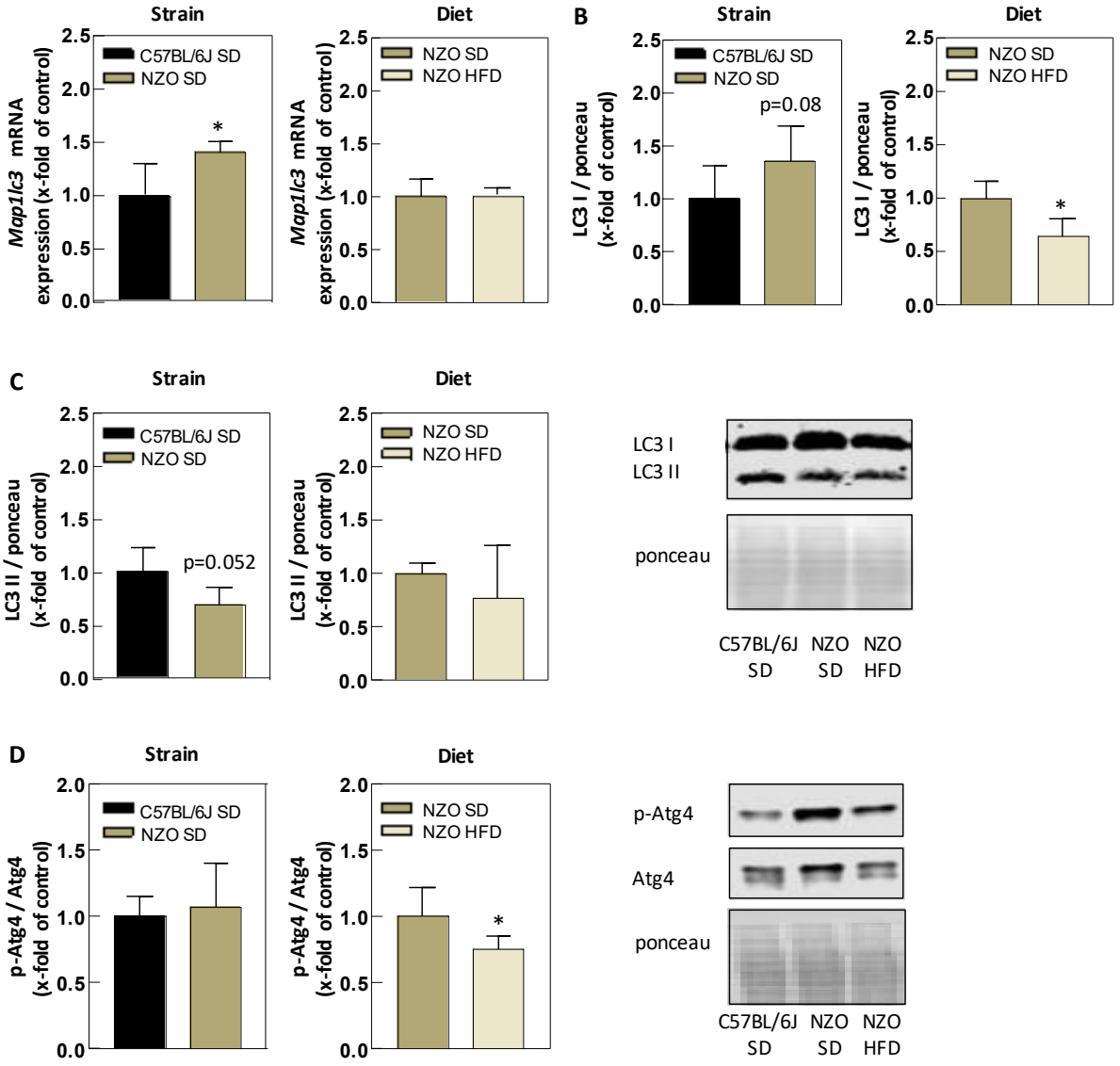

Figure 24: Impact of strain and diet on autophagosome elongation and maturation. A. mRNA expression of *Map1lc3* (LC3). **B-D.** Immunoblot analysis of LC3 I (B), LC3 II (C) and p-Atg4, Atg4 (D). Quantifications and representative immunoblot. Ponceau was used as protein loading control. Statistical significance was given by unpaired t-test at *p < 0.05. Trend was given by p=0.08 and p=0.052. C57BL/6J SD n=8, NZO SD n=6, NZO HFD n=8.

In order to identify whether the low formation of LC3 I is due to lower activity of Atg4, its phosphorylation levels was next analyzed (Figure 24D). Indeed, the ratio p-Atg4/Atg4 was lower only due to diet.

Furthermore, p62 gene and protein levels were detected. As depicted in Figure 25, there are no changes in gene expression, although the protein levels are significantly high by both, strain and diet.

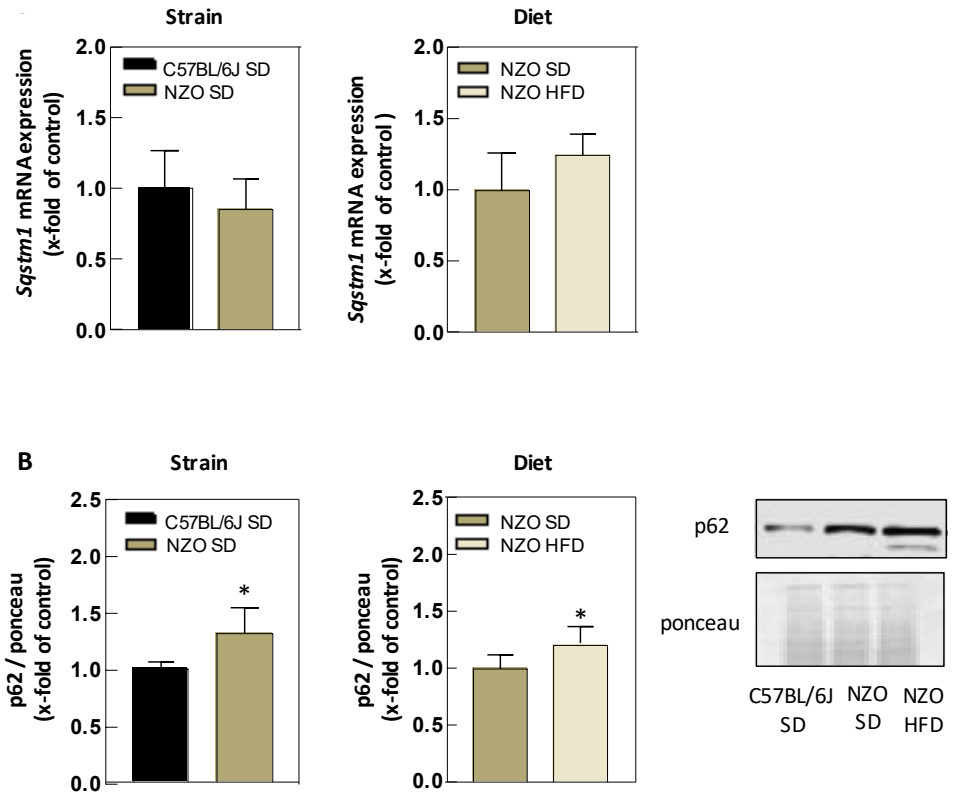

Figure 25: p62 turnover of NZO mice is impaired by strain and diet. A. mRNA expression of *Sqstm1* (p62). **B.** Immunoblot analysis of p62. Quantification and representative immunoblot. Ponceau was used as protein loading control. Statistical significance was given by unpaired t-test at *$p < 0.05$. C57BL/6J SD n=8, NZO SD n=6, NZO HFD n=8.

After investigating the impact of strain and diet on the autophagic system, possible alterations on lysosomal system were further analysed. As depicted in Figure 26A, there are no significant changes on the lysosomal protein LAMP-1. However, the lysosomal cysteine cathepsins activity is tended to be lower in NZO SD mice, comparing to C57BL/6J SD and there are no further changes in NZO mice due to diet (Figure 26B).

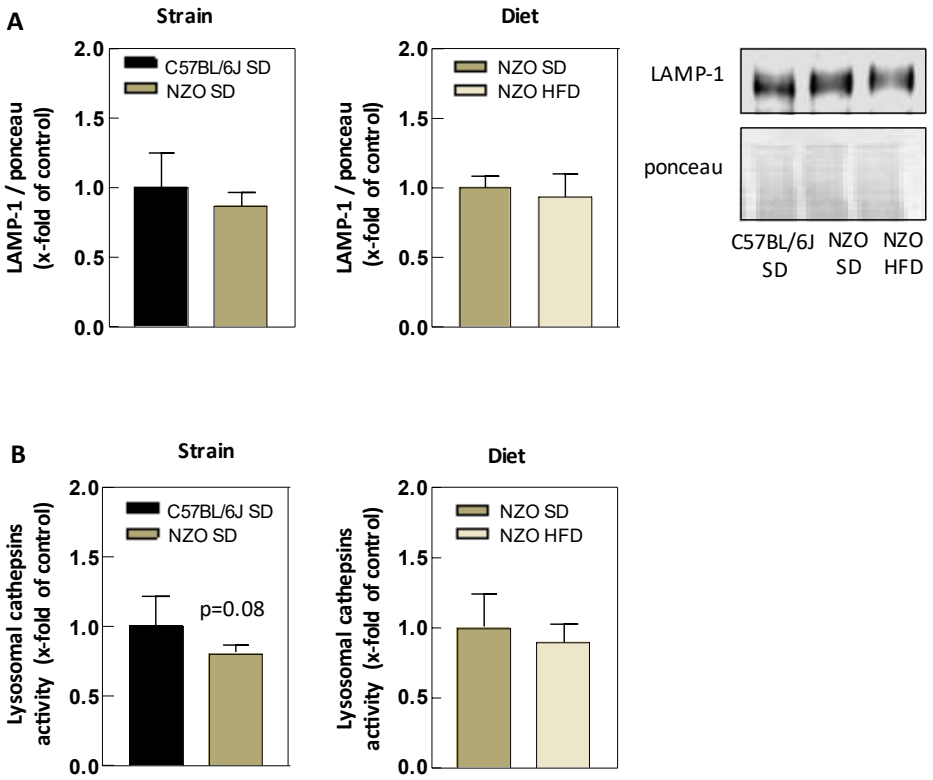

Figure 26: Lysosomal cysteine cathepsins activity and LAMP-1 levels are not affected by strain and diet. A. Immunoblot analysis of LAMP-1. Ponceau was used as protein loading control. **B.** Lysosomal activity of cysteine cathepsins. Trend was given by unpaired t-test at p=0.08. C57BL/6J SD n=8, NZO SD n=6, NZO HFD n=8.

4.2 Impact of palmitate on HepG2 cells - *in vitro* investigation

The next aim was to further investigate the molecular mechanism of LD-induced hepatocellular dysfunction and the role of proteolytic systems on that. Therefore, the second part of this study refers to *in vitro* investigations in HepG2 cells, where PA was used to induce lipid accumulation.

4.2.1 Palmitate induces intracellular lipid accumulation in HepG2 cells and alters the lipid droplet protein content and the redox state

Cell viability of HepG2 cells was firstly assessed after incubation with 500µM and 250µM PA for 24-72h. As depicted in Figure 27A, it was identified that higher concentration of PA (500µM), markedly affect the cell viability. On the contrary, the cells were viable over 72h using 250µM PA. Based on these results it was next tested whether PA can increase the intracellular lipid content in that model (Figure 27B-D).

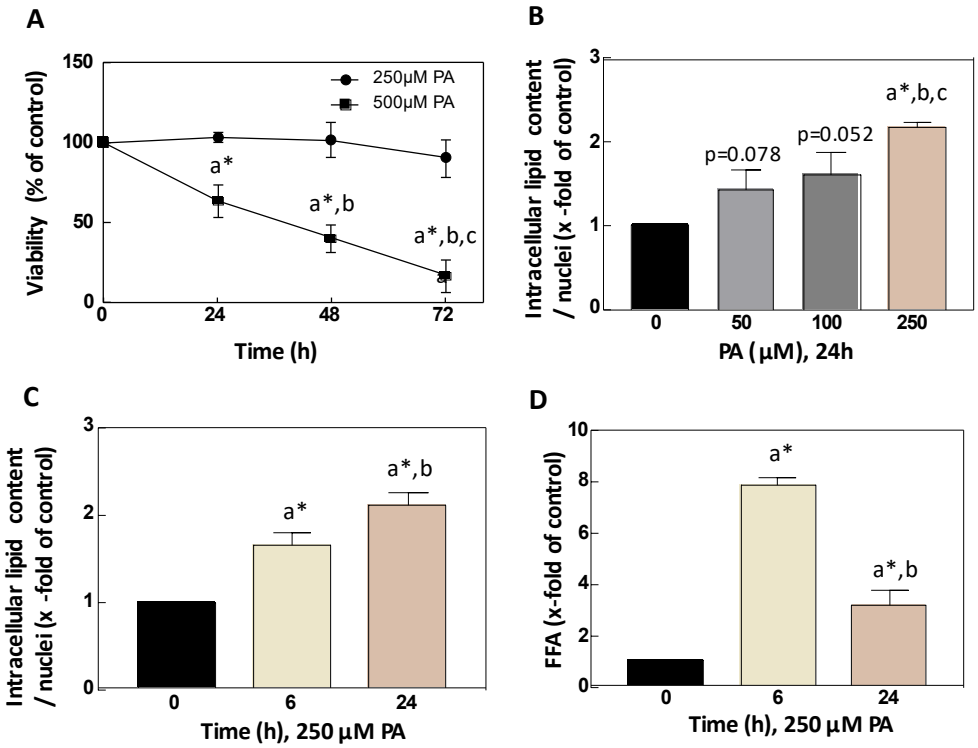

Figure 27: PA induces intracellular lipid accumulation in HepG2 cells. A. Viability measured by neutral red assay. **B, C.** Accumulation of neutral lipids (Oil Red-O staining) in concentration- (B) and time- (C) dependent manner. **D.** Time dependent extracellular FFA content. Statistical significance was given at $p < 0.05$ as follows: one sample t-test indicated with a* vs 0h and one Way ANOVA test, Tukey's multiple comparisons indicated by b vs 24h, 50µM or 6h and c vs 48h or 100 µM. Trend was given at p=0.078 and p=0.052 vs control.

It was observed that treatment with increasing concentrations of PA (up to 250µM) for 24h, progressively induced the intracellular lipid content in a concentration dependent manner (Figure 27B). Similarly, 250µM PA gradually elevates the intracellular lipid accumulation after 6h and 24h (Figure 27C). The amount of FFA was also increased after both 6h and 24h PA treatment. However, FFA where dramatically decreased after 24h, comparing to 6h PA exposure.

The LD protein content altered after 250µM PA treatment for 24h (Figure 28). In Figure 28A is depicted the intracellular lipid accumulation by Oil Red-O staining. The mRNA levels of LD proteins *Cidea* and *Plin2* were significantly increased comparing to control cells (Figure 28B, D). On the contrary, *Plin5* was downregulated due to PA exposure (Figure 28C). A significant upregulation of plin2 protein after 24h PA treatment was additionally detected (Figure 28E). Similar effects in gene and protein expression of LD proteins *Plin2* and *Plin5* were observed *in vivo* due to HFD.

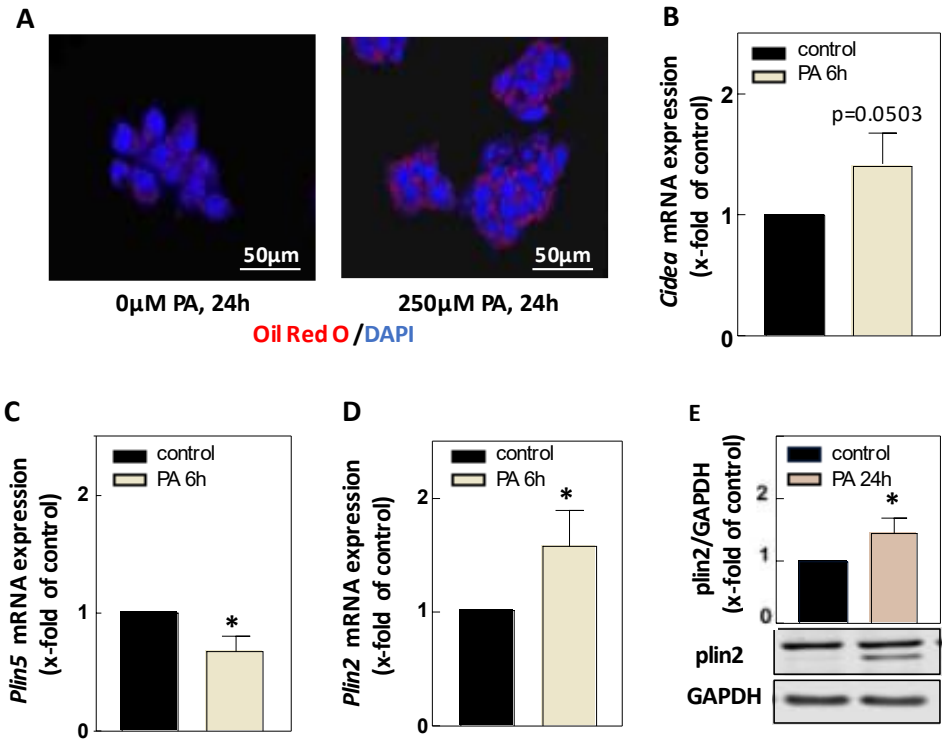

Figure 28: LD protein content after PA treatment. A. Intracellular lipid accumulation after 24h PA treatment. Representative images of Oil Red-O staining by confocal laser-scanning microscope (magnification 10x). **B-D.** mRNA expression of the LD proteins *Cidea* (B), *Plin5* (C) and *Plin2* (D) after 6h, 250µM PA treatment. **E.** Immunoblot analysis of plin2 after 24h, 250µM PA treatment. Quantifications and representative immunoblots. GAPDH was used as protein loading control. Statistical significance was given by one sample t-test at *$p < 0.05$. Trend was given at $p=0.0503$.

The effects of PA on redox homeostasis of the cellular compartments were then examined (Figure 29). Interestingly enough, H_2O_2 formation was not detected on the cytosol, as the dimerization levels of the cytosolic prx2 remained unchanged (Figure 29A). On the contrary, significantly increased dimers of prx3 after 24h PA treatment was observed, indicating a redox shift in mitochondria (Figure 29B). Immunoblot analysis of prx4, a ROS scavenging enzyme in ER, was also performed in order to identify the redox status in ER. Since the native conformation of prx4 is oligomeric [166-168], the monomeric state of the protein was detected by immunoblot analysis in presence of the disulfide-reducing reagent DTT (Suppl. Figure 1A). An upregulation of prx4 was observed, which might indicate a compensatory mechanism in order to eliminate increased ER H_2O_2 levels (Figure 29C). The phosphorylation levels of IRE1α and eIF2α, where also increased, as depicted in Suppl. Figure 1B, C which confirm increased H_2O_2 levels in ER and might indicate ER stress.

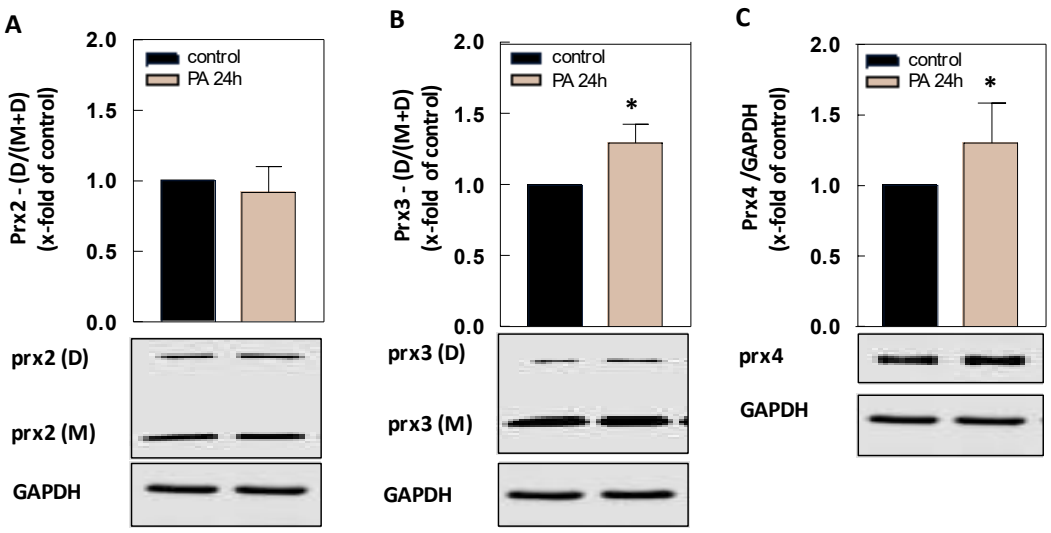

Figure 29: PA affects the redox homeostasis of cellular compartments. A-C. Immunoblot analysis of the cytosolic prx2 (A), mitochondrial prx3 (B) and ER prx4 (C). Quantifications and representative immunoblots. GAPDH was used as protein loading control. Statistical significance was given by one sample t-test at *$p < 0.05$.

4.2.2 Impact of palmitate on proteasome system

In vivo, it was observed that strain and diet only affect the levels of proteasome subunits, but not the 20S or 26S proteasome activity (4.1.2). Therefore, the next aim was to investigate whether also *in vitro*, the PA-mediated LD accumulation and the redox changes in mitochondria and ER have similar impact on proteasome. Proteasome subunits were firstly detected, after 250 µM PA treatment for 6h and 24h in HepG2 cells (Figure 30). The levels of Rpt6, remained unchanged after both 6h and 24h PA treatment, while an upregulation of the 20S core proteasome subunits α4 and the catalytic subunits β1 and β5 was observed only after 24h PA.

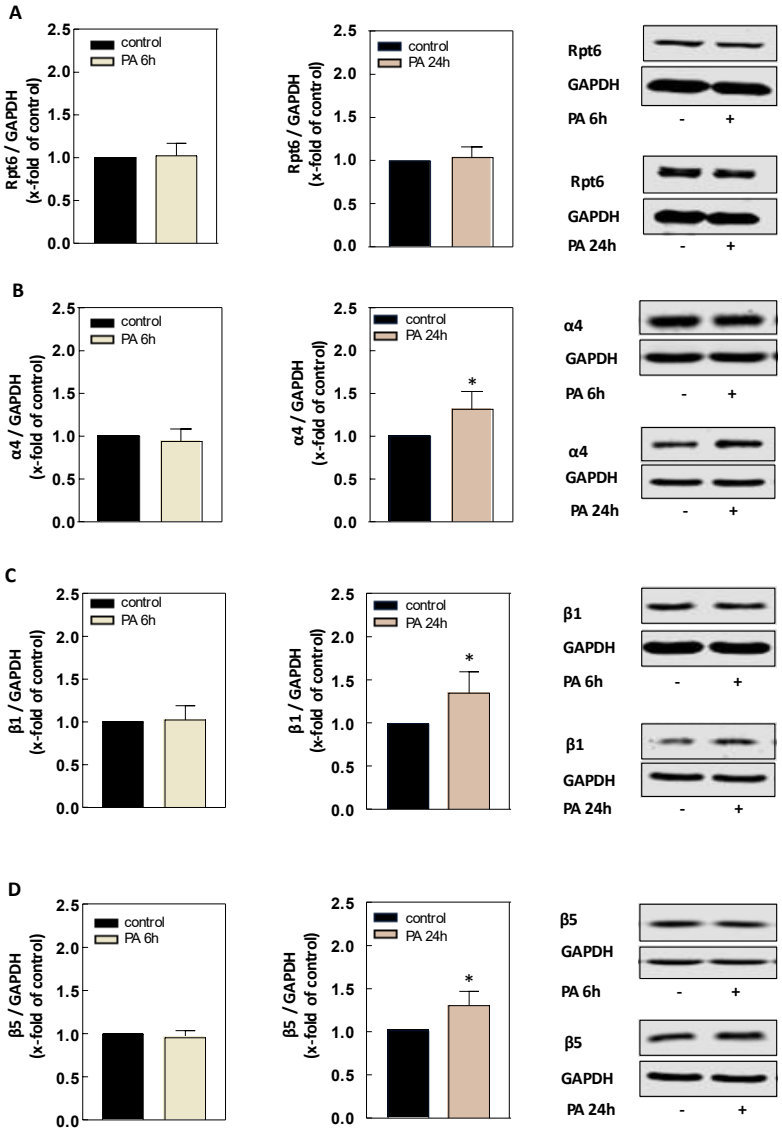

Figure 30: Effects of PA on proteasome subunits in HepG2 cells. A-D. Immunoblot analysis of the proteasome subunits Rpt6, α4, β1, β5 after 6h and 24h PA treatment. Quantification and representative immunoblot. GAPDH was used as protein loading control. Statistical significance was given by one sample t-test at *$p < 0.05$.

The chymotrypsin-like activity (β5) was measured as depicted in Figure 31. 6h PA treatment impairs only the activity of 20S proteasome, while 24h PA impairs also the 26S proteasome activity.

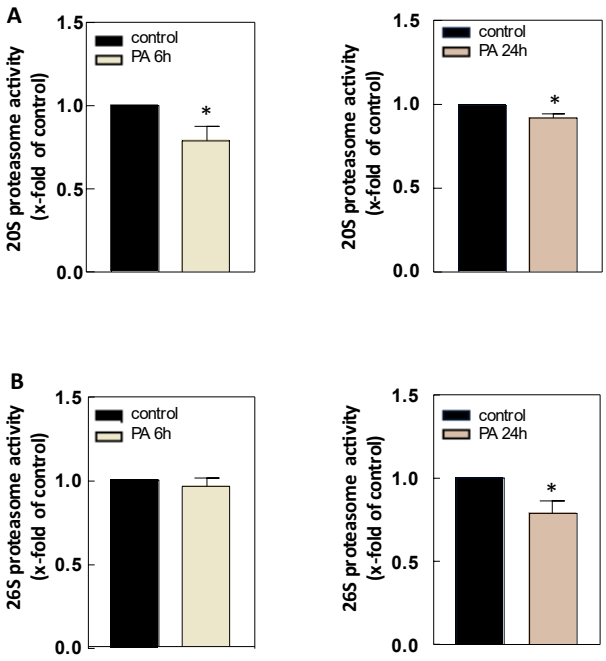

Figure 31: Effects of PA on proteasome activity in HepG2 cells. A. 20S chymotrypsin-like proteasome activity **B.** 26S chymotrypsin-like proteasome activity after 6h and 24h PA treatment. Statistical significance was given by one sample t-test at *p < 0.05.

4.2.2.1 Role of proteasome in lipid droplet degradation

Since PA has a negative impact on proteasome in HepG2 cells, it was next investigated whether proteasome is involved in LD degradation. Possible changes of intracellular lipid accumulation were assessed, in presence of PA and proteasome inhibitor (LC) or proteasome activator (ursolic acid) (Figure 32). However, there are no significant changes on LD content when proteasome activity is manipulated, indicating that proteasome is not involved in the bulk LD degradation.

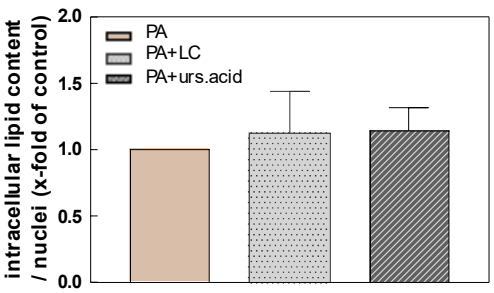

Figure 32: Role of proteasome in the degradation of PA-induced LDs. Quantification of neutral lipids stained by Oil Red-O and measured by spectrometer at 520nm. HepG2 cells were incubated with 250μM PA for 24h and/or LC and ursolic acid, as described on materials and methods.

4.2.3 Impact of palmitate on autophagy-lysosome system

The next aim was to examine whether and how the PA-induced lipotoxicity affects the autophagic process in hepatocytes and to confirm the results of the *in vivo* studies (4.1.3.). Given that the autophagy-lysosome system is highly dynamic, autophagic flux was analyzed as well as the levels of autophagy-related proteins in time, choosing short (6h) and long time (24h) PA exposure.

The autophagy-related proteins Beclin-1, Atg5 and Atg5-Atg12 were firstly detected in order to follow the initial steps of the autophagic process (Figure 33).

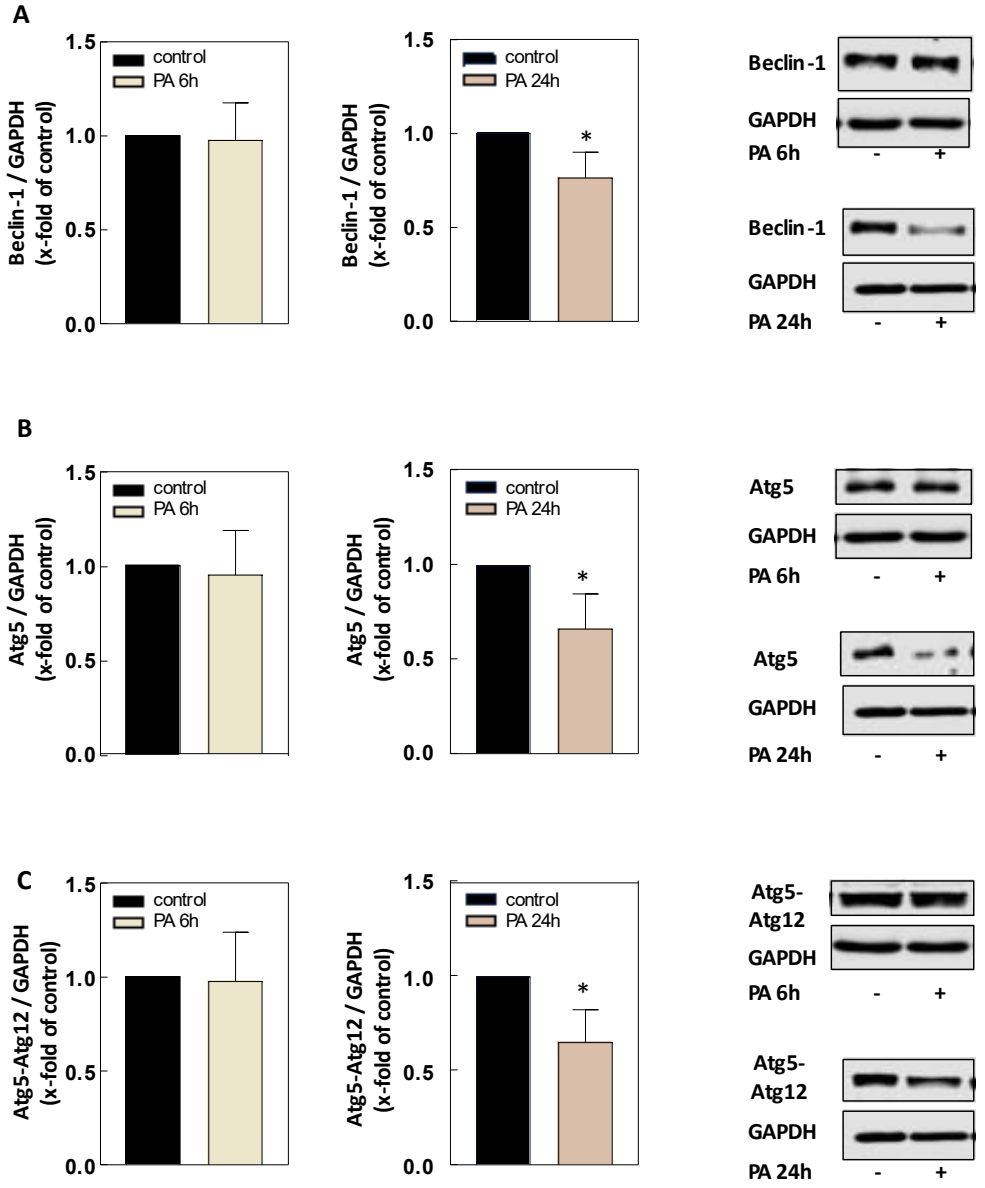

Figure 33: PA restrains the early stages of autophagic pathway in HepG2 cells. A-C. Immunoblot analysis of autophagy-related proteins Beclin-1, Atg5 and Atg5-Atg12 after 6h and 24h PA treatment. Quantifications and representative immunoblots. GAPDH was used as protein loading control. Statistical significance was given by one sample t-test at *$p < 0.05$.

As depicted in Figure 33, all proteins were significantly downregulated after 24h PA treatment, while after 6h PA exposure the levels remained unchanged, comparing to untreated cells. Interestingly, similar changes were observed *in vivo*, as the levels of these proteins were also low in NZO mice fed a HFD.

The gene and protein expression of LC3 as well as the Atg4 activity were next analyzed (Figure 34A, Suppl. Figure 2). After 6h PA treatment the phosphorylation levels of Atg4 and the protein levels of LC3 I remained unchanged, while LC3 II was significantly higher comparing to untreated cells. Analysis of *Map1lc3* (LC3) gene expression after 6h PA and the phosphorylation levels of Atg4 after 24h PA treatment displayed no significant changes in comparison to control. However, both LC3 I and LC3 II proteins were significantly increased after 24h PA treatment, comparing to control cells. These data indicate that in contrast to the *in vivo* results, PA does not affect the initial steps of LC3 I formation.

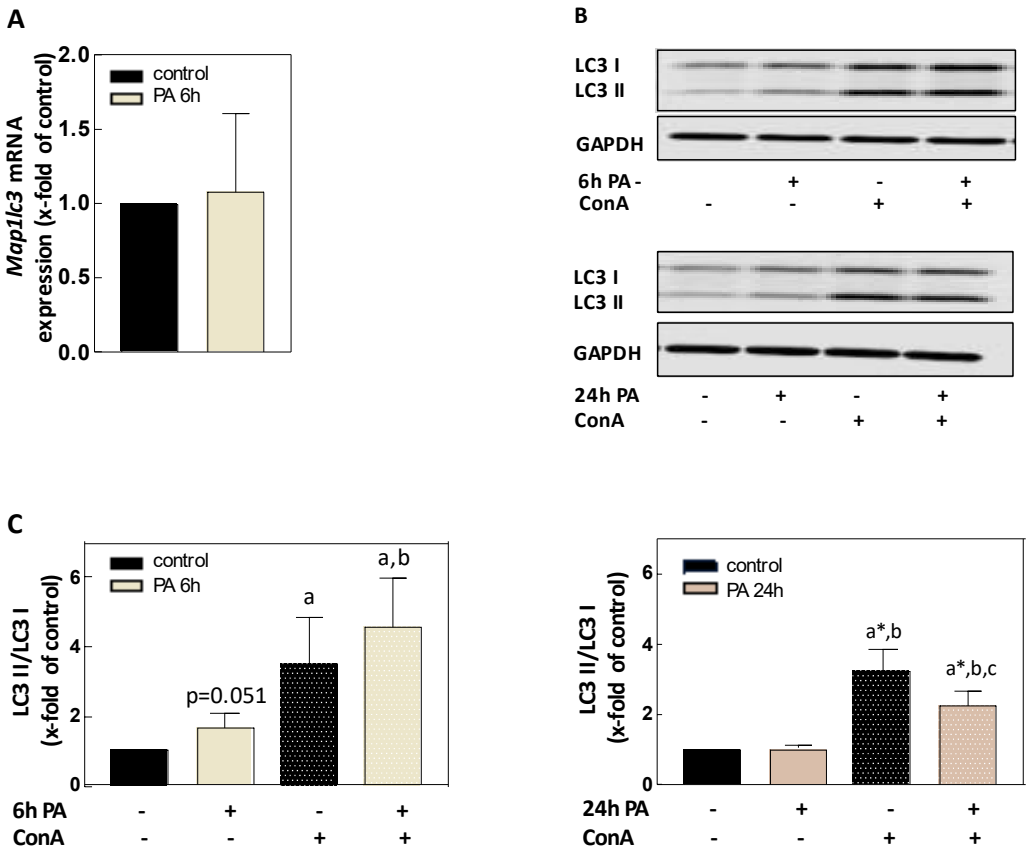

Figure 34: Impact of PA on LC3 II turnover in HepG2 cells. A. mRNA expression of *Map1lc3* (LC3) after 6h PA treatment. **B.** Representative immunoblot of LC3 I and LC3 II after 6h and 24h PA treatment. GAPDH was used as protein loading control. **C.** Normalized LC3 II/LC3 I ratio after 6 and 24h PA treatment. Statistical significance was given at $p < 0.05$ as follows: one Way ANOVA test, Tukey's multiple comparisons indicated by b vs 6 or 24h PA and c vs control+ConA; and one sample t-test indicated by a* vs control. Trend was given by p=0.051 vs control.

To estimate the autophagic flux, LC3 II and p62 turnover were analyzed in presence and absence of the lysosomal inhibitor ConA. The conversion of LC3 II was estimated by the normalized ratio LC3 II/LC3 I (Figure 34B, C). After 6h PA treatment, the ratio LC3 II/LC3 I was significantly increased, comparing to control, whereas in presence of ConA the ratio was increased in both control and PA treated cells. In addition, no differences were obtained by comparing the ratio of LC3 II/LC3 I in ConA vs control with ConA+6h PA vs 6h PA, suggesting that LC3 II is similarly formed in both conditions.

On the contrary, after 24h PA treatment the ratio LC3 II/LC3 I remained unchanged comparing to control cells, although, the protein levels of both LC3 I and LC3 II were significantly increased as described above (Suppl. Figure 2). In addition, in PA+ConA treated cells, the ratio LC3 II/LC3 I was significantly decreased comparing to ConA alone. Additionally, comparing normalized LC3 II/LC3 I in ConA vs control with ConA+24h PA vs 24h PA, the ratio was distinctly reduced after 24h PA treatment. Overall, a progressive decline of LC3 II turnover during time, as indicated by the reduced LC3 II/LC3 I values was observed, after 24h PA in comparison to 6h PA treatment.

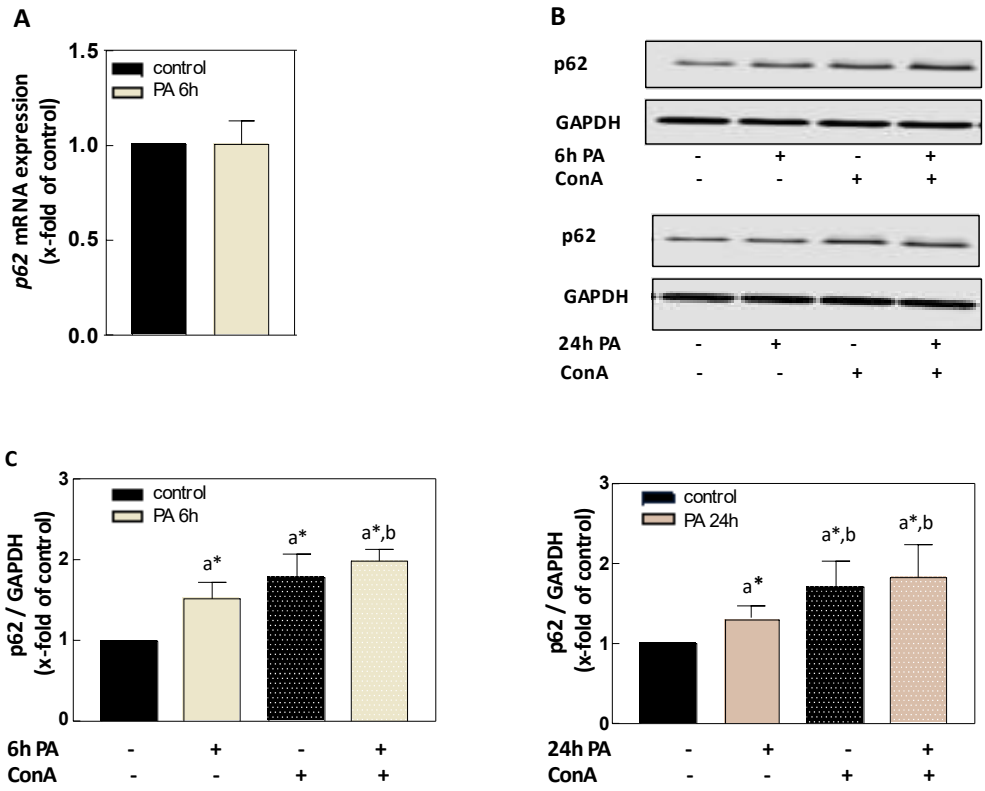

Figure 35: PA impairs p62 turnover in HepG2 cells. A. mRNA expression of *Sqstm1* (p62) after 6h PA treatment. **B.** Representative immunoblot of p62 after 6h and 24h PA treatment. GAPDH was used as protein loading control. **C.** protein expression of p62 after 6 and 24h PA treatment. Statistical significance was given at $p < 0.05$ as follows: one Way ANOVA test, Tukey's multiple comparisons indicated by b vs 6 or 24h PA; and one sample t-test indicated by a* vs control.

To further clarify the role of PA on autophagic flux, the delivery of cytosolic cargo to lysosomes was also estimated by analyzing the p62 protein levels in presence and absence of ConA (Figure 35). As depicted in Figure 35B, C after both 6h and 24h PA treatment, significantly increased p62 protein levels compared to controls were obtained, while inhibition of lysosomal degradation augments this effect. In addition, comparison of p62 levels in ConA vs control with ConA + PA vs PA indicates that the p62 turnover is reduced in both, 6 and 24h PA treatment. To verify that the increased p62 protein levels by PA were not due to increased *Sqstm1* (p62) gene expression, *Sqstm1* mRNA was analyzed after 6h PA treatment (Figure 35A), obtaining no changes in comparison to control, indicating p62 accumulation and decreased turnover. Similar effects were observed *in vivo* as a result of strain and diet.

Considering the impact of PA on lysosomal system, the expression levels of the lysosomal protein LAMP-1 were detected and the lysosomal activity of cysteine cathepsins was measured.

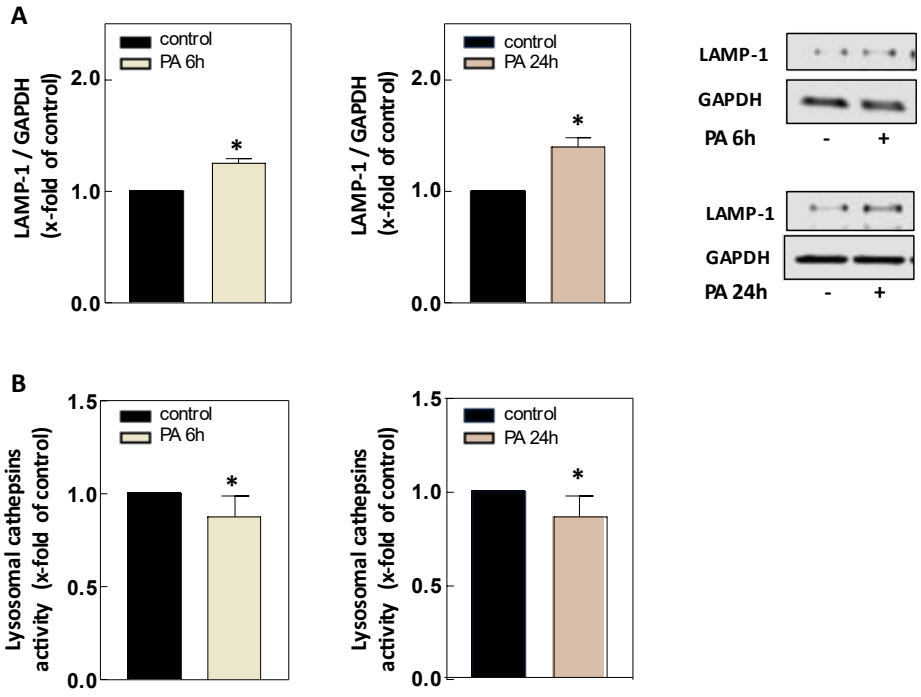

Figure 36: Impact of PA on lysosomal system in HepG2 cells. A. Immunoblot analysis of LAMP-1 after 6h and 24h PA exposure. GAPDH was used as protein loading control. **B.** lysosomal activity of cysteine cathepsins after 6h and 24h PA treatment. Statistical significance was given by one sample t-test at *$p < 0.05$.

As indicated in Figure 36, a significant upregulation of LAMP-1 was observed after both 6h and 24h PA treatment. However, the lysosomal activity of cysteine cathepsins was

significantly decreased at both time points. On the contrary, *in vivo* no negative impact of strain or diet on lysosomal system was observed.

4.2.3.1 Role of autophagy in lipid droplet degradation

Since PA affects the autophagy-lysosome system, it was next investigated whether autophagy is involved in LD degradation. Thus, the autophagic process was chemically manipulated and subsequently the intracellular neutral lipid content and the plin2 protein levels were assessed (Figure 37). Interestingly, both plin2 and intracellular lipid content were significantly increased after inhibition of autophagy with 3MA in PA treated cells. Similar effects were obtained after inhibition of the lysosomal degradation by ConA (Suppl. Figure 3). On the contrary, the PA-induced plin2 level and LD content were significantly decreased after induction of autophagy by Torin 1, indicating that autophagy is involved in the bulk LD degradation.

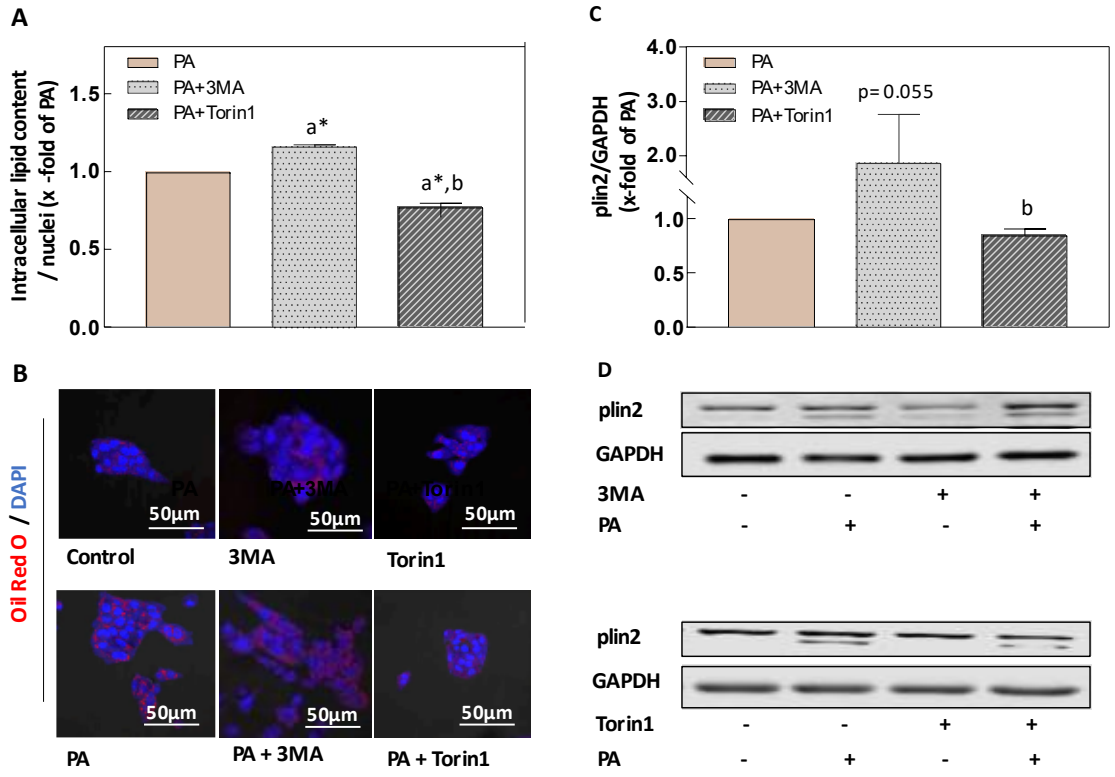

Figure 37: Autophagy is involved in the degradation of PA-induced LDs. HepG2 cells were incubated with PA for 24h and/or 3MA and Torin1. **A.** Quantification of intracellular lipids, stained by Oil Red-O and measured by spectrometer at 520nm and **B.** Representative images by confocal laser-scanning microscopy (magnification 10x). **C.** Quantification of plin2 protein expression by immunoblot analysis and **D.** Representative immunoblots. Statistical significance was given at $p < 0.05$ as follows: one Way ANOVA test, Tukey's multiple comparisons indicated by b vs PA+3MA; and one sample t-test indicated by a* vs PA. Trend is given by p=0.055 vs PA.

4.3 Prevention of palmitate-induced lipotoxicity by punicalagin through induction of autophagy

Since autophagy is involved in LD degradation and PA impairs autophagy, it was next investigated whether punicalagin, a natural autophagic inducer, can prevent the PA-mediated lipotoxicity. Therefore, the cells were cotreated with PA and punicalagin for 24h and the alterations on the LD content, redox homeostasis (4.3.1) and autophagy-lysosome system (4.3.2) were observed.

4.3.1 Punicalagin reduces the lipid droplet content and restores the redox imbalance

Plin2 protein levels as well as intracellular lipid accumulation were firstly analyzed in presence of punicalagin + PA (Figure 38). Interestingly, punicalagin alleviates the PA-induced LD content as both plin2 and intracellular lipid content were significantly decreased in punicalagin + PA treated cells, comparing to PA alone.

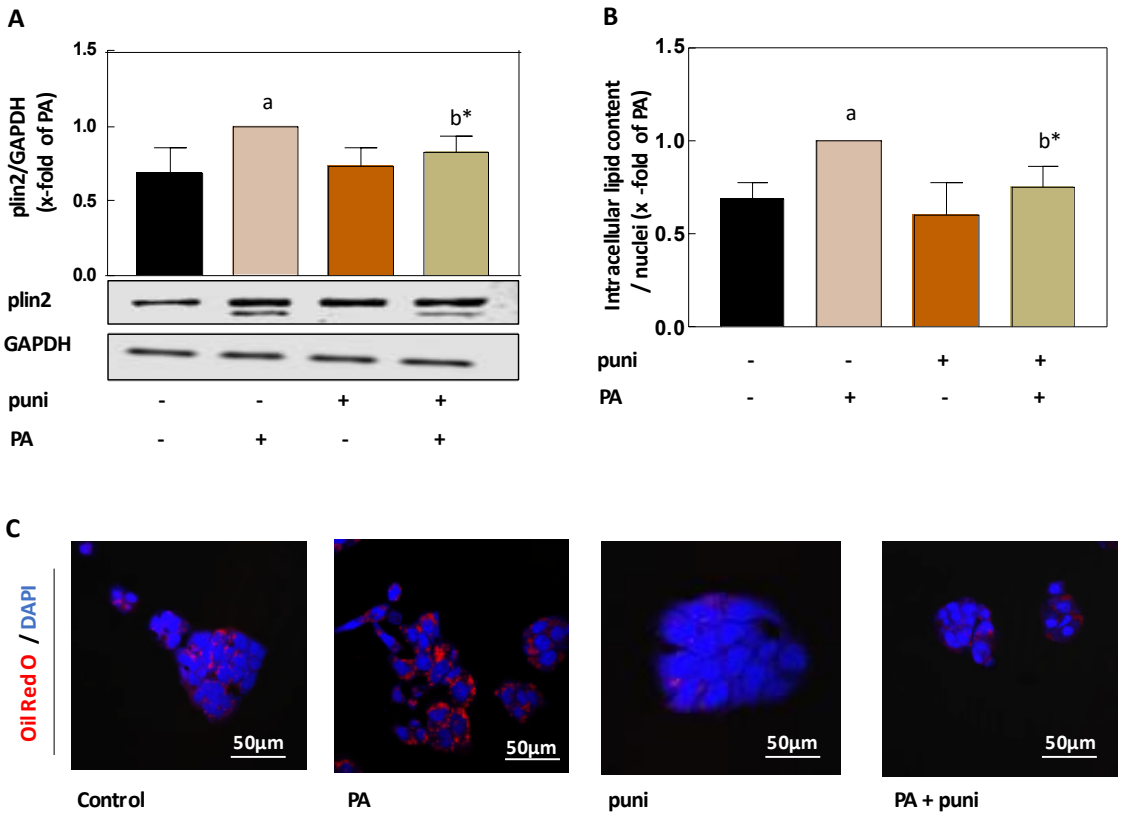

Figure 38: Punicalagin attenuates the PA-induced intracellular lipid accumulation. HepG2 hepatocytes were incubated with 250µM PA for 24h and/or punicalagin (puni) (10µM, 24h) **A.** Immunoblot analysis of plin2 and quantification. **B, C**. Accumulation of neutral lipids (Oil Red-O staining). Quantification by spectrometer at 520nm (B) and representative images by confocal laser-scanning microscopy (magnification 10x) (C). Statistical significance was given at $p < 0.05$ as follows:

one Way ANOVA test, Tukey's multiple comparisons, indicated by a vs control and one sample t-test indicated by b* vs PA.

The effects of punicalagin on LD-induced redox imbalance of the cellular compartments was then examined (Figure 39). As expected, the increased number of prx3 dimers (located in mitochondria) and the high protein levels of prx4 (located in ER) due to PA treatment, are significantly reduced in presence of punicalagin.

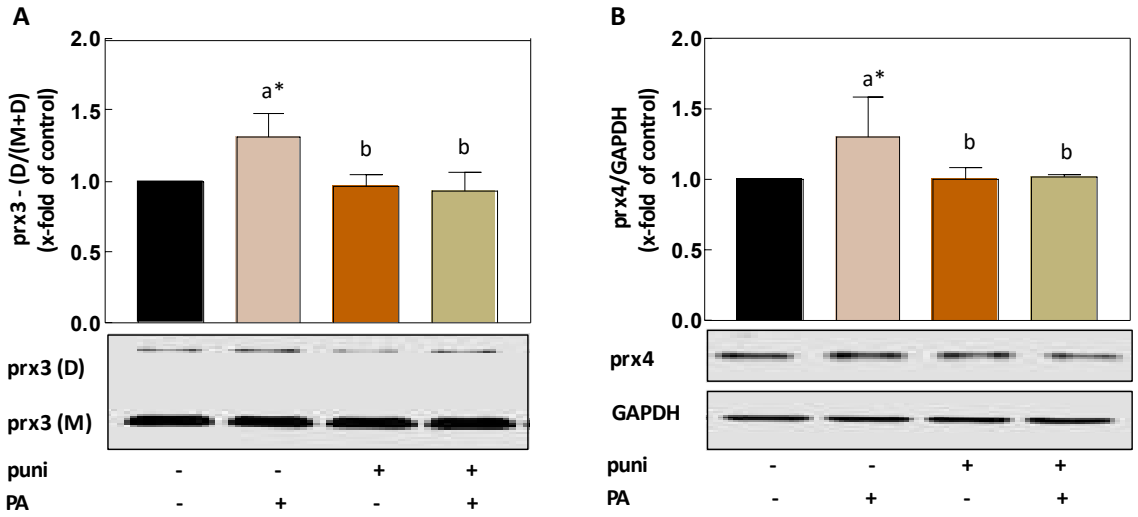

Figure 39: Punicalagin alleviates the PA-induced redox shift in mitochondria and ER. A, B. Immunoblot analysis of mitochondrial prx3 (A) and ER prx4 (B) after punicalagin (puni) and PA treatment. Quantifications and representative immunoblots. GAPDH was used as protein loading control. Statistical significance was given at $p < 0.05$ as follows: one Way ANOVA test, Tukey's multiple comparisons, indicated by b vs PA and one sample t-test indicated with a* vs control.

4.3.2 Punicalagin restores the palmitate-impaired autophagic flux

These observations prompted us to investigate if the reduced LD content and improved redox imbalance is a consequence of induced autophagy by punicalagin. It was therefore tested whether in presence of punicalagin the PA-impaired autophagy is also restored.

The protein levels of autophagy-related proteins Beclin-1, Atg5 and Atg5-Atg12 complex were initially detected (Figure 40). Interestingly, it was observed that the reduced levels of all above mentioned autophagy-related proteins returned to their control levels, in presence of punicalagin.

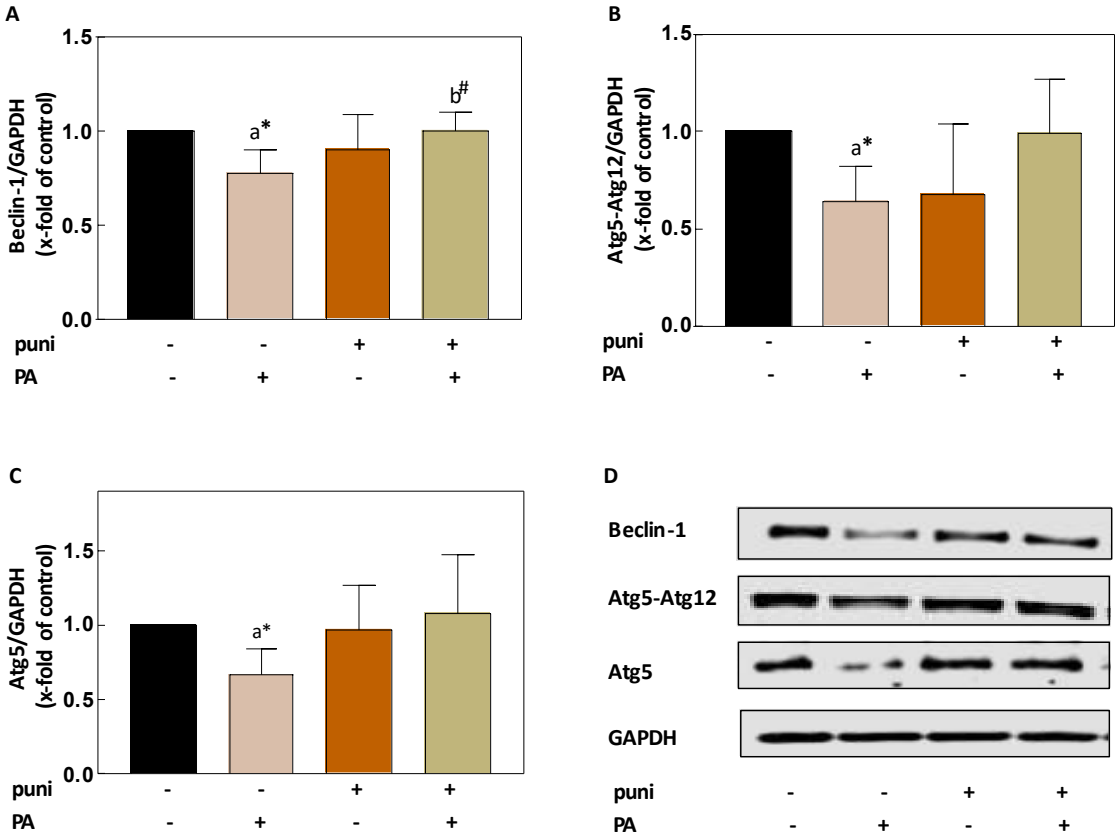

Figure 40: Punicalagin preserves the expression of autophagy-related proteins. Immunoblot analysis of the autophagy-related proteins Beclin-1, Atg5-Atg12 and Atg5. **A-C**. Quantifications and **D.** representative immunoblots. GAPDH was used as a protein loading control. Statistical significance was given at $p < 0.05$ as follows: Mann–Whitney test indicated by $b^{\#}$ vs PA or one sample t-test indicated by a* vs control.

Furthermore, the autophagic flux was analyzed, using the lysosomal inhibitor ConA (Figure 41). Analysis of the normalized ratio LC3 II/LC3 I (Figure 41A, D) indicates that in absence of ConA, the ratio is significantly higher in punicalagin treated cells but unchanged in PA + punicalagin or PA alone, in comparison to control. To estimate the difference in the degradation rate of formed LC3 II between PA and PA + punicalagin, it was calculated and

compared the normalized ratio LC3 II/LC3 I of PA + ConA vs PA and PA + punicalagin + ConA vs PA + punicalagin, obtaining increased turnover of formed LC3 II in punicalagin treated cells (Figure 41B). Therefore, the degradation of formed LC3 II was significantly higher in presence of punicalagin, comparing to PA treated cells, indicating that punicalagin improves the PA-reduced LC3 II turnover.

Analysis of p62 protein levels in absence of ConA (Figure 41C, D) indicated decreased p62 in PA + punicalagin, comparing to PA treated cells. In presence of ConA, p62 is always significantly increased. However, no significant changes between the single ConA treatments were visible, indicating that punicalagin improves also the PA-reduced p62 turnover.

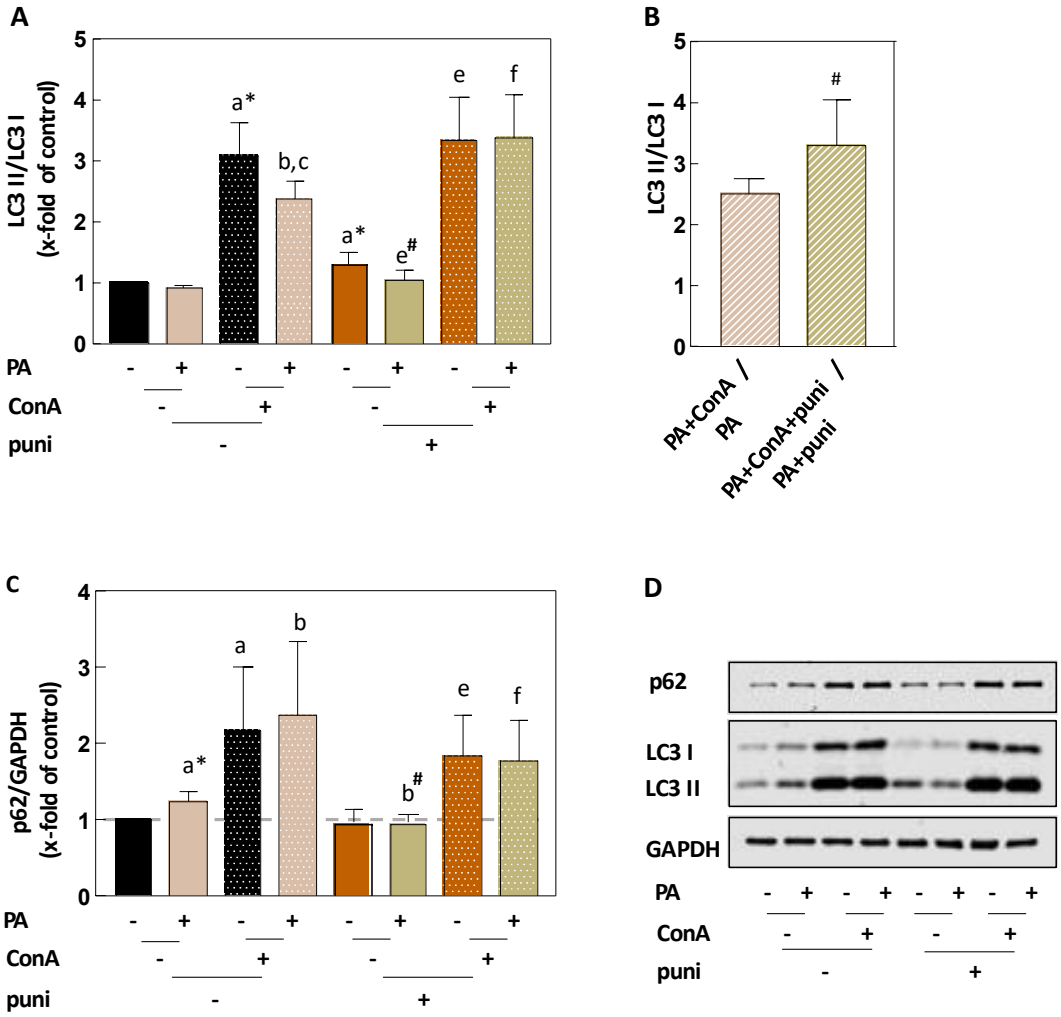

Figure 41: Punicalagin improves the PA-impaired autophagic flux. A-D. Immunoblot analysis of LC3 II and p62 turnover in presence of punicalagin (puni) and PA cotreatment. **A.** Normalized LC3 II/LC3 I ratio. **B.** Degradation of LC3 II in PA vs PA + puni treated cells. **C.** Protein expression of p62. GAPDH was used as a protein loading control. **D.** Representative immunoblots of LC3 I, LC3 II, p62, and GAPDH. Statistical significance was given at $p < 0.05$ as follows: one way ANOVA test, Tukey's multiple comparisons, indicated by b vs PA, c vs ConA, e vs puni, f vs puni+PA. Mann–Whitney test indicated by $b^{\#}$ vs PA, $e^{\#}$ vs puni, and # vs PA/PA+ConA and one sample t-test indicated by a* vs control.

5. Main findings

Regarding the first part of the thesis (4.1) it was shown that HFD induces the LD accumulation and affects both proteolytic systems. In Table 5 are depicted the major proteins which were analyzed in the liver of C57BL/6J and NZO mice and compared with our *in vitro* investigation (HepG2/PA) (4.2).

Table 5: Major protein alterations due to strain, HFD (*in vivo* study) and PA treatment (*in vitro* study).

		In vivo		***In vitro***	
	Parameter	**Strain** (C57BL/6J SD vs NZO SD)	**Diet** (NZO SD vs NZO HFD)	**6h PA vs 0h**	**24h PA vs 0h**
LD proteins	TG/LDs	↑	↑	↑	↑
	Plin5	↓	↓	↓	nd
	Plin2	↓	↑	↑	nd
	plin2	↑	↑	nd	↑
Proteasome	β5	↓	↓	↔	↑
	β1	↔	↓	↔	↑
	Rpt6	↑	↓	↔	↔
	20S proteasome activity	↔	↔	↓	↓
	26S proteasome activity	↔	↔	↔	↓
Autophagic system	Beclin-1	↑	↓	↔	↓
	Atg5	↑	↓	↔	↓
	Atg5-Atg12	↑	↓	↔	↓
	Map1lc3 (LC3)	↑	↔	↔	↔
	p-Atg4/Atg4	↔	↓	↔	↔
	LC3 I	↑	↓	↔	↑
	LC3 II	↓	↔	↑	↑
Lysosomal system	*Sqstm1* (p62)	↔	↔	↔	nd
	p62	↑	↑	↑	↑
	LAMP-1	↔	↔	↑	↑
	lysosomal activity	↓	↔	↓	↓

Briefly, the most important findings are the following:

- HFD and PA induce intracellular lipid accumulation in liver of NZO mice and HepG2 cells respectively. The LD protein content alters similarly both *in vivo* and *in vitro* as increased plin2 (gene and protein) and decreased *Plin5* and levels were observed.
- Proteasome is affected by HFD and PA. In NZO HFD mice decreased proteasome subunit levels were detected comparing to NZO SD. However, there is no impact of HFD on proteasome activity. On the contrary, PA restrains the proteasome activity.
- The autophagy-lysosome system is impaired *in vivo* and *in vitro* by strain/diet and PA respectively. More specifically, the first stages of the autophagic system are mainly affected due to HFD in NZO mice and 24h PA treatment in HepG2 cells. p62 accumulation was also observed, which indicates reduced p62 turnover. Therefore, impairment of late stages of the autophagic process occurs by either inhibiting autophagosome-lysosome fusion or lysosomal degradation. Indeed, the lysosomal activity of cysteine cathepsins was reduced in NZO SD mice, comparing to C57BL/6J SD and in PA treated HepG2 cells comparing to control cells.

The second part of the thesis (4.2), allowed us to better understand the mechanism of PA-induced autophagic impairment and the role of proteolytic systems on LD degradation. In particular:

- Observation of the autophagic flux in time showed that PA primarily impairs the late stages (lysosomal system**,** 6h PA treatment) and secondarily the early stages (autophagy system, 24h PA treatment) of the autophagic process.
- Chemical manipulation of both proteolytic systems indicates that mainly autophagy is involved in the bulk LD degradation.

Finally, the third part of the thesis regards the reversion of the LD-induced effects through parallel treatment by punicalagin (4.3). The PA effects which recover due to punicalagin treatment, are summarized in Figure 42.

Briefly, punicalagin:

- reduces the PA-increased LD content
- reduces the increased ROS formation in mitochondria and ER and
- recovers the PA-impaired autophagic flux

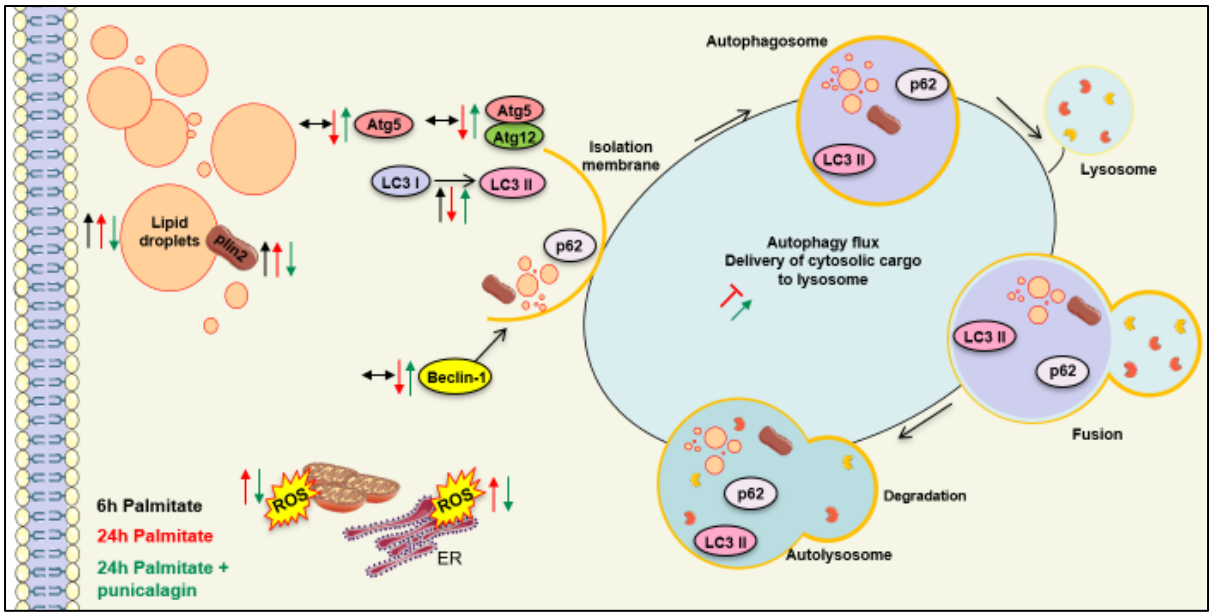

Figure 42: Hepatocellular lipotoxicity is prevented by autophagic removal of excessive LDs. Major alterations of LD- and autophagy related- proteins due to PA treatment in HepG2 cells and recovery after punicalagin treatment. (This figure has been created using templates from Servier Medical Art:SMART [169-172]).

6. Discussion

In the present research, a close examination of the two major intracellular proteolytic systems (ubiquitin-proteasome system and autophagy-lysosome system) was made, in order to examine their potential link with obesity and/or diet-induced hepatocellular damage. The specific research objectives that were addressed and will be discussed on the following sections are:

- Alterations of livers structural integrity and the proteolytic systems functionality due to obesity and HFD - *in vivo* analysis (6.1).
- Insights into the lipotoxic mechanisms in hepatocytes and the involvement of proteolytic systems - *in vitro* analysis (6.2).
- Reversion or limitation of the lipotoxic effects through induction of autophagy by punicalagin, a natural autophagy inducer (6.3).

Overall, clear effects of lipotoxicity on both proteolytic systems were found. Although, it seems that under lipotoxic conditions the function of both proteolytic systems is impaired, there is evidence that autophagy is involved in the bulk LD degradation. Experiments with punicalagin indicate that the lipotoxic effects can be reversed through induction of autophagy. Hence, autophagy can be considered as a therapeutic target.

6.1 Impact of high fat diet on the liver of NZO mice – *in vivo* analysis

Obesity and type 2 diabetes are prevalent metabolic disorders, commonly associated with hepatic steatosis which might have serious consequences on the metabolic performance of hepatocytes [173]. NZO mice is a well-established model of severe obesity and type 2 diabetes, as hyperphagia and reduced energy expenditure in these animal strains, cause adiposity, insulin resistance, dyslipidemia and hypertension [174, 175]. Despite the fact that shortly after weaning, these mouse strains gain weight on a standard diet (SD), a number of different feeding strategies have been proposed to induce an obese phenotype. According to previous investigations, a diet rich in fat induces lipotoxicity and insulin resistance, while additional metabolic challenge with nutritional carbohydrates leads to progressive loss of functional beta-cell mass [174, 176-180]. Despite extensive research in several animal models, the impact of HFD-induced lipotoxicity on proteolytic systems has never been investigated in NZO mice. Since dietary treatment with a diet high in fat is one of the most common strategies to study liver steatosis, a first *in vivo* screening was performed in NZO mice on SD and HFD, in order to get an impression regarding the impact of obesity and diet

on liver proteostasis. Data from C57BL/6J mice on SD were additionally added as a normal wild type control in order to better interpret the results.

6.1.1 High fat diet induces triglyceride, lipid droplet accumulation and cellular injury in the liver of NZO mice

Firstly, possible alterations of liver's structural integrity due to HFD were examined. It was observed that NZO mice have already increased body and liver weight on a SD in comparison to C57BL/6J mice. Indeed, several adipogenic gene variants have been identified that are responsible for accumulation of body fat and hyperphagic behavior [181]. However, NZO mice fed with HFD, containing 30% fat, resulted in severe overweight, accompanied by pronounced high liver weight (Figure 17). It is recognized that oversupply of dietary lipids and reduced capacity of lipid storage in adipose tissue leads to increased circulatory FFA in plasma and lipid accumulation in non-adipose tissues [9]. Hence, FFA in the liver are esterified into TGs, the main constituents of LDs, when lipid uptake is exceeded to lipid utilization [17]. Despite the fact that the presence of LD deposition is a prerequisite for NASH development, it has been proposed that increased FFA levels contribute to hepatocellular lipotoxicity, since their metabolites lead to oxidative stress [182]. A time dependent study in HFD-fed rats demonstrated that prolonged high fat feeding impairs the ability of the liver to synthesize TGs, resulting in significantly elevated serum and hepatic FFA levels [183]. In addition, in clinical settings, increased FFA levels in patients with NASH have been associated with the severity of the disease [184]. In order to determine whether increased TG formation is the cause of the aberrant increased liver weight in HFD-fed NZO mice, hepatic TG and FFA content were measured. A dramatic increase of TG content upon HFD, accompanied by rather unchanged FFA was observed (Figure 18). These findings suggest that after 16 weeks HFD feeding, hepatic FFA were normally converted to TGs and stored in the liver, resulting in increased liver weight and fat mass, which is consistent with signs of fatty liver.

To confirm these data and evaluate histological changes due to HFD, hematoxylin and eosin staining was performed in liver sections (Figure 19). The NAS score was evaluated according to the following three histological features: steatosis, lobular inflammation and hepatocellular ballooning with a categorization: "not NASH" (NAS < 3), "borderline NASH" (NAS 3-4) and "NASH" (NAS $\geq$ 5). Interestingly, NZO mice fed with HFD exhibit pronounced LD accumulation (steatosis) and evident ballooning degeneration, indicating hepatocellular injury. However, no lobular inflammation was observed, obtaining a NAS score of 3.7,

indicating a borderline NASH profile. This could be explained by the duration of HFD feeding. A comparative study in mouse models of obesity induced by hyperphagia or HFD, proposed that over 10 weeks of HFD is needed to develop hepatic steatosis. However, a much longer feeding duration is required, exceeding 40 weeks of HFD, to initiate a mild degree of inflammation, more closely representing NASH [185].

The LD accumulation was further confirmed by detecting the LD-associated proteins plin5 and plin2, since the expression of both perilipins can be modified under physiological conditions such as exercise and aging as well as in pathological states such as obesity [186]. Plin5 is a perilipin protein closely related to FFA catabolism, playing essential role in the delivery of TG from LDs to mitochondria and promoting lipid oxidation. Additionally, plin5 is a protective factor against hepatic lipotoxic damage [187, 188]. Therefore, the gene expression of *Plin5* was analyzed and decreased expression levels in NZO SD mice, comparing to C57BL/6J SD mice was detected (Figure 20A). This could be explained by the fact that NZO mice already on SD exhibit reduced fat oxidation [189]. Interestingly, *Plin5* gene expression was further decreased in HFD fed NZO mice, indicating that plin5 does not participate in HFD-induced LD accumulation and the fatty acid transfer from LD to mitochondria might be downregulated.

Plin2 is the most prevalent perilipin protein in the liver and plays significant role in LD formation and stabilization. In contrast to plin5, plin2 is responsible for fatty acid uptake and lipid storage, while plin2 overexpression has been associated with increased lipogenesis. Additionally, plin2 is positively correlated with cytosolic TG content and LD accumulation under both physiological and pathological conditions [190]. It has been suggested that plin2 expression is critical to induce obesity in HFD-fed mice. According to recent studies in mice, plin2 contributes to the initiation and progression of NAFLD, while its absence reduces the obesity phenotype, by preventing or alleviating the HFD-induced hepatic steatosis and inflammation [191, 192]. In the present study, increased plin2 protein expression in NZO SD mice was detected, comparing to C57BL/6J SD mice (Figure 20C). One potential explanation could be the fact that NZO mice on SD already exhibit increased lipogenesis [193, 194]. The plin2 gene and protein expression were exacerbated in HFD-fed mice as indicated by immunoblot and immunostaining of liver tissues. In Figure 20D it is clearly depicted plin2 surrounding the LD surface in NZO mice fed with HFD. These data suggest the participation of plin2, but not plin5, in the HFD-induced LD accumulation, a finding which is in accordance to the study by Nocetti and colleagues [195].

6.1.2 High fat diet affects the expression of proteasome subunits but not the proteasome activity in NZO mice

The increased LD content and the alteration of LD-associated protein pattern (plin5 and plin2) potentially indicate a decreased LD turnover due to HFD. It is generally assumed that the LD accumulation in the liver is due to extended exposure to high nutritional fat. Liver has the capability to prevent unwanted excessive LD accumulation by initiating the TG transport to the adipose tissue, a process which requires a functional LD breakdown [196]. The degradation or shrinkage of LDs, as described on the introduction (1.5.1), can be mediated by the synergistic action of proteasome, autophagy and lipases.

It has been suggested that proteasome can degrade proteins from the LD surface, including plin2, allowing the access of lipases [48-51, 54]. In addition, proteasome regulates the turnover of proteins involved in signaling pathways, including lipid metabolism and insulin signaling. Hence, misregulation of these pathways underlay the pathophysiology of hepatic steatosis and thereby NAFLD. The impact of HFD on proteasome has never been investigated in NZO mice, while a few studies have been carried out in animal models of type 2 diabetes and obesity, most of them concluding a dysregulated function of proteasome. To investigate whether HFD has any impact on proteasome in NZO mice, proteasome subunits as well as the proteasome activity of both 20S and 26S proteasome were detected. Interestingly, decreased expression of proteasome subunits in HFD-fed mice was observed, although the proteasome activity is not affected (Figure 21, 22). Considering the fact that NZO mice in HFD exhibit insulin resistance, these findings are in accordance to the studies from Rui *et al.* and Ishii *et al.*. These studies described that proteasome activity does not alter under lipotoxic conditions and suggested that enhanced ubiquitination and proteasomal degradation of key insulin signaling proteins are the leading causes of insulin resistance [79, 85]. However, a significant point that should be considered to interpret the present results in NZO mice is the duration of HFD feeding. A time dependent and/or NAFLD stage dependent effect potentially also explains the fact that in spite of the reduced proteasome subunit expression, the proteasome activity is not affected.

6.1.3 High fat diet-induced lipotoxicity affects autophagy

Except for proteasome, LDs can selectively be isolated and degraded by the autophagy-lysosome system (autophagy / lipophagy). Autophagy has emerged as an important regulator in lipid metabolism and has been widely acknowledged for its involvement in the

development of NAFLD. Although several studies have shown that autophagy contributes to the cellular energy balance, providing FFAs and amino acids as energetically essential components, cells not only activate lipolysis upon energetic demand but also as a protective mechanism to prevent stores from becoming enlarged [197]. The impact of HFD-induced lipotoxicity in the autophagic function has controversially been discussed, while investigations in NZO mice have yet to be done. A number of studies in mice with NAFLD support that HFD induces autophagy as a protective mechanism against lipotoxicity [83, 106, 107]. On the contrary, a considerable body of evidence has shown an association between reduced autophagic potential with the development of hepatic steatosis and NAFLD, although, the stage of autophagic process which is impaired is also under discussion [113-125].

In this study, it was observed that in NZO SD mice autophagy-lysosome system is impaired, while HFD further deteriorates the initial steps of the autophagic process. In particular, alterations on the early autophagy stages were firstly investigated by analyzing the protein levels of autophagy related proteins (Atgs). Beclin-1, Atg5 and Atg5-Atg15 along with other proteins are involved in the nucleation and elongation/enclosure step of autophagosome. During this process of autophagosome formation, the soluble LC3 I is released and then conjugated to PE to form LC3 II. The lipidation of LC3 I to LC3 II is critical for the autophagosome maturation and facilitates their fusion with lysosomes and consequent autophagosome degradation. Immunoblot analysis showed elevated levels of Beclin-1, Atg5 and Atg5-Atg12 complex in NZO SD mice, comparing to C57BL/6J SD mice which rather indicate a functional phagophore nucleation. Interestingly, upon HFD reduced expression of all the above mentioned Atgs was observed, indicating its negative impact on autophagosome formation (Figure 23). These findings are in accordance with previous investigations in obese and diabetic mice, which also reported low amount of Atg proteins [114-116, 125-129]. In particular, previous studies in obese mice have demonstrated a direct link between decreased Atg expression, a subsequent impaired autophagy, insulin resistance and hyperinsulinemia [114, 115]. In addition, a study by Yang and colleagues in obese mice demonstrated that Atg5 regulates insulin action, suggesting that its downregulation and impaired autophagosome formation are the leading cause of impaired insulin sensitivity and glucose homeostasis [114]. Indeed, NZO mice upon HFD exhibit the above complications. Alterations in signaling pathways have also been proposed as a potential mechanism for the downregulation of Atgs during HFD. The Peroxisome proliferator-activated receptor δ (PPARδ) for instance, a

stimulator of autophagy flux, was suggested to be involved in the Atg downregulation, as HFD suppresses its expression [116].

To further investigate the impact of HFD on the initial autophagy stages, *Map1lc3* (LC3) gene and LC3 I, LC3 II protein expression were analyzed, as LC3 is involved in phagophore elongation and autophagosome maturation (Figure 24). Increased expression of both *Map1lc3* and LC3 I protein in NZO SD mice comparing to C57BL/6J SD mice were observed, while LC3 II was reduced. This finding rather indicates impairment on the lipidation process of LC3 and therefore, on the autophagosome maturation in NZO SD mice. Studies in obese and type 2 diabetes mouse models also demonstrated reduced LC3 II levels among other Atgs [114-116, 125-129]. Unexpectedly, in NZO mice, upon HFD, the LC3 II levels are not further decreased. In contrast, LC3 I was suppressed accompanied by reduced Atg4 activity (Figure 24D). Since Atg4 is a protein involved in autophagosome biogenesis by facilitating the cleavage process of pro-LC3 into LC3 I [198], this finding gives further evidence that HFD impairs the phagophore processing in NZO mice.

To investigate any alterations on the lysosomal system due to obesity/HFD, the cathepsin lysosomal activity was measured as well as the relative gene and protein expression of the autophagic selective substrate p62 (Figure 25, 26). There is evidence that NZO SD mice exhibit lower cathepsin lysosomal activity comparing to C57BL/6J SD mice. This finding is further supported by unchanged gene expression and elevated levels of p62 protein, indicating accumulation and reduced degradation of p62. At the same time, there is no evidence that HFD further affects the lysosomal system, as there are no changes on the lysosomal activity or number of lysosomes. Additionally, the *Sqstm1* (p62) gene expression remains unaffected while p62 protein further accumulates potentially as a result of the HFD-induced impaired autophagosome formation. These findings are in accordance with previous reports, which proposed that during NAFLD the later steps of autophagy are impaired. In particular, Fukuo and colleagues demonstrated decreased hepatic cathepsin expression in patients with NAFLD [131]. In addition, Fang and colleagues suggested the Transcription factor EB (TFEB), a regulator of lysosomal biogenesis and transcription factor of cathepsin B is decreased upon HFD [126].

Overall, these data give evidence for reduced autophagic potential in obese and diabetic NZO mice. As NZO mice in HFD contain increased LD content and hepatic injury in comparison to NZO in SD, this potentially indicates that the autophagy impairment is highly affected by the

stage of NAFLD. In addition, the decrease in early autophagy initiation proteins might indicate a starting point for the decline in autophagy that is associated with increasing amounts of LDs and TGs in liver of high-fat fed mice. However, a direct connection between impaired autophagy and LD accumulation was not demonstrated in this *in vivo* study. Another limitation is the determination of autophagy flux and alterations of autophagy related proteins in time.

6.2 Impact of palmitate on HepG2 cells - *in vitro* analysis

In order to obtain better insights into the cellular mechanisms of LD-induced lipotoxicity and based on the *in vivo* findings in NZO mice, PA-treated HepG2 cells were used to establish a lipotoxicity model. PA is the most common saturated fatty acid in human serum and Western-style diet, playing a significant role in the pathogenesis of NAFLD [20-22]. Hence, PA-loaded HepG2 cells were used to induce lipotoxicity and investigate its impact on proteolytic systems in the liver.

6.2.1 Palmitate induces lipid droplet accumulation and changes the redox status in HepG2 cells

Since an increased and chronic LD deposition is a hallmark of hepatic steatosis, it was initially investigated whether PA could induce LD retention and subsequently affect the redox state. Consistent with previous related reports it was observed that PA induces intracellular lipid accumulation in a concentration dependent and time dependent manner (Figure 27B, C) [199, 200]. In addition, the FFA content was significantly decreased from 6h to 24h, indicating a rather successful esterification and conversion into TGs (Figure 27D). These findings are in consistency with HFD-fed NZO mice where it was also observed increased LD formation due to diet.

The LD-associated proteins are essential for the normal cellular physiology, regulating the balance between lipid storage and lipolysis. Hence, the differential expression of these proteins is strongly associated with dysegulation of intracellular lipid accumulation and thereafter with several metabolic disorders [190, 201]. During hepatic steatosis, the composition of LD-associated proteins alters and contributes to changes in lipid metabolism [41]. Plin2 and CIDEA are LD-associated proteins that both promote lipid deposition. Most importantly, plin2 provides LD stabilization [202] and inhibits fatty acid oxidation [46], while CIDEA promotes the formation of large LDs [40]. According to a recent study, CIDEA is differentially expressed in liver, depending on stage and severity of NAFLD [203]. Both plin2

and CIDEA are upregulated in rodents and humans with NAFLD and play a significant role in the pathogenesis of hepatic steatosis. By contrast, plin5 has been suggested to play a protective role against lipotoxicity [45, 204-208]. A study in hepatocytes indicated that plin5 reduces the PA-induced apoptotic rates and mitochondrial damage. Plin5 maintains the appropriate balance between fatty acid storage and catabolism during periods of lipid overload. In addition, it specifically antagonizes lipases and facilitates the fatty acid flow, acting as an "active bridge" between LDs and mitochondria, and thereby preventing ROS damage and a consequent lipotoxicity.

In this study, similarly to HFD-fed NZO mice, it was observed that PA induces plin2 (gene and protein) and suppress the gene expression of *Plin5*. In addition, *Cidea*, a LD-associated protein particularly induced upon saturated fatty acids, is also upregulated in presence of PA treatment (Figure 28). The increased LD content results from imbalance between lipid storage and lipolysis or secretion [46]. It is therefore quite interesting the fact that PA upregulates *Plin2* and *Cidea* which promote the LD stabilization, while *Plin5* that facilitates lipolysis is suppressed. Apparently, the protein pattern that covers the LD is a signal for the regulation of TG turnover. On the basis of present knowledge, it seems that LDs which predominantly are coated with plin2 or CIDEA, store neutral lipids and that their excessive accumulation contributes to metabolic dysregulation. On the contrary, LDs that predominantly are covered by plin5 are available for lipolysis, contributing less to disease onset [182].

The increased lipid accumulation and disturbances in lipid metabolism affect different ROS generators, including mitochondria and ER. Hence, the increased H_2O_2 and other ROS formation in cellular compartments might diffuse within the cell and cause alterations in cellular redox status. Given that oxidative stress has been described as an important contributor of PA-induced lipotoxic damage in hepatocytes [209-213], potential redox changes in cellular compartments were next determined. Interestingly, increased H_2O_2 formation was detected in mitochondria and ER but not in the cytosol, suggesting a shift in redox status (Figure 29). Both mitochondria and ER are key mediators of FFA catabolism during hepatic steatosis. In mitochondria fatty acids undergo β-oxidation. However, when the mitochondrial oxidation system is inadequate to metabolize excess fatty acids ω-oxidation, an alternative pathway of fatty acid metabolism, can be activated in ER [214]. It appears therefore that due to PA overload an adapted response stress occurs primarily to mitochondria and secondly to ER as a consequence of mitochondria overworking. The increased ROS generation in mitochondria might be connected to decreased plin5 levels, since it has been

previously reported that plin5 deficiency can increase ROS damage and impair mitochondrial function [216]. Additionally, these findings might indicate a beginning of mitochondrial dysfunction and ER stress. During metabolic dysregulation, many consequences like a slight but chronic redox-shift can be progressed to a more oxidative state, namely systemic inflammation that increased ROS generation, UPR, ER and mitochondrial stress. Indeed, it has been suggested that during metabolic disorders, extensive pathological changes are caused by long-term manifestation of slight but chronic oxidative stress [217]. These changes not only accumulate over time to massive and possibly irreversible pathologies but also affect signaling pathways in lipid metabolism, including insulin sensitivity [218]. In addition, redox changes can also affect proteasome and autophagy, as both proteolytic systems are important sensors of the redox signaling but also highly susceptible to redox changes [56, 219].

6.2.2 Palmitate-induced lipotoxicity affects the proteasome activity

The current knowledge regarding the impact of PA-mediated lipotoxicity on proteasome is limited, although there is evidence that proteasome is involved in the pathogenesis of NAFLD. Impaired proteasome function under lipotoxic conditions has been proposed by a set of studies [76, 78, 83, 84], while other investigations suggest that proteasome is not affected, although it is involved in the pathogenesis of NAFLD by affecting the stability of several key functional proteins [49-52, 72-75, 77, 85, 86]. This discrepancy in the literature might be explained by the fact that there is a lack of investigation regarding the impact of lipotoxicity on proteasome's functionality in time. To investigate therefore whether PA also affects proteasome, proteasome subunits and activity were detected after 6h and 24h PA exposure. It was observed that 6h PA treatment already impairs the activity of 20S proteasome. After 24h PA treatment the proteasome activity of 26S proteasome was also impaired while the β-catalytic subunits were upregulated (Figure 31, 32). In concert with these findings, previous analyses of liver tissue in mouse models with type 2 diabetes and obesity, also revealed a coordinate decrease of 26S proteasome activity and increased proteasome components, which might indicate a compensatory mechanism against impaired proteasome function [78].

Under lipotoxic conditions, proteasome dysfunction has been suggested to be a primary event which mediates UPR activation and ER stress which in turn leads to hepatic insulin resistance, all typical characteristics in NAFLD [78]. The reason that during obesity and type 2 diabetes the proteasome function is impaired remains unclear, although it has been reported that fatty acid, insulin, mitochondrial dysfunction and oxidative stress impairs the proteasome activity [56, 88]. ATP deficiency in NAFLD mice liver due to reduced stability of oxidative

phosphorylation complex subunits in mitochondria has been suggested to contribute to reduced proteasomal degradation [83]. The decreased proteasome activity might also be explained by potential post-translational modifications of proteasome subunits [56]. H_2O_2 derivatives, such as peroxinitrite, have been proposed to inhibit the proteasome activity [220]. In addition, several studies of proteasome oxidation demonstrated that specific subunits of proteasome are preferentially modified by reactive lipids [221-223]. Despite the fact that the precise mechanisms behind the impairment of catalytic activity remain complex, it is evident that post-translational modifications of proteasome subunits is a dynamic regulatory process in proteolysis. However, a direct link between lipotoxic stress and proteasome changes remain to be determined. Although other mechanisms for proteasome impairment cannot be excluded, this conclusion is also consistent with the critical role of ER and mitochondrial stress that characterizes NAFLD.

6.2.3 Palmitate-induced lipotoxicity affects time dependently the autophagy system

As described above, the current *in vivo* study in NZO mice as well as other studies in humans and rodents with NAFLD suggests that lipotoxicity impairs the autophagic potential, although the stage and the underlying mechanisms are under discussion. Hyperinsulinemia and downregulation of Atg proteins have been suggested to contribute to impaired autophagosome formation [114, 115] In contrast, some reports suggest that later steps of autophagosome maturation, such as autophagosome-lysosome fusion and acidification, are impaired, rather than autophagosome formation. Additionally, a study in mouse liver suggested that HFD affects the fusion [130], while in patients with NAFLD decreased hepatic cathepsin expression has been found [131]. Similarly to the above-mentioned *in vivo* studies, the impact of PA-mediated hepatic lipotoxicity on the autophagic system has also extensively been investigated although it has been controversially discussed. A number of studies support that PA induces autophagy as a defensive mechanism against cellular dysfunction [108-110]. By contrast, a study by Ding and colleagues demonstrated that PA fails to induce autophagy [224] and a number of more recent studies indicated that PA impairs the autophagic flux [127-129]. Since NAFLD is a progressed disease, it can be speculated that lipotoxicity can time-dependently impair the autophagic process.

In order to clarify which stage of the autophagic process is impaired and how PA affects autophagy in time, potential alterations of Atg levels as well as the autophagic flux after short (6h) and long time (24h) PA treatment were determined (Figure 33-36). It was observed that 6h PA treatment inhibits the lysosomal degradation while the early stages of the

autophagosome formation as well as the autophagy flux remain unaffected. In particular, after 6h PA exposure there were no significant changes on the protein levels of Beclin-1, Atg5 and Atg5-Atg15, comparing to untreated cells. In addition, increased LC3 II / LC3 I ratio was observed, indicating increased formation of LC3 II and therefore functional autophagosome formation / maturation. However, increased p62 levels were detected, indicating a rather p62 accumulation and reduced turnover. The decreased lysosomal degradation rate is further supported by the reduced cathepsin lysosomal activity. In addition, increased number of lysosomes was detected, as indicated by enhanced LAMP-1 levels, which might explain a compensatory mechanism against the failure in lysosomal degradation.

After long time PA treatment (24h), decreased cathepsin lysosomal activity and increased p62 protein levels were still observed. However, mRNA levels remain unchanged, indicating p62 protein accumulation and reduced turnover. Similarly to 6h, after 24h PA treatment enhanced LAMP-1 levels were detected, suggesting increased lysosome content and a rather compensatory upregulation of lysosomes. A similar observation was demonstrated in a study by Declèves and colleagues in kidneys of obese mice [225]. In this study, electron microscopy demonstrated increased LAMP-1 levels and enlarged lysosomes, suggesting an overload of the lysosomal system and accumulation of lysosomes.

It appears therefore that both, 6h and 24h PA exposure impair the late stage of the autophagic process either by inhibiting the lysosomal degradation, as it is indicated by the reduced lysosomal activity of cysteine cathepsins, or the autophagosome-lysosome fusion. The latter might be explained by alterations in lipid composition of the autophagosomal and lysosomal membrane as a consequence of the increased lipid content. Hence, the ability of autophagosomes to fuse with lysosomes reduces, leading to impairment of the autophagic flux [130]. Rubicon has also been recently suggested as a significant negative regulator of the autophagic process. It is localized at the lysosomes and it is responsible for accelerating hepatic lipid accumulation as well as impaired autophagy maturation. Tanaka and colleagues recently demonstrated that saturated fatty acids, such as PA, specifically upregulate Rubicon which further suppresses the fusion of autophagosomes with lysosomes [129]. Most importantly, Rubicon is partially degraded by the proteasome system. Since the present dissertation and other studies demonstrated that PA impairs the proteasome activity, it can be speculated that the degradation of Rubicon might be further suppressed, eventually leading to its increased expression.

Interestingly, apart from the inhibition of the late stages, 24h PA exposure has also a negative impact on the early stages of autophagy, affecting the protein levels of Atgs Beclin1, Atg5 and Atg5-Atg12 complex as well as the LC3 II conversion. In particular, reduced LC3 II / LC3 I ratio was observed after 24h PA treatment in comparison to 6h PA, suggesting impaired LC3 I conversion to LC3 II. The decreased levels of Atg5-Atg12, a complex that supports the lipidation process, corroborates the notion of impaired LC3 lipidation and consequently autophagosome maturation. Additionally, LC3 I levels further increased, although the activity of Atg4, the protein which facilitates the cleavage process of pro-LC3, is not affected (Suppl. Figure 2). This might indicate a compensatory mechanism against the failure in autophagic flux. The reduced Atg expression suggests impaired autophagosome formation and has extensively been reported in several experimental models with lipotoxicity [116, 126-129]. Several autophagic regulators and transcription factors of Atgs have been reported to differentially be expressed upon PA and HFD treatment. PPARγ and δ for instance, a stimulator of autophagy flux, has been described to be reduced upon PA treatment, leading to reduced Atg expression [116, 199, 226]. In addition, TFEB, a transcription factor of ATGs and lysosomal genes has been demonstrated to be downregulated upon PA treatment [126]. Defective autophagy is closely related to the development of ER stress, mitochondrial dysfunction and hepatic insulin resistance [227]. Therefore, it is possible that impairment of both proteasome- and autophagy-mediated protein degradation under PA-mediated lipotoxic conditions further exacerbate ER and mitochondrial stress and potentially leads after extensive PA exposure to a cellular oxidative stress.

Collectively, these data provide evidence that PA exposure impairs the autophagy-lysosome system, starting from the late stage of the autophagic process either by inhibiting autophagosome-lysosome fusion or the lysosomal degradation and continuing to the initial stages of the autophagosome formation-maturation. Similar findings were observed also in the *in vivo* analysis of NZO mice, where it was also observed reduced Atg expression and lysosomal activity. In addition, these data are consistent with the most recent studies in hepatocytes, which demonstrated that PA impairs the autophagic flux [127-129]. In addition, a study by Ding and colleagues also examined the autophagy dynamics in response to progressive steatosis and proposed an initial activation of autophagic flux as a protective response against lipotoxicity, following a late inhibition as a result of continuous metabolic stress [112]. This recent study by Ding and colleagues and the current dissertation, to the best of knowledge are the first reports that demonstrated a time dependent alteration on the autophagy flux. The current dissertation, however, additionally demonstrates a time-

dependent impairment of the different autophagic stages in response to PA-induced lipotoxicity.

6.2.4 Autophagy but not proteasome regulates the bulk lipid droplet degradation suggesting a therapeutic target for the treatment of palmitate-induced lipotoxicity

Given that both proteasome and autophagy are involved on the LD degradation, it appears that the increased LD accumulation under PA-induced lipotoxic conditions is due to impaired proteolytic function and thus decreased LD turnover. To investigate that assumption, alterations of the intracellular lipid content were observed after induction or inhibition of proteasome and autophagy in PA-treated HepG2 cells (Figure 32, 37). Interestingly, the intracellular lipid content was significantly increased only after inhibition of autophagy and decreased after its induction, indicating a direct control of lipid content by autophagy but not by proteasome. Apparently, despite the fact that proteasome controls the degradation of several LD-associated proteins significant for the LD stabilization, autophagy is critical and rather responsible for the bulk degradation of LD in hepatocytes. Indeed, previous studies performed in hepatocytes and demonstrated that modulation of autophagy affect the intracellular lipid content [105, 228]. However, to the best of knowledge, similar studies regarding the role of proteasome on the regulation of total LD content have not performed before.

These observations suggest that autophagy is a potential therapeutic target against PA-induced lipotoxicity by reducing the increased LD accumulation. Despite the fact that impaired proteasome is implicated in the development of NAFLD its involvement in several metabolic cascades makes it a rather complicated therapeutic target. Due to the fact that proteasome degrades proteins implicated in signaling pathways, a direct targeting of proteasome may cause changes in multiple signaling pathways. By contrast promotion of autophagy potentially has a positive impact due to its ability to remove not only misfolded proteins, but also various cellular components such as damaged mitochondria and excess LDs.

6.3 Punicalagin reverses the palmitate-induced effects through induction of autophagy

In order to investigate whether the PA-induced lipotoxic effects can be reversed via stimulation of the autophagic process, punicalagin was applied to PA-treated HepG2 cells. Punicalagin is a natural compound which has previously been reported to enhance autophagy [145, 146] and have hepatoprotective effects [228, 229]. Although much of the literature has

focused on its antioxidant and anti-inflammatory effects, whether punicalagin can alleviate the PA-induced lipotoxicity via the autophagic pathway has yet to be investigated.

Notably, coincubation of punicalagin with PA attenuates the increased LD content, as well as the protein levels of plin2 (Figure 38). The latter is quite remarkable, given that plin2 levels in the liver are considered as a marker of LD accumulation and it is highly correlated with the degree of hepatic steatosis [191, 192, 230]. Increased plin2 levels are also associated with oxidative damage [195]. Interestingly, the increased H_2O_2 levels in mitochondria and ER, due to PA treatment, are reduced in presence of punicalagin (Figure 39). These findings support previous studies in hepatocytes, showing that the steatosis phenotype can be rescued via treatment with punicalagin, by promoting mitochondrial function and eliminating inflammation and oxidative stress [141, 147]. These observations might indicate mitochondrial efficiency and improved lipid turnover.

In order to investigate whether punicalagin has also a positive impact on the autophagy function, the Atg protein levels as well as the autophagy flux were analyzed. The most striking initial finding is that the reduced levels of autophagy related proteins Beclin1, Atg5 and Atg5-Atg12 complex are restored in presence of punicalagin, which potentially indicates improved LC3 II formation and therefore capable autophagosome formation and LC3 lipidation (Figure 40). Most importantly, the degradation of LC3 II was increased in presence of punicalagin and PA cotreatment in comparison to PA alone (Figure 41B). Additionally, the p62 levels were decreased, indicating increased p62 turnover and therefore a rescued autophagic flux (Figure 41). Since a well characterized mechanism of punicalagin's anti-inflammatory action is the activation of PPARs, one possible explanation of its positive effect on autophagic flux can be the activation of the autophagy stimulator PPARδ [231]. However, further investigations should be performed to justify that hypothesis.

Collectively, these data provide evidence of punicalagins therapeutic effects on PA-induced hepatic lipotoxicity through induction of autophagy. Punicalagin alleviates the PA-induced lipid accumulation as well as the mitochondrial and ER redox imbalance, potentially by modulating the autophagic pathway. Punicalagin induces autophagy and restores the PA-impaired autophagic flux. It appears that acts on the early autophagic stages and upregulates the autophagy-related proteins Beclin1, Atg5 and Atg5-Atg12 complex. Induction of autophagy therefore reduces the burden of FFA transported or synthesized in the liver.

7. Outlook

A better understanding of the molecular mechanisms underlying liver dysfunction during the development of NAFLD, will redirect potent strategies of disease treatment. Therefore, the present doctoral thesis, was performed to improve the current knowledge of diet-induced metabolic stress on liver functionality and integrity, focusing on the role of the two major proteolytic systems, proteasome and autophagy. Undoubtedly, NAFLD is a complex and multifactorial process. Mitochondrial dysfunction, ER stress and perturbation of both autophagy and proteasome are some of the suggested mechanisms of its pathogenesis. In this study, it was demonstrated *in vivo* and *in vitro* that lipotoxicity affects the function of both proteolytic systems. However, despite the fact that proteasome controls the LD stabilization, it appears that autophagy is rather responsible for the bulk degradation of LDs.

These observations suggest that targeting autophagy is a promising therapeutic approach to reduce lipotoxicity. Indeed, experiments with the natural autophagy inducer punicalagin, alleviated the PA-induced lipotoxic effects *in vitro*. However, the exact mechanism of autophagy upregulation due to punicalagin remains unclear. Activation of PPARs is a well characterized mechanism of punicalagin's anti-inflammatory action. Thus, activation of the autophagy stimulator PPARδ could be a possible explanation of its positive effect on autophagic flux. A possible relevance of punicalagin to TFEB induction should also be investigated in further studies, as it has been suggested that pomegranate extract mediates the upregulation of autophagy and lysosomal genes through TFEB activation.

Promotion of autophagy potentially has a positive impact due to the ability of clearance excess LD and damaged cellular components including mitochondria and misfolded proteins. The pharmacological activation and inhibition of autophagy have proven benefits against obesity and metabolic diseases however, only in preclinical studies. Currently, the only therapeutic options for NAFLD remain lifestyle interventions, involving dietary modifications and changes in physical activity. Notably, caloric restriction and exercise are also two main autophagic stimuli. The current study is the first that demonstrates the protective effects of punicalagin on the hepatic lipotoxicity through the induction of autophagic pathway. These findings therefore, should be strengthened by further *in vivo* investigations, in order to test the therapeutic potential of punicalagin in NAFLD.

By contrast, targeting proteasome as a therapeutic approach appears to be more challenging and its role in the development of NAFLD requires further investigation. In this study it was observed that lipotoxicity affects proteasome by altering its subunit expression and/or activity.

However why these alterations occur remains to be elucidated. One possible explanation could be that under lipotoxic conditions post translational modifications can occur to proteasome subunits, resulting in proteasome activity impairment. Additionally, lipotoxicity might affect the activity of transcription factors which control the expression of proteasome subunits. How these alterations of proteasome contribute to the development of NAFLD should also be answered. Despite the fact that proteasome regulates the stabilization of LD, in this study it was observed that under lipotoxic conditions the massive LD amount is not controlled by proteasome. Therefore, proteasome might contribute to the pathogenesis of NAFLD via signaling or metabolic pathways including UPR induction, ER stress and insulin resistance. This hypothesis, however, require additional research.

8. References

1. Zhang, X., et al., *New insight into inter-organ crosstalk contributing to the pathogenesis of non-alcoholic fatty liver disease (NAFLD).* Protein & cell, 2018. **9**(2): p. 164-177.
2. Montgomery, M.K., W. De Nardo, and M.J. Watt, *Impact of Lipotoxicity on Tissue "Cross Talk" and Metabolic Regulation.* Physiology (Bethesda), 2019. **34**(2): p. 134-149.
3. https://smart.servier.com/smart_image/muscle-5/
4. https://smart.servier.com/smart_image/heart-9/
5. https://smart.servier.com/smart_image/pancreas-2/
6. https://smart.servier.com/smart_image/liver-2/
7. Younossi, Z., et al., *Global burden of NAFLD and NASH: trends, predictions, risk factors and prevention.* Nat Rev Gastroenterol Hepatol, 2018. **15**(1): p. 11-20.
8. Lonardo, A., et al., *Epidemiology and pathophysiology of the association between NAFLD and metabolically healthy or metabolically unhealthy obesity.* Ann Hepatol, 2020. **19**(4): p. 359-366.
9. Mundi, M.S., et al., *Evolution of NAFLD and Its Management.* Nutr Clin Pract, 2020. **35**(1): p. 72-84.
10. Samuel, V.T., et al., *Mechanism of hepatic insulin resistance in non-alcoholic fatty liver disease.* J Biol Chem, 2004. **279**(31): p. 32345-53.
11. Irimia, J.M., et al., *Lack of liver glycogen causes hepatic insulin resistance and steatosis in mice.* J Biol Chem, 2017. **292**(25): p. 10455-10464.
12. Gordillo, M., T. Evans, and V. Gouon-Evans, *Orchestrating liver development.* Development, 2015. **142**(12): p. 2094-108.
13. Lorente, S., M. Hautefeuille, and A. Sanchez-Cedillo, *The liver, a functionalized vascular structure.* Sci Rep, 2020. **10**(1): p. 16194.
14. Ricken, T., et al., *Modeling function-perfusion behavior in liver lobules including tissue, blood, glucose, lactate and glycogen by use of a coupled two-scale PDE-ODE approach.* Biomech Model Mechanobiol, 2015. **14**(3): p. 515-36.
15. Sørensen, K.K., et al., *Liver Sinusoidal Endothelial Cells.* Compr Physiol, 2015. **5**(4): p. 1751-74.
16. Mashek, D.G., *Hepatic fatty acid trafficking: multiple forks in the road.* Adv Nutr, 2013. **4**(6): p. 697-710.

17. Gluchowski, N.L., et al., *Lipid droplets and liver disease: from basic biology to clinical implications.* Nat Rev Gastroenterol Hepatol, 2017. **14**(6): p. 343-355.
18. Estadella, D., et al., *Lipotoxicity: effects of dietary saturated and transfatty acids.* Mediators Inflamm, 2013. **2013**: p. 137579.
19. Mendez-Sanchez, N., et al., *New Aspects of Lipotoxicity in Nonalcoholic Steatohepatitis.* Int J Mol Sci, 2018. **19**(7).
20. Carta, G., et al., *Palmitic Acid: Physiological Role, Metabolism and Nutritional Implications.* Front Physiol, 2017. **8**: p. 902.
21. de Almeida, I.T., et al., *Plasma total and free fatty acids composition in human non-alcoholic steatohepatitis.* Clin Nutr, 2002. **21**(3): p. 219-23.
22. Ogawa, Y., et al., *Palmitate-induced lipotoxicity is crucial for the pathogenesis of nonalcoholic fatty liver disease in cooperation with gut-derived endotoxin*. Sci Rep, 2018. **8**(1): p. 11365.
23. Turchinovich, A., et al., *Cell-Free Circulating Nucleic Acids as Early Biomarkers for NAFLD and NAFLD-Associated Disorders.* Front Physiol, 2018. **9**: p. 1256.
24. Brunt, E.M., et al., *Nonalcoholic fatty liver disease (NAFLD) activity score and the histopathologic diagnosis in NAFLD: distinct clinicopathologic meanings.* Hepatology, 2011. **53**(3): p. 810-20.
25. Caldwell, S., et al., *Hepatocellular ballooning in NASH.* J Hepatol, 2010. **53**(4): p. 719-23.
26. Kleiner, D.E., et al., *Design and validation of a histological scoring system for nonalcoholic fatty liver disease.* Hepatology, 2005. **41**(6): p. 1313-21.
27. Takahashi, Y. and T. Fukusato, *Histopathology of nonalcoholic fatty liver disease/nonalcoholic steatohepatitis.* World J Gastroenterol, 2014. **20**(42): p. 15539-48.
28. Chen, Z., et al., *Role of oxidative stress in the pathogenesis of nonalcoholic fatty liver disease*. Free Radic Biol Med, 2020. **152**: p. 116-141.
29. Paradies, G., et al., *Oxidative stress, cardiolipin and mitochondrial dysfunction in nonalcoholic fatty liver disease.* World J Gastroenterol, 2014. **20**(39): p. 14205-18.
30. Simões, I.C.M., et al., *Mitochondria in non-alcoholic fatty liver disease.* Int J Biochem Cell Biol, 2018. **95**: p. 93-99.
31. Lee, J., J.S. Park, and Y.S. Roh, *Molecular insights into the role of mitochondria in non-alcoholic fatty liver disease*. Arch Pharm Res, 2019. **42**(11): p. 935-946.

32. Ashraf, N.U. and T.A. Sheikh, *Endoplasmic reticulum stress and Oxidative stress in the pathogenesis of Non-alcoholic fatty liver disease.* Free Radic Res, 2015. **49**(12): p. 1405-18.
33. Lebeaupin, C., et al., *Endoplasmic reticulum stress signalling and the pathogenesis of non-alcoholic fatty liver disease.* J Hepatol, 2018. **69**(4): p. 927-947.
34. Mantzaris, M.D., E.V. Tsianos, and D. Galaris, *Interruption of triacylglycerol synthesis in the endoplasmic reticulum is the initiating event for saturated fatty acid-induced lipotoxicity in liver cells.* Febs j, 2011. **278**(3): p. 519-30.
35. Hetz, C., K. Zhang, and R.J. Kaufman, *Mechanisms, regulation and functions of the unfolded protein response.* Nat Rev Mol Cell Biol, 2020. **21**(8): p. 421-438.
36. Li, Y.R., H. Zhu, and I. Danelisen, *Role of Peroxiredoxins in Protecting Against Cardiovascular and Related Disorders.* Cardiovasc Toxicol, 2020. **20**(5): p. 448-453.
37. Cox, A.G., C.C. Winterbourn, and M.B. Hampton, *Measuring the redox state of cellular peroxiredoxins by immunoblotting.* Methods Enzymol, 2010. **474**: p. 51-66.
38. Onal, G., et al., *Lipid Droplets in Health and Disease.* Lipids Health Dis, 2017. **16**(1): p. 128.
39. Xu, S., X. Zhang, and P. Liu, *Lipid droplet proteins and metabolic diseases.* Biochim Biophys Acta Mol Basis Dis, 2018. **1864**(5 Pt B): p. 1968-1983.
40. Olzmann, J.A. and P. Carvalho, *Dynamics and functions of lipid droplets.* Nat Rev Mol Cell Biol, 2019. **20**(3): p. 137-155.
41. Zhang, S., et al., *Morphologically and Functionally Distinct Lipid Droplet Subpopulations.* Sci Rep, 2016. **6**: p. 29539.
42. Sztalryd, C. and D.L. Brasaemle, *The perilipin family of lipid droplet proteins: Gatekeepers of intracellular lipolysis.* Biochim Biophys Acta Mol Cell Biol Lipids, 2017. **1862**(10 Pt B): p. 1221-1232.
43. Zhang, X., Y. Wang, and P. Liu, *Omic studies reveal the pathogenic lipid droplet proteins in non-alcoholic fatty liver disease.* Protein Cell, 2017. **8**(1): p. 4-13.
44. Itabe, H., et al., *Perilipins: a diversity of intracellular lipid droplet proteins.* Lipids Health Dis, 2017. **16**(1): p. 83.
45. Wang, H., et al., *Perilipin 5, a lipid droplet-associated protein, provides physical and metabolic linkage to mitochondria.* J Lipid Res, 2011. **52**(12): p. 2159-68.
46. Carr, R.M. and R.S. Ahima, *Pathophysiology of lipid droplet proteins in liver diseases.* Exp Cell Res, 2016. **340**(2): p. 187-92.

47. Zhou, L., et al., *Cidea promotes hepatic steatosis by sensing dietary fatty acids.* Hepatology, 2012. **56**(1): p. 95-107.
48. Kory, N., et al., *Protein Crowding Is a Determinant of Lipid Droplet Protein Composition.* Dev Cell, 2015. **34**(3): p. 351-63.
49. Masuda, Y., et al., *ADRP/adipophilin is degraded through the proteasome-dependent pathway during regression of lipid-storing cells.* J Lipid Res, 2006. **47**(1): p. 87-98.
50. Xu, G., et al., *Post-translational regulation of adipose differentiation-related protein by the ubiquitin/proteasome pathway.* J Biol Chem, 2005. **280**(52): p. 42841-7.
51. Choi, K., et al., *Regulation of diacylglycerol acyltransferase 2 protein stability by gp78-associated endoplasmic-reticulum-associated degradation.* Febs j, 2014. **281**(13): p. 3048-60.
52. Ghosh, M., et al., *Ubiquitin Ligase COP1 Controls Hepatic Fat Metabolism by Targeting ATGL for Degradation.* Diabetes, 2016. **65**(12): p. 3561-3572.
53. Kaushik, S. and A.M. Cuervo, *Degradation of lipid droplet-associated proteins by chaperone-mediated autophagy facilitates lipolysis.* Nat Cell Biol, 2015. **17**(6): p. 759-70.
54. Kaushik, S. and A.M. Cuervo, *AMPK-dependent phosphorylation of lipid droplet protein PLIN2 triggers its degradation by CMA.* Autophagy, 2016. **12**(2): p. 432-8.
55. Kory, N., R.V. Farese, Jr., and T.C. Walther, *Targeting Fat: Mechanisms of Protein Localization to Lipid Droplets.* Trends Cell Biol, 2016. **26**(7): p. 535-546.
56. Korovila, I., et al., *Proteostasis, oxidative stress and aging.* Redox Biol, 2017. **13**: p. 550-567.
57. Schulze, R.J., A. Sathyanarayan, and D.G. Mashek, *Breaking fat: The regulation and mechanisms of lipophagy.* Biochim Biophys Acta Mol Cell Biol Lipids, 2017. **1862**(10 Pt B): p. 1178-1187.
58. Zhang, X., et al., *Classical and alternative roles for autophagy in lipid metabolism.* Curr Opin Lipidol, 2018. **29**(3): p. 203-211.
59. Schulze, R.J., et al., *Hepatic Lipophagy: New Insights into Autophagic Catabolism of Lipid Droplets in the Liver.* Hepatol Commun, 2017. **1**(5): p. 359-369.
60. Chondrogianni, N., et al., *Protein damage, repair and proteolysis.* Mol Aspects Med, 2014. **35**: p. 1-71.
61. Pickering, A.M. and K.J. Davies, *Degradation of damaged proteins: the main function of the 20S proteasome.* Prog Mol Biol Transl Sci, 2012. **109**: p. 227-48.

62. Ben-Nissan, G. and M. Sharon, *Regulating the 20S proteasome ubiquitin-independent degradation pathway.* Biomolecules, 2014. **4**(3): p. 862-84.
63. Hugo, M., et al., *Early cysteine-dependent inactivation of 26S proteasomes does not involve particle disassembly.* Redox Biol, 2018. **16**: p. 123-128.
64. Jung, T. and T. Grune, *The proteasome and the degradation of oxidized proteins: Part I-structure of proteasomes.* Redox Biol, 2013. **1**(1): p. 178-82.
65. Maupin-Furlow, J., *Proteasomes and protein conjugation across domains of life*. Nat Rev Microbiol, 2011. **10**(2): p. 100-11.
66. Jung, T., B. Catalgol, and T. Grune, *The proteasomal system.* Mol Aspects Med, 2009. **30**(4): p. 191-296.
67. Liu, C.W., et al., *Conformational remodeling of proteasomal substrates by PA700, the 19 S regulatory complex of the 26 S proteasome.* J Biol Chem, 2002. **277**(30): p. 26815-20.
68. Collins, G.A. and A.L. Goldberg, *The Logic of the 26S Proteasome*. Cell, 2017. **169**(5): p. 792-806.
69. Bar-Nun, S. and M.H. Glickman, *Proteasomal AAA-ATPases: structure and function*. Biochim Biophys Acta, 2012. **1823**(1): p. 67-82.
70. Schulman, B.A. and J.W. Harper, *Ubiquitin-like protein activation by E1 enzymes: the apex for downstream signalling pathways.* Nat Rev Mol Cell Biol, 2009. **10**(5): p. 319-31.
71. Metzger, M.B., et al., *RING-type E3 ligases: master manipulators of E2 ubiquitin-conjugating enzymes and ubiquitination.* Biochim Biophys Acta, 2014. **1843**(1): p. 47-60.
72. Eastman, S.W., M. Yassaee, and P.D. Bieniasz, *A role for ubiquitin ligases and Spartin/SPG20 in lipid droplet turnover.* J Cell Biol, 2009. **184**(6): p. 881-94.
73. Hooper, C., et al., *Spartin activates atrophin-1-interacting protein 4 (AIP4) E3 ubiquitin ligase and promotes ubiquitination of adipophilin on lipid droplets.* BMC Biol, 2010. **8**: p. 72.
74. Alberts, P. and D. Rotin, *Regulation of lipid droplet turnover by ubiquitin ligases.* BMC Biol, 2010. **8**: p. 94.
75. Weisshaar, N., et al., *Phospholipase Lpl1 links lipid droplet function with quality control protein degradation.* Mol Biol Cell, 2017. **28**(6): p. 716-725.

76. Tomaru, U., et al., *Decreased proteasomal activity causes age-related phenotypes and promotes the development of metabolic abnormalities.* Am J Pathol, 2012. **180**(3): p. 963-972.
77. Nagarajan, S.R., et al., *Correction: Insulin and diet-induced changes in the ubiquitin-modified proteome of rat liver.* PLoS One, 2017. **12**(9): p. e0184610.
78. Otoda, T., et al., *Proteasome dysfunction mediates obesity-induced endoplasmic reticulum stress and insulin resistance in the liver.* Diabetes, 2013. **62**(3): p. 811-24.
79. Rui, L., et al., *SOCS-1 and SOCS-3 block insulin signaling by ubiquitin-mediated degradation of IRS1 and IRS2.* J Biol Chem, 2002. **277**(44): p. 42394-8.
80. Litwak, S.A., et al., *Lipotoxic Stress Induces Pancreatic β-Cell Apoptosis through Modulation of Bcl-2 Proteins by the Ubiquitin-Proteasome System.* J Diabetes Res, 2015. **2015**: p. 280615.
81. López-Avalos, M.D., et al., *Evidence for a role of the ubiquitin-proteasome pathway in pancreatic islets.* Diabetes, 2006. **55**(5): p. 1223-31.
82. Díaz-Ruiz, A., et al., *Proteasome Dysfunction Associated to Oxidative Stress and Proteotoxicity in Adipocytes Compromises Insulin Sensitivity in Human Obesity.* Antioxid Redox Signal, 2015. **23**(7): p. 597-612.
83. Lee, K., et al., *Hepatic Mitochondrial Defects in a Nonalcoholic Fatty Liver Disease Mouse Model Are Associated with Increased Degradation of Oxidative Phosphorylation Subunits.* Mol Cell Proteomics, 2018. **17**(12): p. 2371-2386.
84. Hamel, F.G., *Preliminary report: inhibition of cellular proteasome activity by free fatty acids.* Metabolism, 2009. **58**(8): p. 1047-9.
85. Ishii, M., et al., *Palmitate induces insulin resistance in human HepG2 hepatocytes by enhancing ubiquitination and proteasomal degradation of key insulin signaling molecules.* Arch Biochem Biophys, 2015. **566**: p. 26-35.
86. Waller-Evans, H., et al., *Nutrigenomics of high fat diet induced obesity in mice suggests relationships between susceptibility to fatty liver disease and the proteasome.* PLoS One, 2013. **8**(12): p. e82825.
87. Kounakis, K., et al., *Emerging Roles of Lipophagy in Health and Disease.* Front Cell Dev Biol, 2019. **7**: p. 185.
88. Höhn, A., et al., *Happily (n)ever after: Aging in the context of oxidative stress, proteostasis loss and cellular senescence.* Redox Biol, 2017. **11**: p. 482-501.
89. Menon, M.B. and S. Dhamija, *Beclin 1 Phosphorylation - at the Center of Autophagy Regulation.* Front Cell Dev Biol, 2018. **6**: p. 137.

90. Walczak, M. and S. Martens, *Dissecting the role of the Atg12-Atg5-Atg16 complex during autophagosome formation*. Autophagy, 2013. **9**(3): p. 424-5.
91. Fujita, N., et al., *The Atg16L complex specifies the site of LC3 lipidation for membrane biogenesis in autophagy*. Mol Biol Cell, 2008. **19**(5): p. 2092-100.
92. Maruyama, T. and N.N. Noda, *Autophagy-regulating protease Atg4: structure, function, regulation and inhibition*. J Antibiot (Tokyo), 2017. **71**(1): p. 72-8.
93. Koukourakis, M.I., et al., *Autophagosome Proteins LC3A, LC3B and LC3C Have Distinct Subcellular Distribution Kinetics and Expression in Cancer Cell Lines*. PLoS One, 2015. **10**(9): p. e0137675.
94. Lee, Y.K. and J.A. Lee, *Role of the mammalian ATG8/LC3 family in autophagy: differential and compensatory roles in the spatiotemporal regulation of autophagy*. BMB Rep, 2016. **49**(8): p. 424-30.
95. Noda, N.N., et al., *Structure of the Atg12-Atg5 conjugate reveals a platform for stimulating Atg8-PE conjugation*. EMBO Rep, 2013. **14**(2): p. 206-11.
96. Bjørkøy, G., et al., *Monitoring autophagic degradation of p62/SQSTM1*. Methods Enzymol, 2009. **452**: p. 181-97.
97. Zhang, X.J., et al., *Why should autophagic flux be assessed?* Acta Pharmacol Sin, 2013. **34**(5): p. 595-9.
98. https://smart.servier.com/smart_image/mitochondria/
99. https://smart.servier.com/smart_image/enzyme-2/
100. https://smart.servier.com/smart_image/enzyme-9/
101. Eskelinen, E.L., *Roles of LAMP-1 and LAMP-2 in lysosome biogenesis and autophagy*. Mol Aspects Med, 2006. **27**(5-6): p. 495-502.
102. Stoka, V., V. Turk, and B. Turk, *Lysosomal cathepsins and their regulation in aging and neurodegeneration*. Ageing Res Rev, 2016. **32**: p. 22-37.
103. Li, F. and H. Zhang, *Lysosomal Acid Lipase in Lipid Metabolism and Beyond*. Arterioscler Thromb Vasc Biol, 2019. **39**(5): p. 850-856.
104. Zechner, R., F. Madeo, and D. Kratky, *Cytosolic lipolysis and lipophagy: two sides of the same coin*. Nat Rev Mol Cell Biol, 2017. **18**(11): p. 671-684.
105. Singh, R., et al., *Autophagy regulates lipid metabolism*. Nature, 2009. **458**(7242): p. 1131-5.
106. Kim, R.S., et al., *The XBP1 Arm of the Unfolded Protein Response Induces Fibrogenic Activity in Hepatic Stellate Cells Through Autophagy*. Sci Rep, 2016. **6**: p. 39342.

107. Shen, L., et al., *Phosphorylated heat shock protein 27 promotes lipid clearance in hepatic cells through interacting with STAT3 and activating autophagy.* Cell Signal, 2016. **28**(8): p. 1086-98.
108. Cai, N., et al., *Autophagy protects against palmitate-induced apoptosis in hepatocytes.* Cell Biosci, 2014. **4**: p. 28.
109. Tan, S.H., et al., *Induction of autophagy by palmitic acid via protein kinase C-mediated signaling pathway independent of mTOR (mammalian target of rapamycin).* J Biol Chem, 2012. **287**(18): p. 14364-76.
110. Tu, Q.Q., et al., *Palmitic acid induces autophagy in hepatocytes via JNK2 activation.* Acta Pharmacol Sin, 2014. **35**(4): p. 504-12.
111. Ogata, M., et al., *Autophagy is activated for cell survival after endoplasmic reticulum stress.* Mol Cell Biol, 2006. **26**(24): p. 9220-31.
112. Ding, H., et al., *Hepatic autophagy fluctuates during the development of non-alcoholic fatty liver disease.* Ann Hepatol, 2020. **19**(5): p. 516-522.
113. González-Rodríguez, A., et al., *Impaired autophagic flux is associated with increased endoplasmic reticulum stress during the development of NAFLD.* Cell Death Dis, 2014. **5**(4): p. e1179.
114. Yang, L., et al., *Defective hepatic autophagy in obesity promotes ER stress and causes insulin resistance.* Cell Metab, 2010. **11**(6): p. 467-78.
115. Liu, H.Y., et al., *Hepatic autophagy is suppressed in the presence of insulin resistance and hyperinsulinemia: inhibition of FoxO1-dependent expression of key autophagy genes by insulin.* J Biol Chem, 2009. **284**(45): p. 31484-92.
116. Tong, L., et al., *PPARδ attenuates hepatic steatosis through autophagy-mediated fatty acid oxidation.* Cell Death Dis, 2019. **10**(3): p. 197.
117. Li, R., et al., *1,25(OH)(2) D(3) attenuates hepatic steatosis by inducing autophagy in mice.* Obesity (Silver Spring), 2017. **25**(3): p. 561-571.
118. Sinha, R.A., et al., *Caffeine stimulates hepatic lipid metabolism by the autophagy-lysosomal pathway in mice.* Hepatology, 2014. **59**(4): p. 1366-80.
119. Zhang, E., et al., *Glycycoumarin inhibits hepatocyte lipoapoptosis through activation of autophagy and inhibition of ER stress/GSK-3-mediated mitochondrial pathway.* Sci Rep, 2016. **6**: p. 38138.
120. Zhang, Y., et al., *Resveratrol improves hepatic steatosis by inducing autophagy through the cAMP signaling pathway.* Mol Nutr Food Res, 2015. **59**(8): p. 1443-57.

121. Zhang, R., et al., *Corilagin Alleviates Nonalcoholic Fatty Liver Disease in High-Fat Diet-Induced C57BL/6 Mice by Ameliorating Oxidative Stress and Restoring Autophagic Flux.* Front Pharmacol, 2019. **10**: p. 1693.
122. Lou, J., et al., *Hepatic CD147 knockout modulates liver steatosis and up-regulates autophagy in high-fat-diet-induced NAFLD mice.* Biochem Biophys Res Commun, 2020. **524**(4): p. 1010-1017.
123. Song, Y.M., et al., *Metformin alleviates hepatosteatosis by restoring SIRT1-mediated autophagy induction via an AMP-activated protein kinase-independent pathway.* Autophagy, 2015. **11**(1): p. 46-59.
124. Xue, W., et al., *Caveolin-1 alleviates lipid accumulation in NAFLD associated with promoting autophagy by inhibiting the Akt/mTOR pathway.* Eur J Pharmacol, 2020. **871**: p. 172910.
125. Zhu, S., et al., *FGF21 ameliorates nonalcoholic fatty liver disease by inducing autophagy.* Mol Cell Biochem, 2016. **420**(1-2): p. 107-19.
126. Fang, Y., et al., *Liraglutide Alleviates Hepatic Steatosis by Activating the TFEB-Regulated Autophagy-Lysosomal Pathway.* Front Cell Dev Biol, 2020. **8**: p. 602574.
127. He, Y., et al., *The preventive effect of liraglutide on the lipotoxic liver injury via increasing autophagy.* Ann Hepatol, 2020. **19**(1): p. 44-52.
128. Zheng, Y.Y., et al., *Autophagy activation by Jiang Zhi Granule protects against metabolic stress-induced hepatocyte injury.* World J Gastroenterol, 2018. **24**(9): p. 992-1003.
129. Tanaka, S., et al., *Rubicon inhibits autophagy and accelerates hepatocyte apoptosis and lipid accumulation in nonalcoholic fatty liver disease in mice.* Hepatology, 2016. **64**(6): p. 1994-2014.
130. Koga, H., S. Kaushik, and A.M. Cuervo, *Altered lipid content inhibits autophagic vesicular fusion.* Faseb j, 2010. **24**(8): p. 3052-65.
131. Fukuo, Y., et al., *Abnormality of autophagic function and cathepsin expression in the liver from patients with non-alcoholic fatty liver disease.* Hepatol Res, 2014. **44**(9): p. 1026-36.
132. Anan, A., et al., *Proteasome inhibition induces hepatic stellate cell apoptosis.* Hepatology, 2006. **43**(2): p. 335-44.
133. Boozari, B., et al., *Antitumoural immunity by virus-mediated immunogenic apoptosis inhibits metastatic growth of hepatocellular carcinoma.* Gut, 2010. **59**(10): p. 1416-26.

134. Umemura, A., et al., *Liver damage, inflammation, and enhanced tumorigenesis after persistent mTORC1 inhibition*. Cell Metab, 2014. **20**(1): p. 133-44.
135. Huang, X., et al., *The HGF-MET axis coordinates liver cancer metabolism and autophagy for chemotherapeutic resistance.* Autophagy, 2019. **15**(7): p. 1258-1279.
136. Tan, S., et al., *β-Arrestin1 enhances liver fibrosis through autophagy-mediated Snail signaling*. Faseb j, 2019. **33**(2): p. 2000-2016.
137. Ma, J.Q., et al., *Ampelopsin attenuates carbon tetrachloride-induced mouse liver fibrosis and hepatic stellate cell activation associated with the SIRT1/TGF-β1/Smad3 and autophagy pathway*. Int Immunopharmacol, 2019. **77**: p. 105984.
138. https://pubchem.ncbi.nlm.nih.gov/compound/Punicalagin#section=Structures
139. Zou, X., et al., *Mitochondrial dysfunction in obesity-associated nonalcoholic fatty liver disease: the protective effects of pomegranate with its active component punicalagin*. Antioxid Redox Signal, 2014. **21**(11): p. 1557-70.
140. Kang, B., et al., *Punicalagin, a Pomegranate-Derived Ellagitannin, Suppresses Obesity and Obesity-Induced Inflammatory Responses Via the Nrf2/Keap1 Signaling Pathway*. Mol Nutr Food Res, 2019. **63**(22): p. e1900574.
141. Zhang, Y., et al., *A New Possible Mechanism by Which Punicalagin Protects against Liver Injury Induced by Type 2 Diabetes Mellitus: Upregulation of Autophagy via the Akt/FoxO3a Signaling Pathway*. J Agric Food Chem, 2019. **67**(50): p. 13948-13959.
142. Cao, K., et al., *Punicalagin, an active component in pomegranate, ameliorates cardiac mitochondrial impairment in obese rats via AMPK activation*. Sci Rep, 2015. **5**: p. 14014.
143. Jin, D., et al., *Effect of punicalagin on multiple targets in streptozotocin/high-fat diet-induced diabetic mice*. Food Funct, 2020. **11**(12): p. 10617-10634.
144. Yan, C., et al., *Punicalagin attenuates palmitate-induced lipotoxicity in HepG2 cells by activating the Keap1-Nrf2 antioxidant defense system.* Mol Nutr Food Res, 2016. **60**(5): p. 1139-49.
145. Wang, Y., et al., *Punicalagin promotes autophagy to protect primary human syncytiotrophoblasts from apoptosis.* Reproduction, 2016. **151**(2): p. 97-104.
146. Tan, S., et al., *Pomegranate activates TFEB to promote autophagy-lysosomal fitness and mitophagy*. Sci Rep, 2019. **9**(1): p. 727.
147. Feldman, A.T. and D. Wolfe, *Tissue processing and hematoxylin and eosin staining*. Methods Mol Biol, 2014. **1180**: p. 31-43.

148. Sonali Joshi, D.Y., *Chapter 8 - Immunofluorescence*. Basic Science Methods for Clinical Researchers, ed. F.Y.L.S. Morteza Jalali, Mehdi Jalali. 2017, Boston: Academic Press.
149. Shi, S.R., R.J. Cote, and C.R. Taylor, *Antigen retrieval techniques: current perspectives.* J Histochem Cytochem, 2001. **49**(8): p. 931-7.
150. Brenna, J.T., et al., *Best practices for the design, laboratory analysis, and reporting of trials involving fatty acids.* Am J Clin Nutr, 2018. **108**(2): p. 211-227.
151. Coleman, R.A. and D.J. Trader, *Development and Application of a Sensitive Peptide Reporter to Discover 20S Proteasome Stimulators.* ACS Comb Sci, 2018. **20**(5): p. 269-276.
152. Njomen, E. and J.J. Tepe, *Proteasome Activation as a New Therapeutic Approach To Target Proteotoxic Disorders.* J Med Chem, 2019. **62**(14): p. 6469-6481.
153. Ōmura, S. and A. Crump, *Lactacystin: first-in-class proteasome inhibitor still excelling and an exemplar for future antibiotic research.* J Antibiot (Tokyo), 2019. **72**(4): p. 189-201.
154. Zheng, Y. and Y. Jiang, *mTOR Inhibitors at a Glance.* Mol Cell Pharmacol, 2015. **7**(2): p. 15-20.
155. Thoreen, C.C., et al., *An ATP-competitive mammalian target of rapamycin inhibitor reveals rapamycin-resistant functions of mTORC1.* J Biol Chem, 2009. **284**(12): p. 8023-32.
156. Wu, Y.T., et al., *Dual role of 3-methyladenine in modulation of autophagy via different temporal patterns of inhibition on class I and III phosphoinositide 3-kinase.* J Biol Chem, 2010. **285**(14): p. 10850-61.
157. Repetto, G., A. del Peso, and J.L. Zurita, *Neutral red uptake assay for the estimation of cell viability/cytotoxicity.* Nat Protoc, 2008. **3**(7): p. 1125-31.
158. Mehlem, A., et al., *Imaging of neutral lipids by oil red O for analyzing the metabolic status in health and disease.* Nat Protoc, 2013. **8**(6): p. 1149-54.
159. Nolan, T., R.E. Hands, and S.A. Bustin, *Quantification of mRNA using real-time RT-PCR.* Nat Protoc, 2006. **1**(3): p. 1559-82.
160. Schmittgen, T.D. and K.J. Livak, *Analyzing real-time PCR data by the comparative C(T) method.* Nat Protoc, 2008. **3**(6): p. 1101-8.
161. Bonetta, L., *Prime time for real-time PCR.* Nature Methods, 2005. **2**(4): p. 305-312.

162. Vandesompele, J., et al., *Accurate normalization of real-time quantitative RT-PCR data by geometric averaging of multiple internal control genes.* Genome Biol, 2002. **3**(7): p. Research0034.
163. Olson, B.J. and J. Markwell, *Assays for determination of protein concentration*. Curr Protoc Pharmacol, 2007. **Appendix 3**: p. 3a.
164. Lowry, O.H., et al., *Protein measurement with the Folin phenol reagent.* J Biol Chem, 1951. **193**(1): p. 265-75.
165. Bradford, M.M., *A rapid and sensitive method for the quantitation of microgram quantities of protein utilizing the principle of protein-dye binding.* Anal Biochem, 1976. **72**: p. 248-54.
166. Tavender, T.J., A.M., Sheppard, and N.J., Bulleid, *Peroxiredoxin IV is an endoplasmic reticulum-localized enzyme forming oligomeric complexes in human cells*. Biochem J, 2008. **411**(1): p. 191-9.
167. Tavender, T.J., and N.J., Bulleid, *Peroxiredoxin IV protects cells from oxidative stress by removing H_2O_2 produced during disulphide formation.* J Cell Sci, 2010. **123**(15): p. 2672-9.
168. Zhu, L., et al., *A novel reaction of peroxiredoxin 4 towards substrates in oxidative protein folding*. PLoS One, 2014. **9**(8): p. 105529.
169. https://smart.servier.com/smart_image/endoplasmic-reticulum/
170. https://smart.servier.com/smart_image/enzyme-2/
171. https://smart.servier.com/smart_image/enzyme-9/
172. https://smart.servier.com/smart_image/protein-7/
173. Pelusi, S. and L. Valenti, *Hepatic fat as clinical outcome and therapeutic target for nonalcoholic fatty liver disease.* Liver Int, 2019. **39**(2): p. 250-256.
174. Kehm, R., et al., *Redox homeostasis and cell cycle activation mediate beta-cell mass expansion in aged, diabetes-prone mice under metabolic stress conditions: Role of thioredoxin-interacting protein (TXNIP).* Redox Biol, 2020. **37**: p. 101748.
175. Becker, W., et al., *Differential hepatic gene expression in a polygenic mouse model with insulin resistance and hyperglycemia: evidence for a combined transcriptional dysregulation of gluconeogenesis and fatty acid synthesis.* J Mol Endocrinol, 2004. **32**(1): p. 195-208.
176. Kluth, O., et al., *Identification of Four Mouse Diabetes Candidate Genes Altering beta-Cell Proliferation*. PLoS Genet, 2015. **11**(9): p. e1005506.

177. Jurgens, H.S., et al., *Development of diabetes in obese, insulin-resistant mice: essential role of dietary carbohydrate in beta cell destruction*. Diabetologia, 2007. **50**(7): p. 1481-9.
178. Kluth, O., et al., *Dissociation of lipotoxicity and glucotoxicity in a mouse model of obesity associated diabetes: role of forkhead box O1 (FOXO1) in glucose-induced beta cell failure*. Diabetologia, 2011. **54**(3): p. 605-16.
179. Kluth, O., et al., *Decreased Expression of Cilia Genes in Pancreatic Islets as a Risk Factor for Type 2 Diabetes in Mice and Humans.* Cell Rep, 2019. **26**(11): p. 3027-3036 e3.
180. Kluth, O., et al., *Differential transcriptome analysis of diabetes-resistant and -sensitive mouse islets reveals significant overlap with human diabetes susceptibility genes*. Diabetes, 2014. **63**(12): p. 4230-8.
181. Kluge, R., et al., *Pathophysiology and genetics of obesity and diabetes in the New Zealand obese mouse: a model of the human metabolic syndrome.* Methods Mol Biol, 2012. **933**: p. 59-73.
182. Geng, Y., et al., *How does hepatic lipid accumulation lead to lipotoxicity in non-alcoholic fatty liver disease?* Hepatol Int, 2021. **15**(1): p. 21-35.
183. Liu, J., et al., *Free fatty acids, not triglycerides, are associated with non-alcoholic liver injury progression in high fat diet induced obese rats.* Lipids Health Dis, 2016. **15**: p. 27.
184. Bhala, N., R. Younes, and E. Bugianesi, *Epidemiology and natural history of patients with NAFLD.* Curr Pharm Des, 2013. **19**(29): p. 5169-76.
185. Hennig, E.E., et al., *Extracellular matrix and cytochrome P450 gene expression can distinguish steatohepatitis from steatosis in mice*. J Cell Mol Med, 2014. **18**(9): p. 1762-72.
186. Rinnankoski-Tuikka, R., et al., *Lipid droplet-associated proteins in high-fat fed mice with the effects of voluntary running and diet change.* Metabolism, 2014. **63**(8): p. 1031-40.
187. Zacharewicz, E., M.K.C. Hesselink, and P. Schrauwen, *Exercise counteracts lipotoxicity by improving lipid turnover and lipid droplet quality*. J Intern Med, 2018. **284**(5): p. 505-518.
188. Wang, C., et al., *Perilipin 5 improves hepatic lipotoxicity by inhibiting lipolysis.* Hepatology, 2015. **61**(3): p. 870-82.

189. Joost, H.G., *The genetic basis of obesity and type 2 diabetes: lessons from the new zealand obese mouse, a polygenic model of the metabolic syndrome.* Results Probl Cell Differ, 2010. **52**: p. 1-11.
190. Conte, M., et al., *Perilipin 2 and Age-Related Metabolic Diseases: A New Perspective.* Trends Endocrinol Metab, 2016. **27**(12): p. 893-903.
191. Orlicky, D.J., et al., *Perilipin-2 promotes obesity and progressive fatty liver disease in mice through mechanistically distinct hepatocyte and extra-hepatocyte actions.* J Physiol, 2019. **597**(6): p. 1565-1584.
192. McManaman, J.L., et al., *Perilipin-2-null mice are protected against diet-induced obesity, adipose inflammation, and fatty liver disease.* J Lipid Res, 2013. **54**(5): p. 1346-59.
193. Knebel, B., et al., *Alteration of Liver Peroxisomal and Mitochondrial Functionality in the NZO Mouse Model of Metabolic Syndrome.* Proteomics Clin Appl, 2018. **12**(1).
194. Henkel, J., et al., *Stimulation of fat accumulation in hepatocytes by PGE_2-dependent repression of hepatic lipolysis, β-oxidation and VLDL-synthesis.* Lab Invest, 2012. **92**(11): p. 1597-606.
195. Nocetti, D., et al., *Lipid droplets are both highly oxidized and Plin2-covered in hepatocytes of diet-induced obese mice.* Appl Physiol Nutr Metab, 2020. **45**(12): p. 1368-1376.
196. Coleman, R.A., *The "discovery" of lipid droplets: A brief history of organelles hidden in plain sight.* Biochim Biophys Acta Mol Cell Biol Lipids, 2020. **1865**(9): p. 158762.
197. Lass, A., et al., *Lipolysis - a highly regulated multi-enzyme complex mediates the catabolism of cellular fat stores.* Prog Lipid Res, 2011. **50**(1): p. 14-27.
198. Sánchez-Wandelmer, J. and F. Reggiori, *Atg4 in autophagosome biogenesis.* Oncotarget, 2017. **8**(65): p. 108290-108291.
199. Zhao, N.Q., et al., *Palmitate induces fat accumulation by activating C/EBPβ-mediated G0S2 expression in HepG2 cells.* World J Gastroenterol, 2017. **23**(43): p. 7705-7715.
200. Zhou, Y., et al., *LXRa participates in the mTOR/S6K1/SREBP-1c signaling pathway during sodium palmitate-induced lipogenesis in HepG2 cells.* Nutr Metab (Lond), 2018. **15**: p. 31.
201. Krahmer, N., R.V. Farese, Jr., and T.C. Walther, *Balancing the fat: lipid droplets and human disease.* EMBO Mol Med, 2013. **5**(7): p. 973-83.
202. Xu, S., et al., *Perilipin 2 and lipid droplets provide reciprocal stabilization.* Biophysics Reports, 2019. **5**(3): p. 145-160.

203. Sans, A., et al., *The Differential Expression of Cide Family Members is Associated with Nafld Progression from Steatosis to Steatohepatitis.* Sci Rep, 2019. **9**(1): p. 7501.
204. Kuramoto, K., et al., *Perilipin 5, a lipid droplet-binding protein, protects heart from oxidative burden by sequestering fatty acid from excessive oxidation.* J Biol Chem, 2012. **287**(28): p. 23852-63.
205. Wang, C., et al., *Plin5 deficiency exacerbates pressure overload-induced cardiac hypertrophy and heart failure by enhancing myocardial fatty acid oxidation and oxidative stress.* Free Radic Biol Med, 2019. **141**: p. 372-382.
206. Tan, Y., et al., *Perilipin 5 Protects against Cellular Oxidative Stress by Enhancing Mitochondrial Function in HepG2 Cells.* Cells, 2019. **8**(10).
207. Gao, X., et al., *Atorvastatin reduces lipid accumulation in the liver by activating protein kinase A-mediated phosphorylation of perilipin 5.* Biochim Biophys Acta Mol Cell Biol Lipids, 2017. **1862**(12): p. 1512-1519.
208. Ma, X., et al., *Lipid storage droplet protein 5 reduces sodium palmitate-induced lipotoxicity in human normal liver cells by regulating lipid metabolism-related factors.* Mol Med Rep, 2019. **20**(2): p. 879-886.
209. Egnatchik, R.A., et al., *Palmitate-induced activation of mitochondrial metabolism promotes oxidative stress and apoptosis in H4IIEC3 rat hepatocytes.* Metabolism, 2014. **63**(2): p. 283-95.
210. Hauck, A.K. and D.A. Bernlohr, *Oxidative stress and lipotoxicity.* J Lipid Res, 2016. **57**(11): p. 1976-1986.
211. Gao, D., et al., *The effects of palmitate on hepatic insulin resistance are mediated by NADPH Oxidase 3-derived reactive oxygen species through JNK and p38MAPK pathways.* J Biol Chem, 2010. **285**(39): p. 29965-73.
212. Nakamura, S., et al., *Palmitate induces insulin resistance in H4IIEC3 hepatocytes through reactive oxygen species produced by mitochondria.* J Biol Chem, 2009. **284**(22): p. 14809-18.
213. He, L., et al., *ER stress-mediated cell damage contributes to the release of EDA(+) fibronectin from hepatocytes in nonalcoholic fatty liver disease.* J Huazhong Univ Sci Technolog Med Sci, 2017. **37**(2): p. 217-225.
214. Grasselli, E., et al., *Models of non-Alcoholic Fatty Liver Disease and Potential Translational Value: the Effects of 3,5-L-diiodothyronine.* Ann Hepatol, 2017. **16**(5):p. 707-719.

215. Zheng, P., et al., *Plin5 alleviates myocardial ischaemia/reperfusion injury by reducing oxidative stress through inhibiting the lipolysis of lipid droplets.* Sci Rep, 2017. **7**: p. 42574.
216. Höhn, A., J. König, and T. Jung, *Metabolic Syndrome, Redox State, and the Proteasomal System.* Antioxid Redox Signal, 2016. **25**(16): p. 902-917.
217. Achard, C.S. and D.R. Laybutt, *Lipid-induced endoplasmic reticulum stress in liver cells results in two distinct outcomes: adaptation with enhanced insulin signaling or insulin resistance.* Endocrinology, 2012. **153**(5): p. 2164-77.
218. Yun, H.R., et al., *Roles of Autophagy in Oxidative Stress.* Int J Mol Sci, 2020. **21**(9).
219. Osna, N.A., et al., *Peroxynitrite alters the catalytic activity of rodent liver proteasome in vitro and in vivo.* Hepatology, 2004. **40**(3): p. 574-82.
220. Just, J., et al., *Identification of an unstable 4-hydroxynoneal modification on the 20S proteasome subunit α7 by recombinant antibody technology.* Free Radic Biol Med, 2015. **89**: p. 786-92.
221. Ferrington, D.A. and R.J. Kapphahn, *Catalytic site-specific inhibition of the 20S proteasome by 4-hydroxynonenal.* FEBS Lett, 2004. **578**(3): p. 217-23.
222. Farout, L., et al., *Inactivation of the proteasome by 4-hydroxy-2-nonenal is site specific and dependant on 20S proteasome subtypes.* Arch Biochem Biophys, 2006. **453**(1): p. 135-42.
223. Mei, S., et al., *Differential roles of unsaturated and saturated fatty acids on autophagy and apoptosis in hepatocytes.* J Pharmacol Exp Ther, 2011. **339**(2): p. 487-98.
224. Declèves, A.E., et al., *Regulation of lipid accumulation by AMP-activated kinase [corrected] in high fat diet-induced kidney injury.* Kidney Int, 2014. **85**(3): p. 611-23.
225. Jung, T.W., et al., *BAIBA attenuates insulin resistance and inflammation induced by palmitate or a high fat diet via an AMPK-PPARδ-dependent pathway in mice.* Diabetologia, 2015. **58**(9): p. 2096-105.
226. Yuan, Y., et al., *Mitochondrial ROS-induced lysosomal dysfunction impairs autophagic flux and contributes to M1 macrophage polarization in a diabetic condition.* Clin Sci (Lond), 2019. **133**(15): p. 1759-1777.
227. Song, Y.M., et al., *Dimethyl sulfoxide reduces hepatocellular lipid accumulation through autophagy induction.* Autophagy, 2012. **8**(7): p. 1085-97.
228. Fouad, A.A., H.O. Qutub, and W.N. Al-Melhim, *Punicalagin alleviates hepatotoxicity in rats challenged with cyclophosphamide.* Environ Toxicol Pharmacol, 2016. **45**: p. 158-62.

229. Luo, J., et al., *Punicalagin Reversed the Hepatic Injury of Tetrachloromethane by Antioxidation and Enhancement of Autophagy.* J Med Food, 2019.

230. Najt, C.P., et al., *Liver-specific loss of Perilipin 2 alleviates diet-induced hepatic steatosis, inflammation, and fibrosis.* Am J Physiol Gastrointest Liver Physiol, 2016. **310**(9): p. G726-38.

231. Viladomiu, M., et al., *Preventive and prophylactic mechanisms of action of pomegranate bioactive constituents.* Evid Based Complement Alternat Med, 2013. **2013**: p. 789764.

9. Supplementary Figures

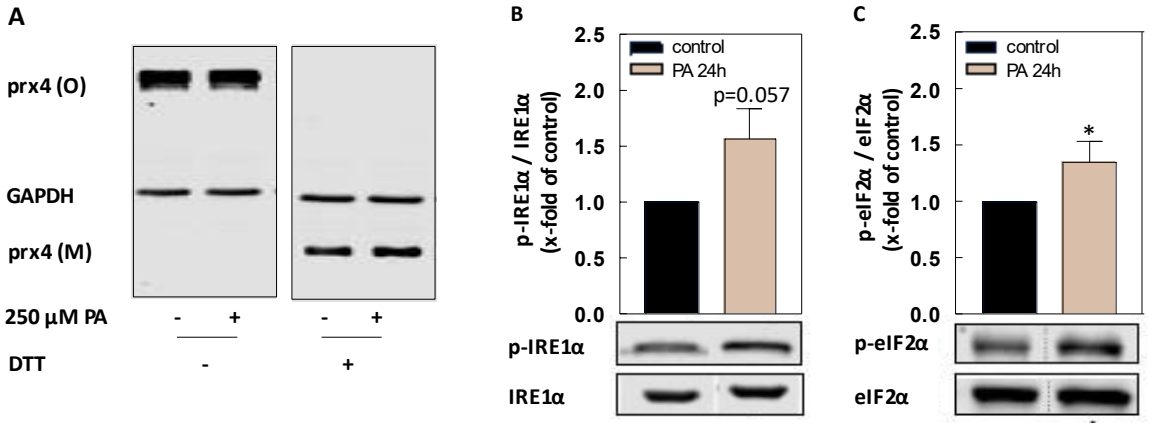

Suppl. Figure 1: ER stress sensors in PA treated HepG2 cells. A. Immunoblot analysis of prx4 under non-reducing (left blot) and reducing conditions (right blot), representing the oligomeric (O) and monomeric (M) state respectively. **B, C.** Analysis of phosphorylation levels of IRE1α (B) and eIF2α (C) by immunoblot after 24h PA treatment. Quantifications and representative immunoblots. Statistical significance was given by one sample t-test at *$p < 0.05$. Trend is given by $p=0.057$.

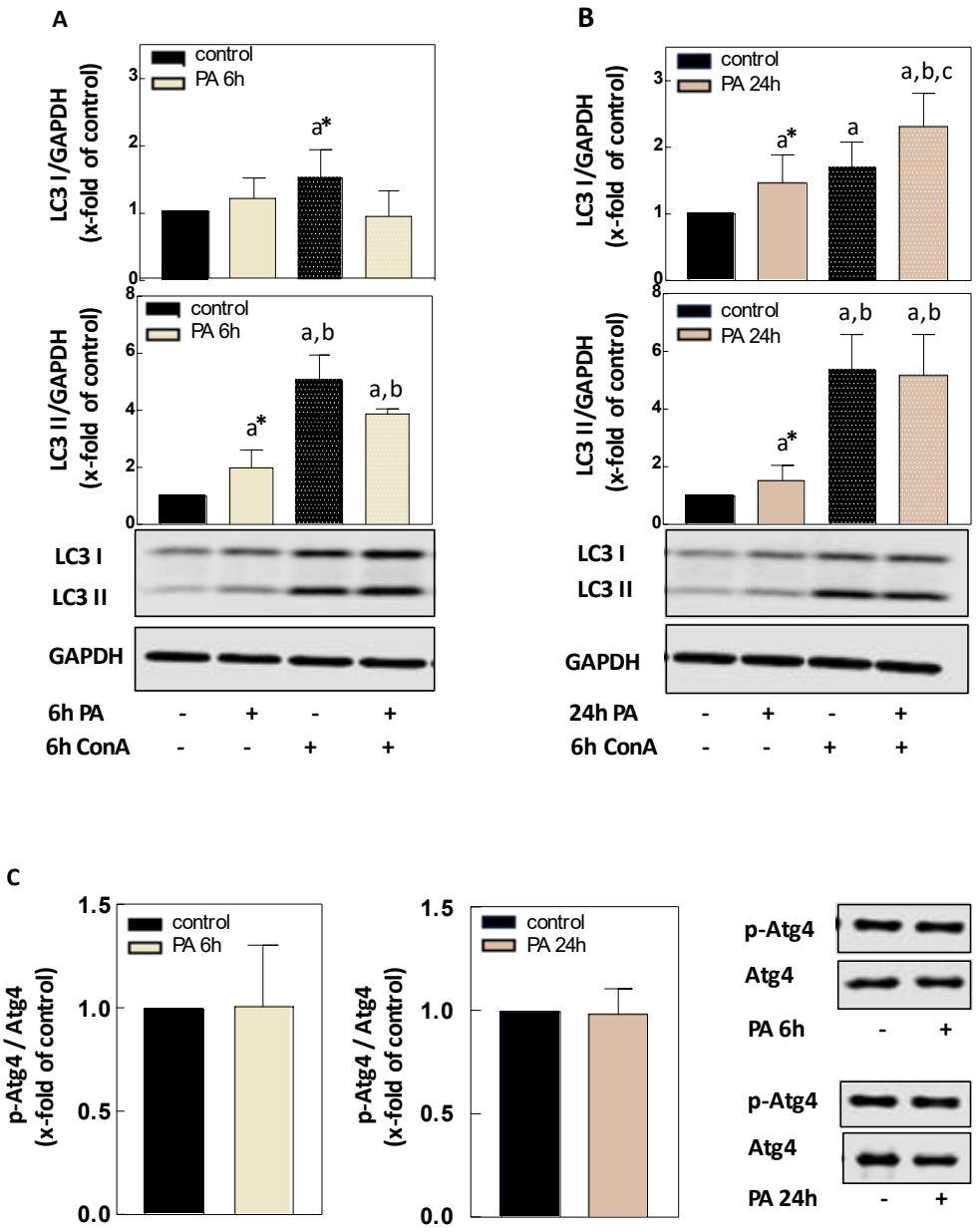

Suppl. Figure 2: Impact of PA on autophagosome elongation and maturation in HepG2 cells. A-C. Immunoblot analysis of LC3 I, LC3 II and p-Atg4/Atg4 ratio after 6h and 24h PA exposure. Quantifications and representative immunoblots. GAPDH was used as protein loading control. Statistical significance was given at $p < 0.05$ as follows: One way ANOVA test, Tukey's multiple comparisons, indicated by a vs control, b vs PA and c vs ConA; one sample t-test indicated with a* vs control.

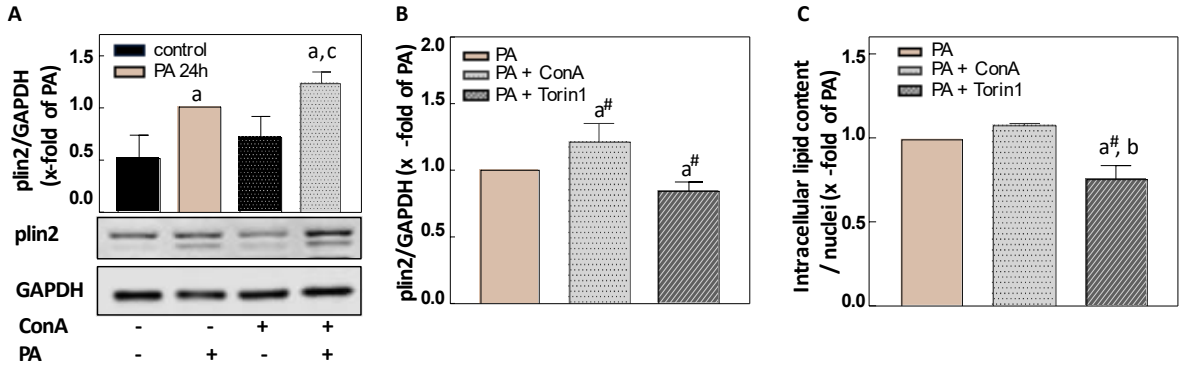

Suppl. Figure 3: Inhibition of lysosomal degradation by ConA further increases the accumulation of LDs. A. Immunoblot analysis of plin2 and quantification. **B, C.** Alterations of plin2 levels (B) and intracellular lipid content (C) due to treatment with ConA and Torin 1 in PA-treated HepG2 cells. Statistical significance was given as follows: one Way ANOVA test, Tukey's multiple comparisons with $p < 0.05$, indicated by a vs control, b vs PA+ConA, c vs ConA and one sample t-test indicated with $a^{\#}$ vs PA.

Selbständigkeitserklärung

Hiermit erkläre ich, dass ich die vorliegende Arbeit selbständig angefertigt und keine anderen als die angegebenen Quellen und Hilfsmittel benutzt habe. Diese Arbeit wurde an keiner anderen Hochschule eingereicht.

Potsdam, November 2021

_____

Ioanna Korovila